MASSACHUSETTS INSTITUTE OF TECHNOLOGY
LINCOLN LABORATORY

EXPERIMENTAL VALIDATION OF PALM - A SYSTEM FOR PRECISE AIRCRAFT LOCATION

J.E. Evans, R.R. LaFrey, I.G. Stiglitz, D. Karp, R.J. McAulay

TECHNICAL NOTE 1975-29

29 Apr 1975

LEXINGTON MASSACHUSETTS

Technical Report Documentation Page

1. Report No.	2. Government Accession No.	3. Recipient's Catalog No.
ESD-TR-75-166		

4. Title and Subtitle	5. Report Date
Experimental Validation of PALM – A System for Precise Aircraft Location	29 April 1975
	6. Performing Organization Code
7. Author(s)	8. Performing Organization Report No.
J. E. Evans R. R. LaFrey I. G. Stiglitz D. Karp R. J. McAulay	Technical Note 1975-29
9. Performing Organization Name and Address	10. Work Unit No. (TRAIS) 15434 022-243-012 & 033-241-062
Lincoln Laboratory, M.I.T. P.O. Box 73 Lexington, MA 02173	11. Contract or Grant No. IAG DOT-FA72WAI-242
	13. Type of Report and Period Covered
12. Sponsoring Agency Name and Address	Technical Note
Department of Transportation Federal Aviation Administration Systems Research and Development Service Washington, DC 20591	14. Sponsoring Agency Code

15. Supplementary Notes

The work reported in this document was performed at Lincoln Laboratory, a center for research operated by the Massachusetts Institute of Technology under Air Force Contract F19628-73-C-0002.

16. Abstract

A ground based system to precisely locate aircraft in three dimensions based on transponder replies has been designed. Field tests have been conducted to validate the design of the elevation performance. This document reports on the principle of operation, experimental hardware and field test of the Precision Altitude and Landing Monitor (PALM).

The key features incorporated in the PALM design include: (a) no new avionics required, i.e., uses standard aircraft transponder; (b) high accuracy position data, i.e., a 1-mrad (0.06°) rms error in elevation and in azimuth; (c) broad airspace coverage, e.g., 40° in elevation, 120° in azimuth (expandable to 360°) and several 10s of miles in range; and (d) low life cycle equipment cost. The high accuracy in the difficult airport multipath environment is a direct result of (a) a newly developed antenna synthesis procedure, (b) the development of adaptive multipath suppression techniques, and (c) the use of digital signal processing.

The program, to date, has focused on an experimental evaluation of the elevation performance. The electronics required for the tests have been built into a self-powered van to facilitate experiments at remote airports. The actual flight test data demonstrated experimental errors on the order of 1 mrad; moreover, as predicted by theory, the resulting errors were essentially independent of elevation angle.

Potential applications for the PALM position data include parallel approach monitoring, independent altitude monitoring, and/or performance assurance monitoring of landing guidance systems.

17. Key Words		18. Distribution Statement
landing monitor performance assurance monitor altitude monitor landing guidance aperture sampling	multipath PALM	Document is available to the public through the National Technical Information Service, Springfield, Virginia 22151.

19. Security Classif. (of this report)	20. Security Classif. (of this page)	21. No. of Pages	
Unclassified	Unclassified	120	

Form DOT F 1700.7 (8-72) Reproduction of completed page authorized

TABLE OF CONTENTS

TABLE OF CONTENTS (continued)

LIST OF ILLUSTRATIONS

ILLUSTRATIONS (continued)

ILLUSTRATIONS (continued)

LIST OF TABLES

1.0 INTRODUCTION AND SUMMARY OF CONCLUSIONS

The Precision Altitude and Landing Monitor (PALM) is intended to provide accurate stand-alone three-dimensional position data for aircraft equipped with standard beacon transponders using ground equipment designed for low life-cycle cost. The PALM program, to date, has focused on an experimental evaluation of the elevation measurements accuracy. These measurement results have successfully validated the theoretical prediction of a 1-mrad elevation accuracy. This report provides a description of the principle of operation and the experimental hardware and presents the experimental results.

A runway equipped with an operational version of PALM would employ two fixed antenna arrays probably located near the glide path intercept point. Typical coverage of a PALM module* would include a sector 120° in azimuth, 40° in elevation (1° to 41°) and several tens of miles in range. Elevation data would be provided by a vertical array of five fixed broad beam antennas mounted on a 30-ft pole. Azimuth data would be obtained using a line array of five fixed broad beam antennas along a 50- to 150-ft baseline. The received transponder replies would provide data to a multichannel receiver. The data from the receivers would then be digitized and transferred to a minicomputer for processing and formatting of the resulting azimuth, elevation, distance, and identity data for transmission over a telephone line to the TRACON and/or TRACAB.

---

*Three modules would be required for full 360° coverage.

Angular accuracy (in elevation and azimuth) better than 0.06° rms (5 ft at 1 mile, 50 ft at 10 miles) and peak range error of 250 ft would be achieved out to a range of at least 30 miles. A special ATCRBS (or DABS)* terminal area interrogator under minicomputer control would provide for position updates every 0.1 sec on aircraft equipped with a standard transponder.

The electronics equipment required for the tests has been built into a self-powered van to facilitate any follow-on experiments at remote airports. The experimental antenna system has been installed at the Lincoln Laboratory Antenna Test Range (Fig. 1) where test flights have been conducted.

A set of flight tests were performed to exercise the various modes of the PALM sensor and to validate both the theoretical design concepts and the theoretically predicted performance accuracy. In one typical test flight, the aircraft flew at constant altitude, covering an elevation sector from 2 to 6 degrees. Elevation angle estimates were subdivided into 1/4-degree cells, statistically averaged and the rms values computed as a function of elevation angle. Not only were the errors of the order of 1 milliradian, as predicted by theory, but the resulting errors were essentially independent of elevation angle which was also predicted theoretically.

---

*Nearly all military and commercial aircraft and an estimated 40% of general aviation aircraft are currently equipped with transponders for Air Traffic Control Radar Beacon System (ATCRBS) service. The Discrete Address Beacon System (DABS) is the planned compatible upgrading to provide improved surveillance (accuracy and reliability) and two-way digital communications for a number of services including Intermittent Positive Control (IPC).

Fig. 1. PALM experimental equipment.

The PALM design concept exploits modern technology to economically satisfy several particular needs for high accuracy, high data rate position data. The brief discussion here of the motivating applications is intended to provide the perspective on the major technical issues addressed during the program (to date).

The position data could be processed and presented to the controller on a standard ARTS or a special stand-alone display. This could provide the surveillance data base required to ensure safe (blunder free) operation of closely spaced dual parallel runways. This application requires an azimuth accuracy of 1 mrad and an update rate of one second* [1,2]. Other applications include independent altitude monitoring, e.g., for Mode C correspondence checking [3,4], independent backup of the ATC surveillance system in high density airspace, low altitude surveillance coverage at airports without ASRs and performance assurance monitoring of the landing guidance system (ILS and MLS) [5].

This same data could serve as a data base for certain ground-to-air messages. Terrain avoidance alerts could automatically be sent to the pilot over the VHF voice link and/or the DABS data link coupled to the IPC display. The actual position data could be transmitted over the DABS data link for landing guidance during low visibility conditions, e.g., this data could be used to drive cross-point needles or an independent landing monitor display in the cockpit. The design accuracy and data rate are comparable to those of the MLS [6].

---

*By way of contrast, the ASR provides an accuracy of ~4 mrad and an update rate of 4 sec. Even the improved accuracy and data link capacity of DABS cannot displace the need for a higher update rate.

For en route applications a similar vertical array would provide altitude data (independent of the barometric altimeter) for aircraft at ranges out to 100 miles. Operating at an update rate of 0.1 Hz, independent altitude data would complement that of the en route radars. Applications for this data would include Mode C correspondence checking and backup. This data could also provide the data base for automated terrain avoidance alerts.

There are several design features that make the PALM concept especially attractive. In particular, no special avionics equipment is required, i.e., a standard ATCRBS transponder will suffice. The system is designed to also operate with DABS equipped aircraft. If PALM is used as a data base for certain ground-to-air messages, a standard VHF voice link and/or DABS data link and IPC display could easily be employed.

The PALM concept incorporates ground equipment designed for low life cycle cost. The antennas are (mechanically) fixed and incorporate no active phase shifters. The signal processing for interference rejection is performed digitally by a general purpose minicomputer for low procurement, operating and maintenance costs. The output data is provided digitally for easy remote display and interface with the ATC system.

The technical details of the PALM program, to date, are described in the following three sections. Section 2 is devoted to providing the theoretical foundation for the PALM design. The aperture synthesis procedures are described, and techniques for resolving ambiguities are investigated. Signal-

to-noise ratio requirements are evaluated to ensure that the partially filled array used for aperture synthesis has sufficient gain. The three basic techniques for rejecting multipath are evaluated. Off-axis multipath, e.g., from buildings, mountains, aircraft, etc., is rejected with time gating. Ground reflection multipath is suppressed by the rapid rolloff in antenna gain about the horizon and by using processing algorithms that exploit the structured interference produced by the (nearly) known (ground) reflector location.

Section 3 is devoted to describing the experimental hardware and to evaluating the equipment errors. The phase accuracy and noise level of the rf section are described, and the antenna characteristics are defined. In addition, the capabilities of the system timing and control subsystem are described. The theodolite calibration used to provide a measurement of "true" aircraft position is characterized.

Experimental results for flight tests conducted at the Lincoln Laboratory Antenna Range are presented in Section 4. These results validate the theoretical analysis presented in Section 2. The results of an analysis of the effects of asynchronous fruit on PALM performance (presented in Appendix A) have demonstrated that this interference will affect less than 6% of the total replies even in the high density 1980 airspace. The results of an analysis of the effects of PALM on ATCRBS uplink reliability and downlink fruit rate (presented in Appendix B) indicate that within the anticipated lifetime of the ATCRBS system, the addition of a limited number of PALM sensors should cause no significant performance degradation.

2.0 PRINCIPLE OF OPERATION

2.1 Design of the Basic Sensor

This section focuses on the design of the PALM sensor for elevation angle determination for aircraft during the approach and landing phase of its flight. The sensor design exploits the fact that the beacon signal returns are typically at high power levels. The interferometer principle is well suited to applications of this type in which large aperture high gain antennas are unnecessary. Furthermore, as will be shown in subsequent sections, the basic interferometer involves relatively simple processing and, hence, is well suited for minicomputer implementation. In this section the basic interferometer processor will be presented with a discussion of more complicated algorithms to follow later in the report.

A simple interferometer is formed by placing two antennas a vertical distance D apart. As shown in Fig. 2, a plane wave of wavelength λ, produced by an aircraft transmission at elevation angle e, will arrive at one of the antennas before the other, inducing a phase shift given by

$$\phi = 2\pi \frac{D}{\lambda} \sin e \tag{2-1}$$

which can be measured by feeding the antenna outputs into a phase detector. Hence the estimated angle is

$$\hat{e} = \sin^{-1}(\widehat{\sin e}) \tag{2-2}$$

where

$$\widehat{\sin e} = \frac{\phi}{2\pi \frac{D}{\lambda}} \tag{2-3}$$

is the estimate of the direction cosine of the elevation angle.

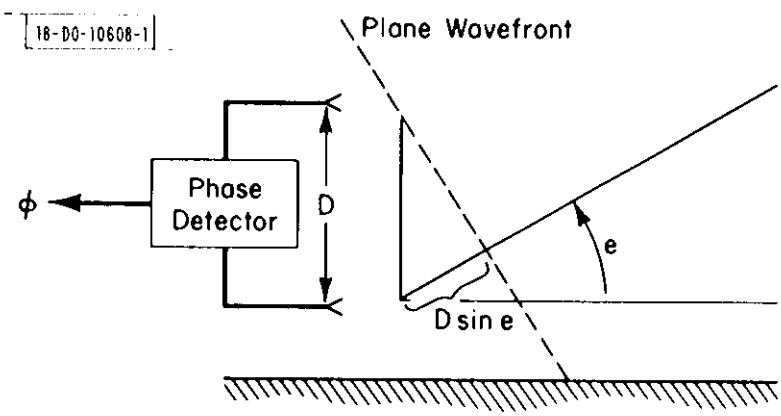

Fig. 2. The basic interferometer.

It is immediately apparent that since a phase detector can only measure phase modulo 2π, the elevation angle estimate will be ambiguous whenever sin e increases by more than λ/D. It will be shown subsequently that apertures spanning approximately 25 wavelengths will be needed to obtain the requisite accuracy and since coverage up to 30° in elevation is required for the PALM application, it is clear that multiple ambiguity lobes will occur. It is well known [7], however, that the ambiguities can be resolved by the judicious placement of additional antennas to form a sparsely filled array. This is an important issue and will be discussed in more detail in Section 2.3. At this time the discussion will focus on the estimation performance of the simple interferometer due to phase measurement errors that arise as a result of the presence of receiver noise, hardware imperfections and multipath. In the next subsections the basic design equation will be derived which accounts for these errors in a quantitative way and illuminates the hardware design tradeoffs that are possible.

2.1.1 Front End Noise Analysis

In practice the mixer preamplifiers in the front end of each of the channels introduce a noise component, which, through the action of the limiters preceding the phase detectors, results in a noise component being added to the phase term in (2-1). This noise term places a fundamental limitation on the accuracy with which the elevation angle can be estimated. Using the Cramer-Rao bounding technique [8], it can be shown that this performance limitation for a two-antenna array is given by

$$\sigma_l = (2\pi \frac{D}{\lambda})^{-1} \text{SNR}^{-1/2} \qquad (2\text{-}4)$$

where σ_l refers to the rms error in the estimate of the direction cosine, and SNR denotes the signal-to-noise ratio at the input to the mixer preamplifier. The rms error in the elevation angle estimate is therefore

$$\sigma_e = \sigma_l / \cos e \qquad (2\text{-}5)$$

which, of course, for small e is essentially the same as (2-4). Clearly, the estimation error can be made small by either increasing the separation of the antenna pair or by increasing the SNR.

For typical applications, the signal-to-noise ratio has been conservatively estimated to be 25 dB for an aircraft at 20 mi as can be seen from the power budget itemized in Table 1. As a ground rule it was reasonable to work with a 100-watt aircraft transponder giving an effective radiated power (ERP) of 20 dB relative to 1 watt. For almost all terminal area applications, aircraft will enter the system no farther than 20 miles in range which yields a path loss of -126 dB. The ground antennas are modest dipole array antennas which cover an azimuth-elevation sector 120° x 40°, having a peak gain of 13 dB. Approximately 4-1/2 feet of vertical aperture are used to obtain a sharp lower edge cutoff of the antenna pattern for obtaining some discrimination against ground reflection multipath. Since it may be necessary to monitor the target aircraft at elevation angles as low as 1°, there is a 9-dB loss in power due to this sharp rolloff of the antenna pattern (it is not possible to obtain a peak gain at 1° and a sharp

TABLE 1

POWER BUDGET FOR PALM ELEVATION

Aircraft ERP	20 dBW	100 Watts
Path Loss	-123 dB	20-Mile Range
Antenna Gain (Peak)	13 dB	120° by 40° Coverage Sector
Loss at 1° Elevation	-9 dB	
Loss at Beam Edge	-3 dB	60° Off Boresight
Multipath Fading	-5 dB	7.2-dB Antenna Rolloff
Integration Time	-67 dB sec	200 nsec
Noise Power Density	-199 dBW/Hz	1000° K Noise Temperature
E/N_o	25 dB	
Required E/N_o for 1-mrad Accuracy	16 dB	For $\frac{d}{\lambda} = 25.5$
Single-Pulse Margin	9 dB	0 dB at 55 Miles
Gain from Averaging Over Separate Pulses of a Reply	9 dB	8 Pulses Present on the Average

cutoff to eliminate multipath simultaneously). Furthermore since coverage extends to ±60° about the azimuth boresight, another 3-dB loss must be anticipated for a target aircraft at the 3-dB beam edge. For an aircraft at 1° in elevation, flat earth ground reflection multipath could give rise to a signal at -1°. Although attenuated by the cutoff of the vertical antenna pattern, this signal, if added out of phase to the direct signal, could reduce the incident signal power by another 5 dB. In order to eliminate multipath signals due to buildings, hills, and other aircraft that may be in the coverage region, only 0.2 μsec of the 0.45-μsec pulse is integrated in the receiver. Since the received energy is the power times the time duration, then the factor, $10 \log 0.2 \times 10^{-6} = -67$ dB, accounts for the associated energy loss. The noise power density, N_o, is -199 dBw/Hz corresponding to a receiver with an effective temperature of 1000°K. The signal-to-noise ratio, E/N_o, is therefore found to be at least 25 dB. For an antenna pair spaced 25.5 wavelengths apart (the choice for the experimental system), the SNR needed for a 1-milliradian accuracy is 16 dB. This would permit a 9-dB design margin that may be used up by other interference sources, such as phase measurement hardware errors, multipath, fruit, etc. Higher accuracy or increased margin could be achieved by averaging the angle estimates for separate pulses within an ATCRBS reply. For example, using the 8 pulses present on the average would provide an additional 9 dB of margin.

2.1.2 Instrumental Errors

Hardware errors manifest themselves as phase measurement errors due to the fact that the phase detector characteristics are not perfectly sinusoidal and cannot be completely accounted for using calibration tables. Furthermore, imperfectly cut cable lengths and temporal variations in receiver

characteristics also result in drifts that are difficult to completely eliminate. It is estimated (Section 3) that the rms error of the combination of these effects corresponds to an electrical phase measurement error of 3°. Since

$$\phi = 2\pi \frac{D}{\lambda} \sin e \tag{2-6}$$

then

$$\sigma_2 = \left(2\pi \frac{D}{\lambda}\right)^{-1} \sigma_\phi \tag{2-7}$$

where σ_2 is the corresponding error in the estimate of the direction cosine, and σ_ϕ is the rms phase measurement error which we estimate to be 3°.

2.1.3 Multipath Errors

The final source of error that we shall consider is due to ground multipath. It has been shown [9] that multipath will produce a phase measurement error given by

$$\delta\phi = \tan^{-1}\left(\frac{\rho \sin \theta_1}{1 + \rho \cos \theta_1}\right) - \tan^{-1}\left(\frac{\sin \theta_2}{1 + \rho \cos \theta_2}\right) \tag{2-8}$$

where ρ is the ratio of the multipath to direct signal level measured at the output of the antennas, and θ_i is the phase of the multipath relative to the direct signal at the i^{th} antenna. Considering a worst case for θ_1 and θ_2*, we get

$$\delta\phi = 2 \sin^{-1} \rho \tag{2-9}$$

*This is $\theta_1 = \cos^{-1}\rho$ and $\theta_2 = \pm \cos^{-1}\rho$.

Since our previous error expressions have been in terms of rms values, introducing the worst case multipath error may result in an overly pessimistic design, especially since the worst case values of θ_i are not $\pm\pi$. If instead we assume that the θ_i are independent random variables uniformly distributed over $(-\pi,\pi)$, we find that

$$\overline{\delta\phi} = 0$$

$$\overline{\delta\phi^2} \approx \rho^2 \quad \text{to terms in } \rho^4 \tag{2-10}$$

Using σ_3 to denote the corresponding (rms) error in the elevation angle direction cosine, and applying (2-6) we see that*

$$\sigma_3 = \left(2\pi \frac{D}{\lambda}\right)^{-1} \rho \tag{2-11}$$

2.1.4 The Sensor Design Equation

Since the errors due to noise, hardware imperfections and multipath are independent, they can be added in an rms sense to give the total error design equation. Therefore, combining (2-4), (2-7) and (2-11), this equation becomes

$$\begin{aligned} \sigma_{\sin e} &= \left[\sigma_1^2 + \sigma_2^2 + \sigma_3^2\right]^{1/2} \\ &= \left(2\pi \frac{D}{\lambda}\right)^{-1}\left[\frac{1}{SNR} + \sigma_\phi^2 + \rho^2\right]^{1/2} \end{aligned} \tag{2-12}$$

In Fig. 3 we use (2-12) to plot the 1-sigma error in the estimate of sin e as a function of the multipath level for the following parameters:

*For small values of ρ, the rms error is half the peak error.

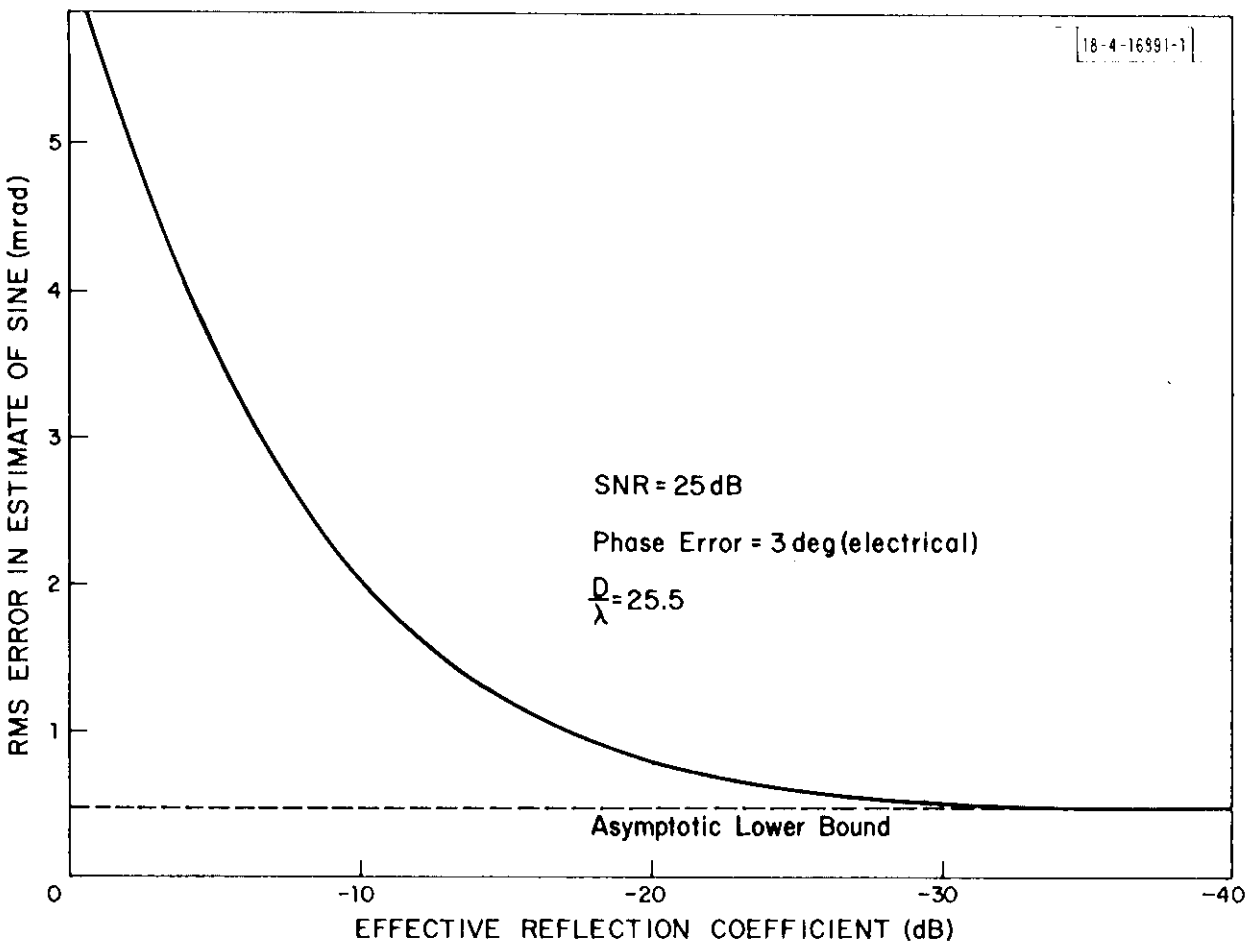

Fig. 3. Theoretical error performance of PALM interferometer.

σ_ϕ = 52 milliradians (3° electrical)

SNR = 316 (25 dB)

D/λ = 25.5

It can be seen that for multipath levels less than 30 dB, the accuracy is limited by the hardware errors in the phase measurement channels. It is also clear from this figure that multipath begins to dominate the performance even at levels as low as 20 dB relative to the direct signal. It is this fact that demands a very careful consideration of multipath effects. Certain hardware design and signal processing options that reduce the effective multipath level are discussed in the next section.

2.2 PALM Multipath Suppression Techniques

In this section we present some of the methods by which the PALM sensor reduces the multipath induced errors to acceptably low levels. In Fig. 4 we summarize the multipath suppression techniques used in the PALM system. The greatest threat to successful PALM operation is ground reflection multipath. This is primarily attacked by using antennas which roll off rapidly at the horizon, as described in Section 2.2.1.

Additionally, there are potential reflections from vertical surfaces such as hangars, aircraft, etc., which can cause significant errors because they are at positive elevation angles and hence not subject to pattern rolloff. The prime mechanism for rejecting these multipath signals is time discrimination. This technique will be discussed in Section 2.2.2. For aircraft on final approach, the rolloff in the gain at wide azimuths also helps reject multipath signals of this type.

The hard limiter capture effect implicit in phase only processing provides an additional direct signal enhancement which is of considerable aid for the resolution of ambiguities. This issue will be discussed in Section 2.3 where the ambiguity issue is treated in detail.

In certain situations, e.g., very low elevation angles (under 2°), the multipath rejection provided by the features discussed above may be inadequate. In such cases, additional rejection can be achieved by "optimally" estimating the elevation angle from all the sensor measurements considered together [as opposed to estimation based only on the (ambiguity resolved) phase between the sensors with widest spacing]. An algorithm based on phase data alone is discussed in Section 2.4.

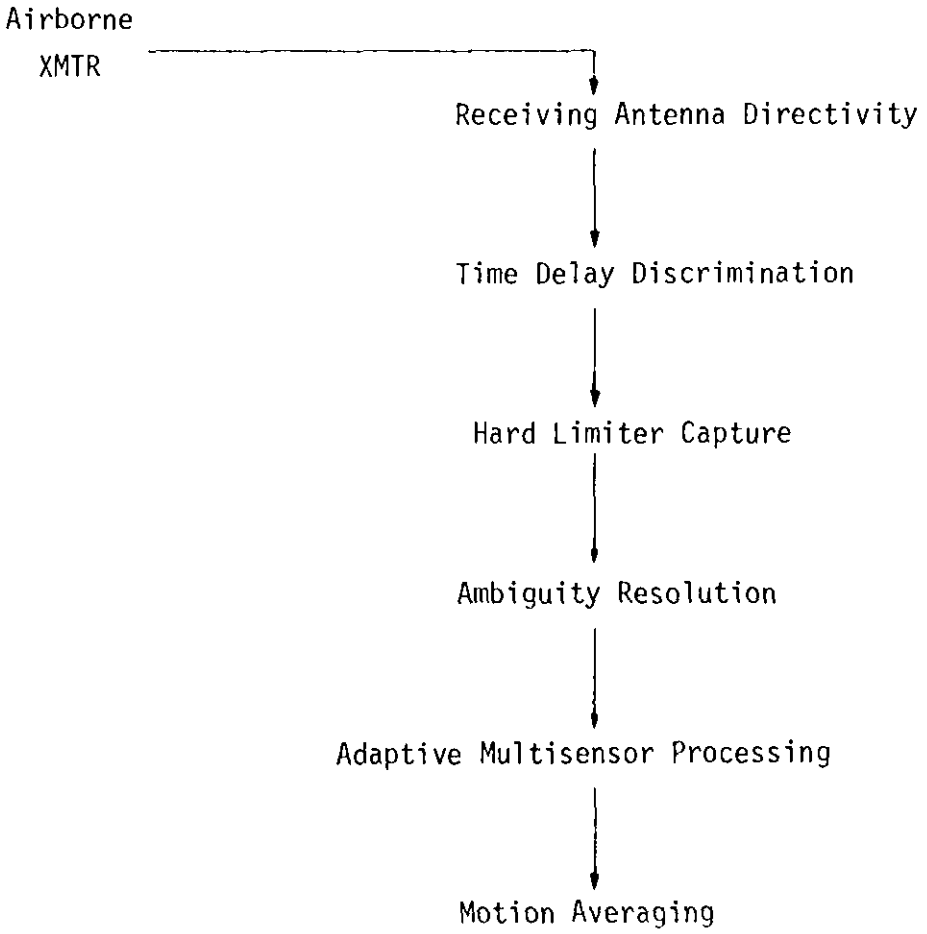

Fig. 4. PALM multipath suppression features.

It is well known that the multipath errors oscillate in sign along the flight path due to the varying rf phase difference between the direct and reflected signals. Consequently, when the PALM measurement rate is higher than the required data rate, there exists the opportunity to reduce the multipath error by averaging several measurements together. In Section 2.2.3, we indicate situations in which this motion averaging scheme provides a substantial improvement in the reduction of the multipath related errors.

2.2.1 Ground Reflection Multipath Suppression Via Sensor Elevation Pattern Shaping

Ground reflection multipath is a prime threat for any L-band elevation sensor due to its omnipresence and the physical difficulties in utilizing large apertures (e.g., 120 λ). Indeed, many interferometer systems conceived in the past have failed due to poor ground reflection multipath rejection [9,10]. The prime mechanism by which this rejection is accomplished in the PALM system is the use of sensors whose antennas have elevation patterns that roll off rapidly at the horizon.

In order to estimate the extent to which the sensor antennas must be designed to reject multipath, it is necessary to examine typical ground reflection multipath levels that are likely to arise in practice. In Fig. 5 we have plotted the reflection coefficient for flat dry land for vertical polarization at L-band that would be measured at the antenna input. It is clear that the multipath levels can be quite high in the regions of interest; hence, a significant amount of multipath rejection will have to be achieved by proper design of the vertical antenna patterns.

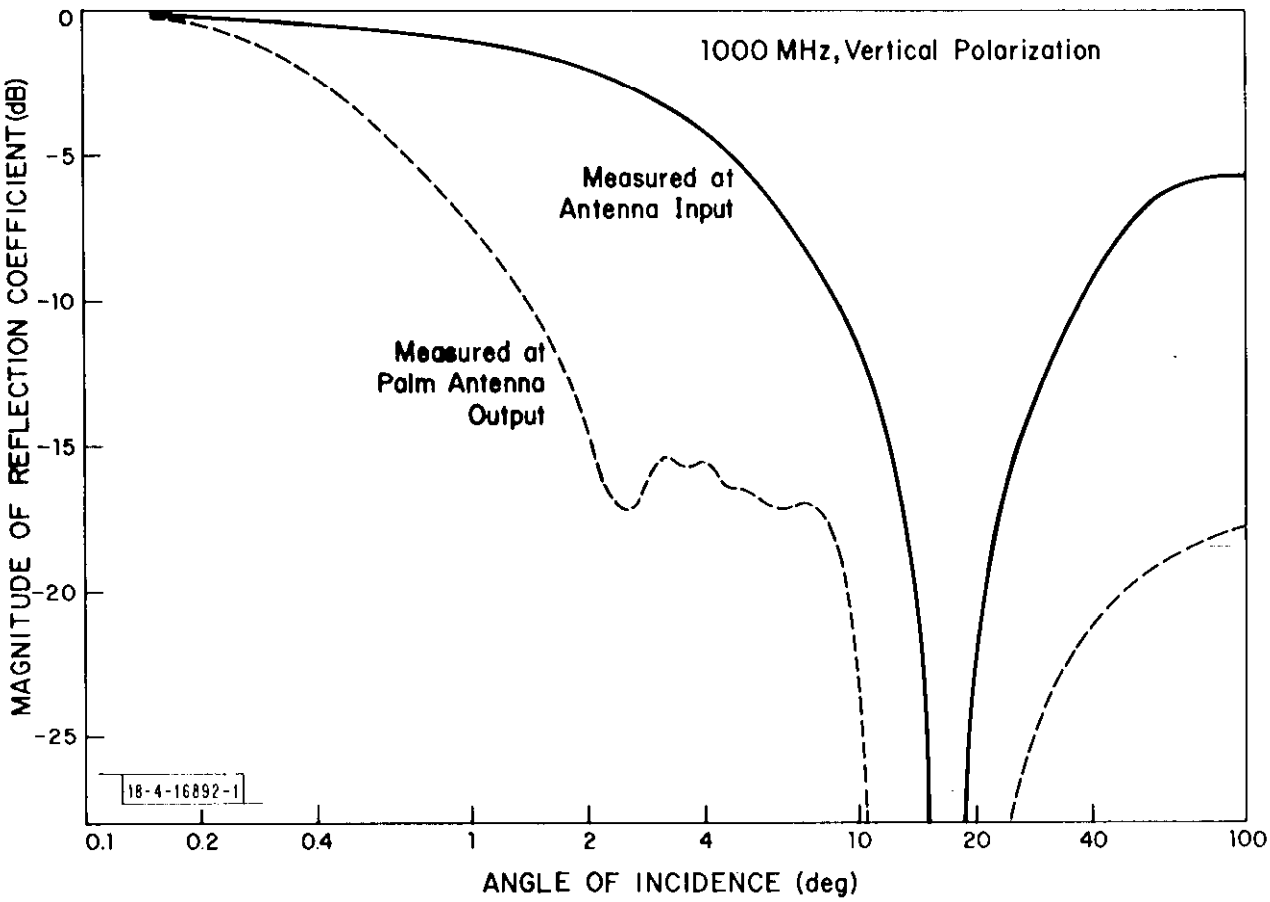

Fig. 5. Reflection coefficient for smooth, flat, dry land versus angle of incidence.

Computing the magnitude of the ratio of the multipath to direct signal levels for an individual antenna requires specification of both the beam pattern and the beam tilt. This ratio was computed for a variety of vertical apertures and tilt parameter values. The study showed that a reasonable reduction in multipath level could be achieved using a 4-ft aperture antenna. A new antenna synthesis procedure was developed to obtain an antenna pattern having a rapid rolloff in gain about the horizon subject to constraints on the sidelobe level and mainbeam ripple [12]. The procedure is based on techniques which have recently been successful in the design of finite impulse response digital filters. Its importance to the current problem is in the fact that the 4-ft aperture is being used optimally with regard to multipath discrimination.

The efficacy of the method is demonstrated in Fig. 6 which compares the measured gain of the PALM antenna with that of the ESCAN and DABSEF antennas. Even though the PALM aperture is half that of the other antennas, its rolloff around the indicated horizon* is nearly as sharp as the other two. In comparison the PALM antenna pattern exhibits a higher sidelobe level; however, this should cause no significant problems for the PALM application.

A theoretical prediction of the rms error in the elevation angle estimate when this antenna is used can be computed in the following way. For an elevation angle e, we can find the multipath reflection coefficient for dry land, for example, from Fig. 5. If the value so determined in $\rho(e)$, then at the

*The ESCAN and DABSEF antennas are normally pointed so that the horizon appears 5 to 6 dB down from the first peak.

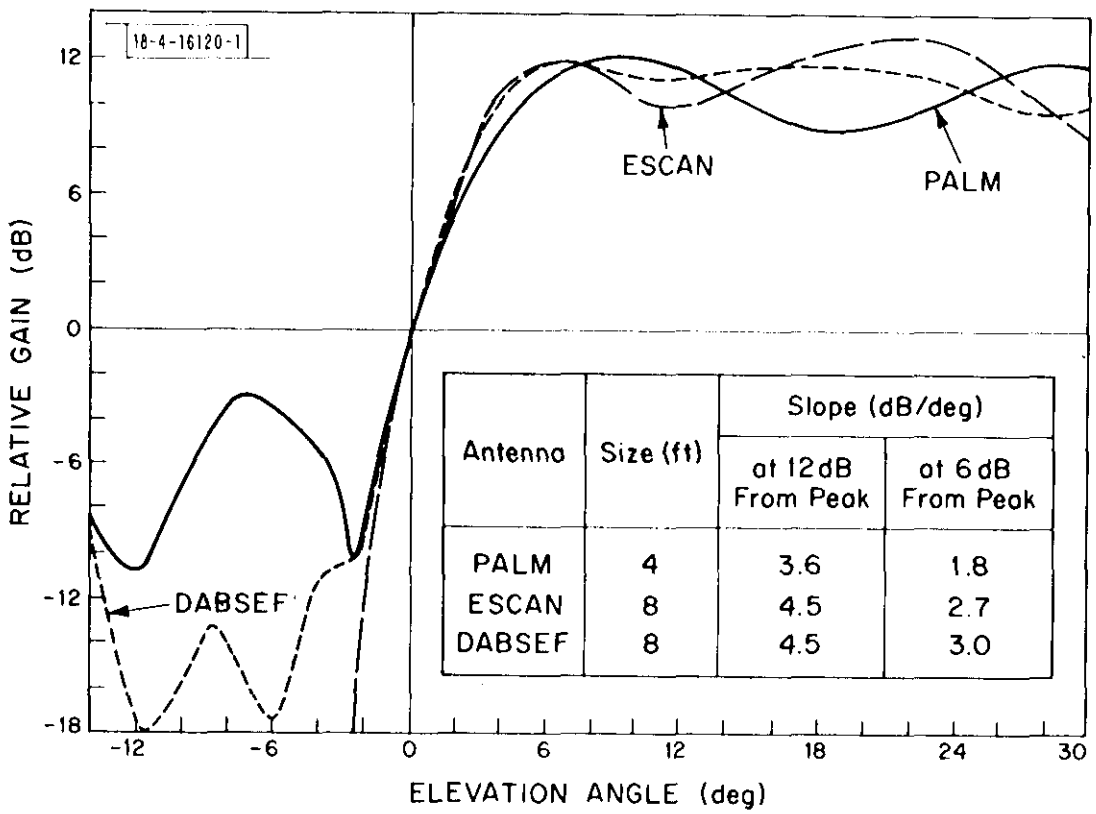

Antenna	Size (ft)	Slope (dB/deg)	
		at 12 dB From Peak	at 6 dB From Peak
PALM	4	3.6	1.8
ESCAN	8	4.5	2.7
DABSEF	8	4.5	3.0

Fig. 6. Measured antenna patterns at 1090 MHz.

output of the antenna its value will be $\rho_{eff}(e) = \rho(e)[G(e)/G(-e)]$, where G(e), G(-e) represent the attenuations of the direct and multipath signals due to the PALM antenna.* Values of G(±e) can be obtained from Fig. 6. They were combined with the results of Fig. 5 for the dry land case and used to compute ρ_{eff} which is also plotted in Fig. 5 for comparison. The effect of the antenna is, of course, quite significant. The resulting value for $\rho_{eff}(e)$ is then used in (2-12) to compute $\sigma_{sine}(e)$ which can be normalized by cos e to give the desired rms error $\sigma(e)$. Using this procedure the rms error versus elevation angle was plotted in Fig. 7 for the case of reflections due to dry land. The results for fresh snow were also computed but were not found to be significantly larger, hence we take these results as indicative of what our experimental performance can be expected to be in most cases of practical interest.

It should be noted that the approximately 1-milliradian constant performance versus elevation angle for the 2.5-to 10-degree elevation angle sector is due to the presence of the first sidelobe in the PALM antenna pattern as shown in Fig. 6. Significantly improved performance in this region can be achieved by designing for a lower sidelobe level by using an equiripple approximation to a cosec-squared pattern which will give better sidelobe performance without sacrificing SNR at 1° or the slope at the horizon. The rapid rolloff at the horizon is the essential factor in the suppression of ground reflection multipath.

---

*For a direct signal at angle e, the multipath reflection from a flat earth will be at angle -e.

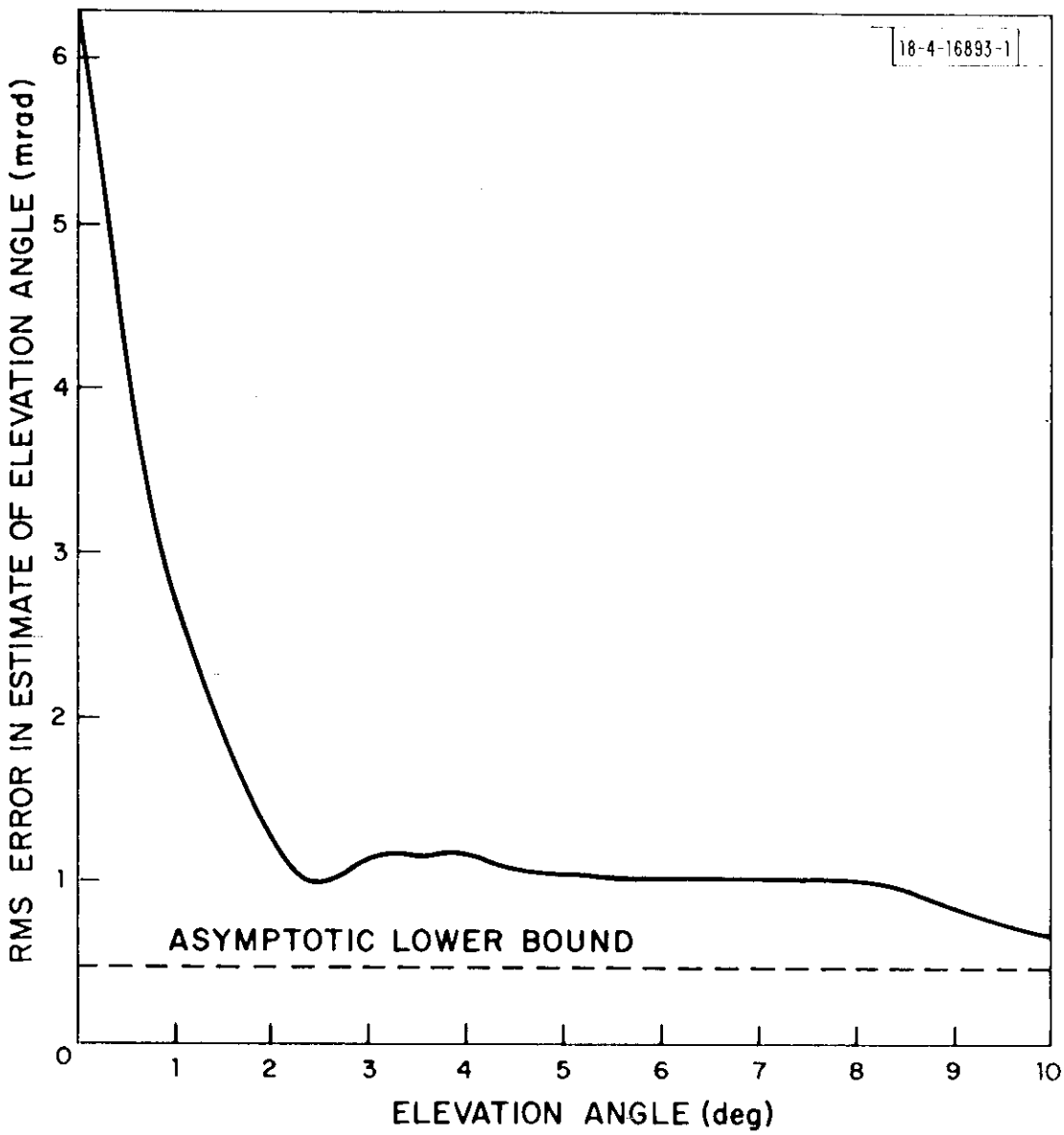

Fig. 7. Rms error versus elevation angle for flat, smooth, dry ground.

The predicted rms error of Fig. 3 presupposed a 25-dB signal to noise, corresponding to an aircraft at a 20-mile range. At the decision height ($\leq$ 200-ft altitude), there would be a considerably higher signal-to-noise ratio and, hence, an error even lower than that predicted in Fig. 7.

2.2.2 Multipath Reduction Via Time Delay Discrimination

Multipath components, which arrive after the PALM array has made its phase and amplitude measurements on a given reply pulse, cause no errors in the aircraft position determination irrespective of the angular position of the scatterer or magnitude of the multipath. In this section, we quantify the improvement afforded by this time delay discrimination. We shall see that this represents quite a powerful tool in avoiding the hangar wall elevation multipath which has been identified as a prime threat to microwave landing system (MLS) operation.

If the PALM phase and amplitude measurement are made T_M seconds after the arrival of a pulse*, one need be concerned only with multipath scatterers lying within the prolate spheroid whose

1. Focal points are the aircraft and PALM array, respectively
2. Major axis, a, is $(T_M + D/c)/2$ where D is the distance of aircraft from PALM array, and c is the velocity of light
3. Minor axis, b, is approximately $\sqrt{T_M D/2c}$

The surface region encompassed by this spheroid can be overbounded by assuming the aircraft and PALM array are at zero height, and plotting the resulting ellipse on an airport plan view.

In Fig. 8, we plot this upper bound for two cases at runway 13L at JFK airport. The two cases are:

1. Aircraft at middle marker ($\simeq$ 200 ft height)
2. Aircraft on centerline at an infinite distance

*Measured, for example, from the 10% point on the leading edge of the arriving pulse.

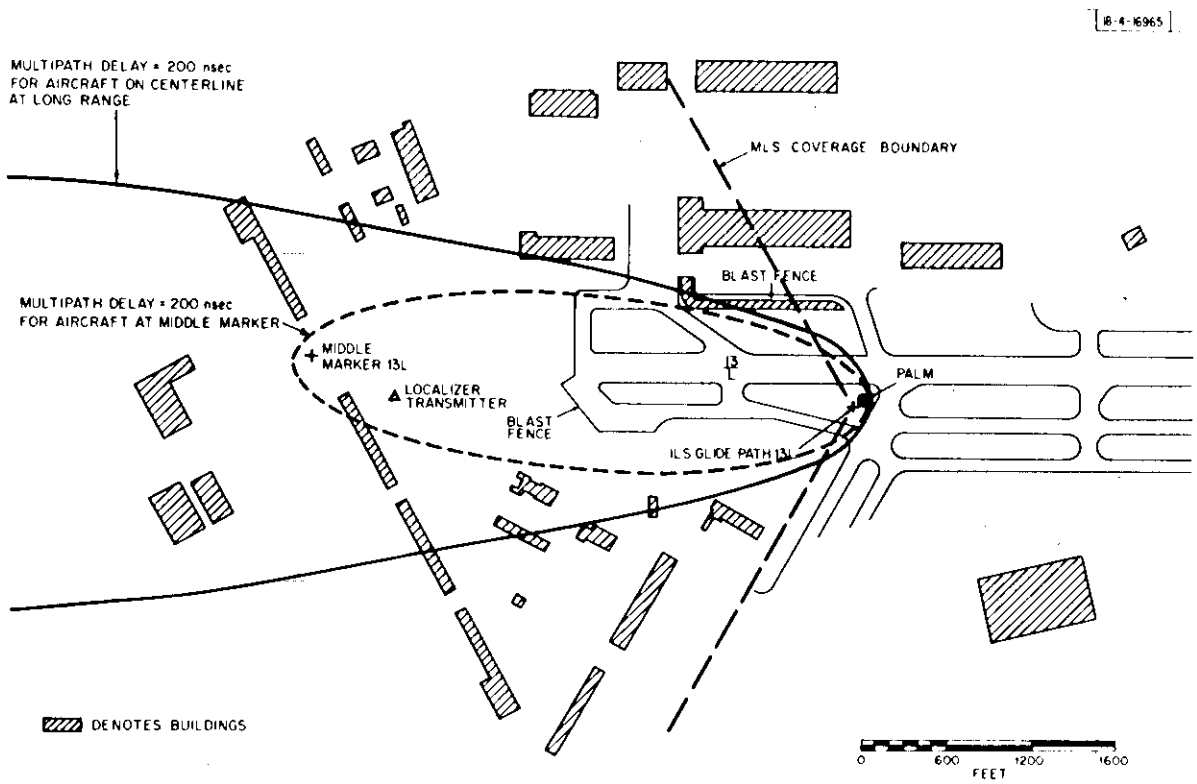

Fig. 8. Time delay discrimination at JFK runway 13L.

The latter curve represents an upper bound on the region in which multipath scatterers will produce signals that will arrive before the PALM sampling time T_M for an aircraft on centerline. Also shown in Fig. 8 are the coverage limits proposed for the MLS elevation function [6].

Both of the principal techniques under consideration (Doppler and Scanning Beam) for the next generation MLS radiate elevation signals which are, in effect, narrow in the elevation plane (e.g., 1°) and very wide in the azimuth plane. Consequently, any vertical structure within the azimuthal coverage region which subtends a vertical angle within 1° to 2° of the glide slope (e.g., an elevation angle $\geq$ 1° for a 2.86° glide slope), represents a threat to successful MLS elevation system operation. Since the MLS techniques essentially have no time delay discrimination, they must rely on aircraft motion effects and/or azimuthal pattern shaping to achieve adequate elevation performance [13,14].

The receiving antenna patterns synthesized by the experimental PALM array are similar to those of the MLS arrays in that they are narrow in elevation and wide in azimuth, and thus one might think PALM is subject to the same hangar multipath problems. However, Fig. 8 shows that virtually all the buildings which might be a threat to MLS at runway 13L are not threats for PALM due to the PALM time delay discrimination.

Although concrete airport examples such as Fig. 8 are instructive, they are possibly misleading in that:

1. Many buildings that might in fact appear to be problems are not because their orientation is such that no significant multipath would be generated in practice.

2. Future construction might yield much higher buildings or buildings that are closer to the runway.

Thus, it is useful to also consider what is possible "theoretically" if buildings adhering to the current obstruction clearance criteria are constructed at arbitrary orientations. Such a treatment of building multipath threats was studied by S. Sussman of Lincoln Laboratory in connection with the assessment of multipath effects on MLS performance.

In Fig. 9 we show the locus of potential hangar threats together with the ellipses corresponding to a multipath delay of 200 nsec which corresponds to the PALM sampling time after leading edge detection. This locus of potential hangar threats are those locations at which a hangar meeting the FAA obstruction clearance criteria* (with appropriate orientation) could generate vertical surface specular multipath for the given aircraft and PALM locations. We see that the PALM delay discrimination eliminates virtually all of the hangar elevation multipath threats for an aircraft on centerline.

An interesting feature of the PALM time delay discrimination is its "self-focusing" property when the target aircraft is off centerline as illustrated in Fig. 10. At many airports, the hangars most likely to cause multipath are parallel to the runway centerline. Consequently, the time delay discrimination is very effective at eliminating hangar multipath for aircraft far off the runway centerline. By contrast, the pattern control (or "centerline emphasis") used to mitigate hangar multipath for MLS systems [13] is generally ineffective (and, in some cases, actually detrimental) when the aircraft is not on centerline.

---

*FAA circular No. AC-150 [11] sets a height limit of 150 ft within 13,000 ft of airport center. Within 500 ft of runway centerline, there are to be no buildings (other than navaids, etc.). A transition surface begins at 500 ft and rises in the ratio of at least 1 to 7 with distance until the 150-ft height is reached.

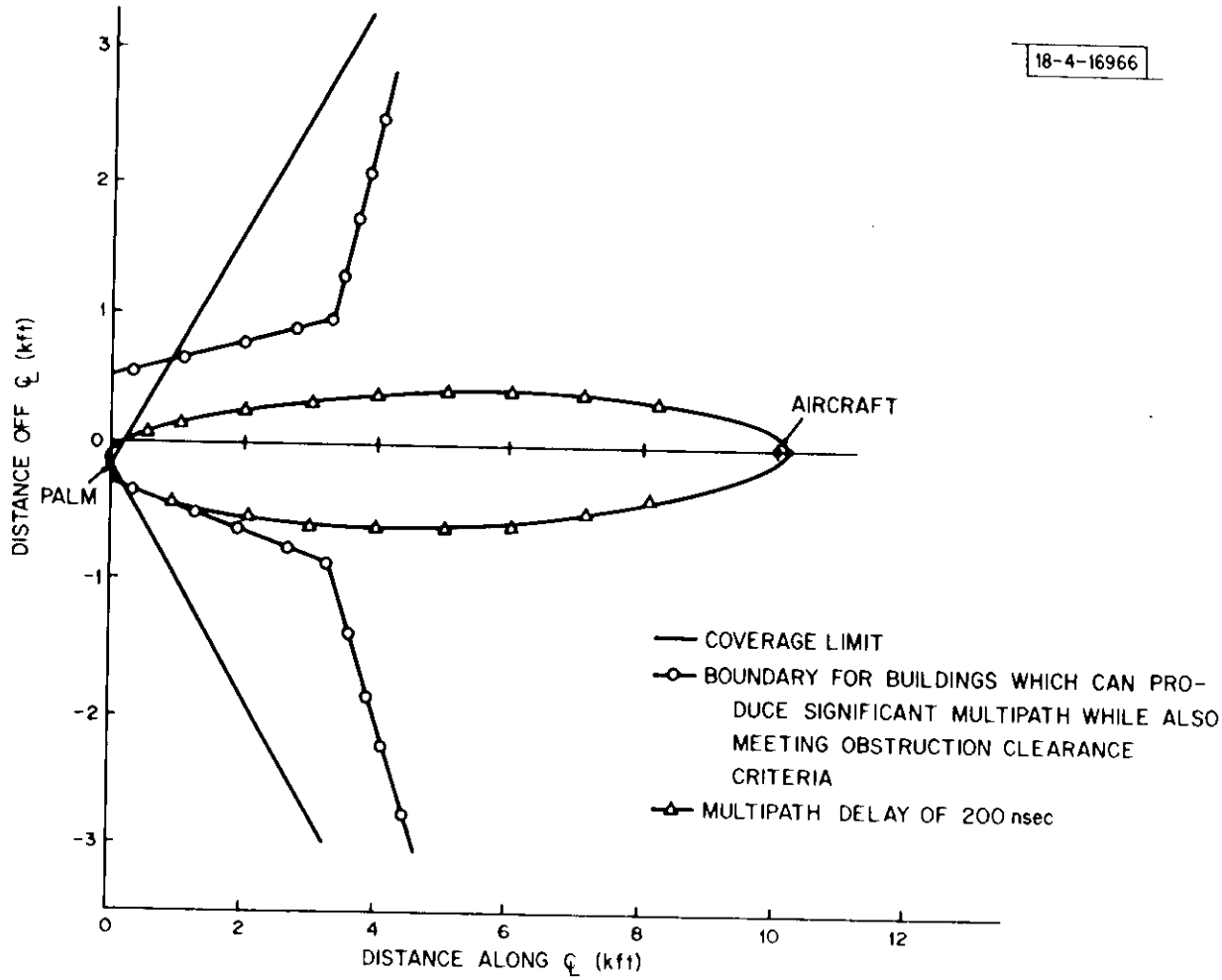

PALM time delay discrimination against theoretically possible hangar elevation multipath threats.

Fig. 9(a) Aircraft at 500-ft altitude on 2.86° glide slope.

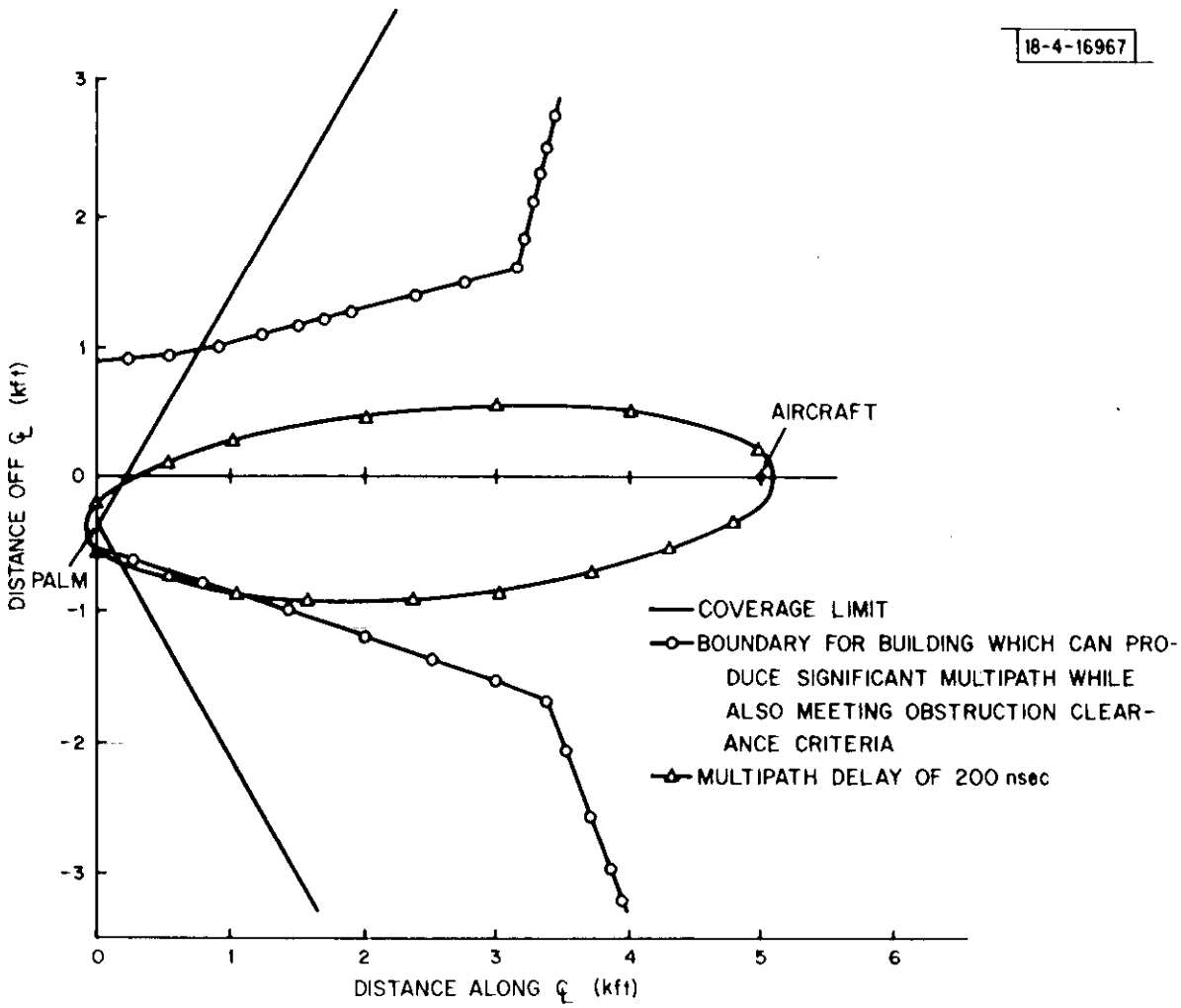

PALM time delay discrimination against theoretically possible hangar elevation multipath threats.

Fig. 9(b) Aircraft at 250-ft altitude on 2.86° glide slope.

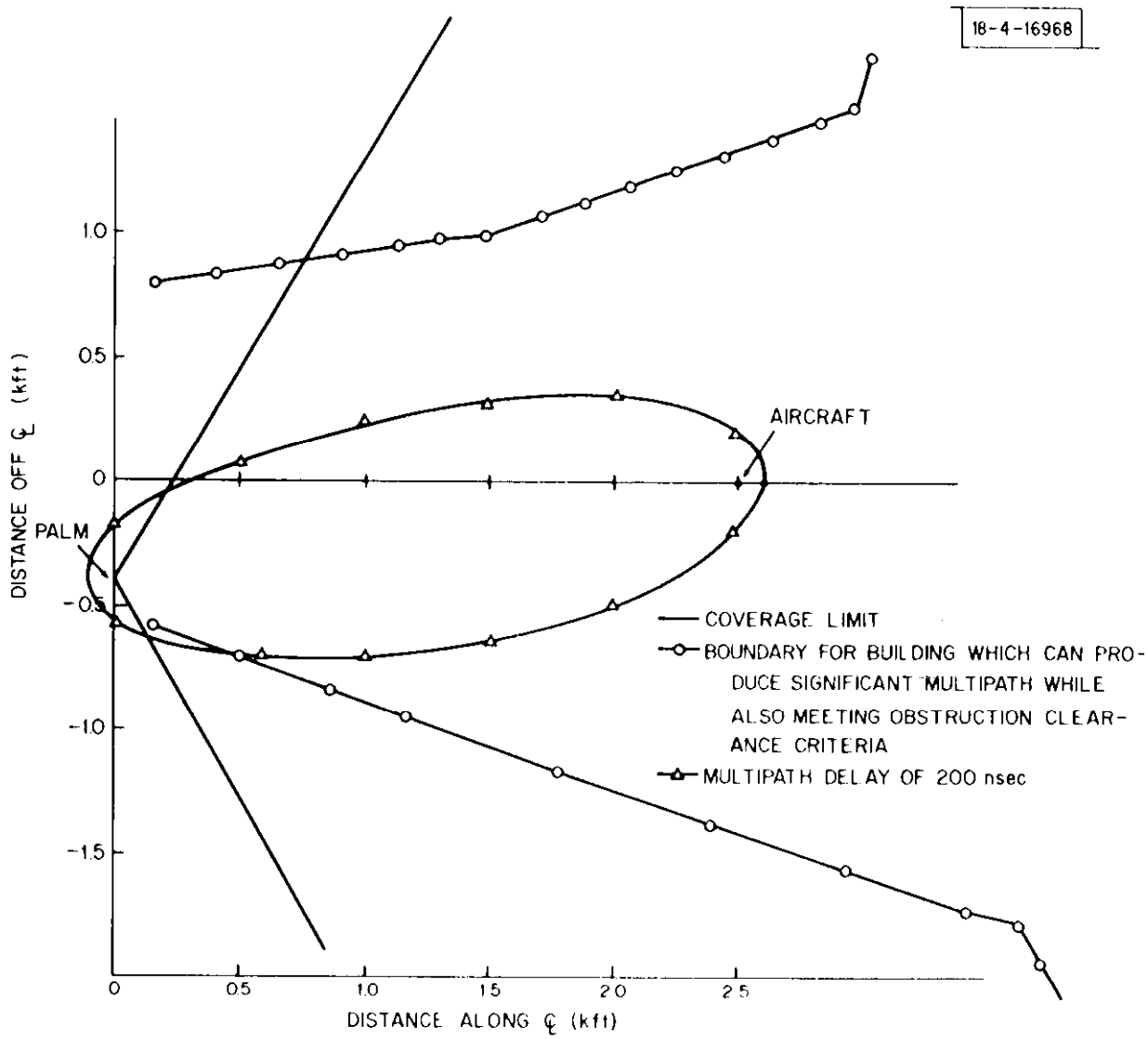

PALM time delay discrimination against theoretically possible hangar elevation multipath threats.

Fig. 9(c) Aircraft at 125-ft altitude on 2.86° glide slope.

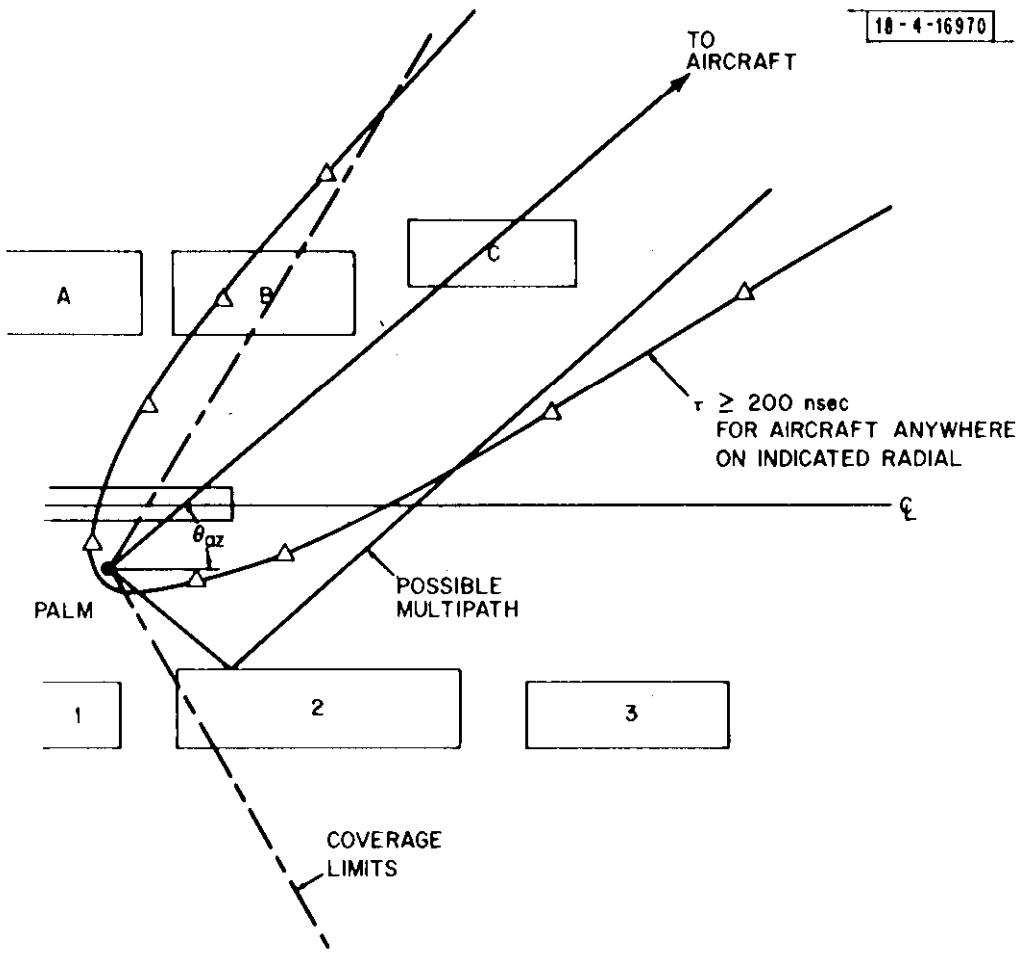

NOTE: WALLS OF BUILDINGS A-C ARE NOT ORIENTED TO YIELD MULTIPATH FOR INDICATED AZIMUTH (although they could yield shadowing.)

SITUATION REVERSES FOR AIRCRAFT ON OTHER SIDE OF CENTERLINE. ($\theta_{az}<0$)

Fig. 10. PALM time delay discrimination against parallel hangar threat for aircraft not on centerline.

2.2.3 PALM Multipath Error Reduction Via Motion Averaging

One possibility for reduction of errors that are due to multipath is the averaging of a number of measurement samples. This method can be used if two conditions prevail:

1. The measurement rate must be sufficiently high to permit accumulation of numerous samples for averaging such that the averaged data is provided at the required system update rate.
2. The errors encountered in the series of measurements must not be the same from sample to sample, but must vary either randomly or cyclically.

The first condition is met for the PALM system because the average interrogation rate for aircraft on final approach is 2 to 5 times that which is probably required.* The second condition can be met if the moving aircraft transponder produces different closing velocities along the paths of the direct and reflected signal. This difference in closing velocities causes a progressive phase variation between the direct and reflected signals received at the PALM sensor [i.e., the quantities θ_1 and θ_2 in Eq. (2-8) will change]. The nature of the PALM processing is such that this progressive phase change causes the error to vary cyclically, thus permitting the error to be reduced by averaging. Since the resultant error reduction is a result of aircraft motion, the effect is called "error reduction by motion averaging" and has been studied at great length in the MLS context (see, e.g., Appendix H of [14]).

In Fig. 11, we illustrate how the error varies along the flight path as the aircraft moves through the hyperbolic interference pattern that exists

*For autopilot coupled landing service, 5 Hz is evidently adequate [6] while 1 Hz is needed for surveillance and cross pointer displays.

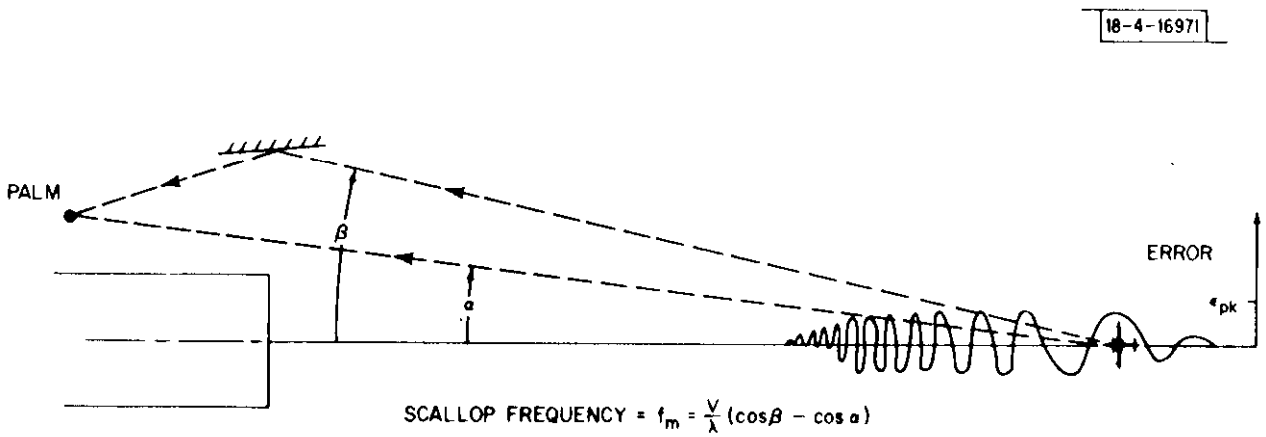

Fig. 11. Cyclical nature of error in bearing measurement due to multipath.

between the PALM array and its image in the multipath reflector. The amount of averaging improvement obtained in a given situation depends on:

1. The number and location in time of the position measurements that are averaged
2. The rate of error cycling (i.e., the motion frequency f_m).

By straightforward geometry, the motion frequency is given by

$$f_m = \frac{v}{\lambda} (\cos \beta - \cos \alpha) \qquad (2\text{-}13)$$

$$= 221 (\cos \beta - \cos \alpha) \quad \text{Hz}$$

for v = 200 ft/sec (120 knots) where α and β are the angles of PALM and its image with respect to the aircraft velocity vector. The error is not purely sinusoidal in Fig. 11 or in practice because α and β increase as the aircraft approaches the runway.

There are a number of options for the PALM measurement format. If the measurements are made uniformly in time, the averaged error is related to the measurement error by

$$e_a \leq A_f \; e_m \qquad (2\text{-}14)$$

where

$$A_f \triangleq \text{averaging factor} = |(\sin M\pi f_m T)/(M \sin \pi f_m T)| \qquad (2\text{-}15)$$

M = number of replies averaged

T = spacing between replies ($\approx$0.1 second)

e_m = rms error on single reply

e_a = rms error of averaged replies

This particular interrogation format yields "grating lobes" at f_m values which are multiples of 1/T. However, these may be essentially eliminated by using a jittered interrogation timing (as is done to avoid "blind" velocities in MTI radar). By doing this, one would achieve an averaging factor of

$$A_f \approx \begin{cases} \dfrac{\sin M \pi f_m T}{M \sin \pi f_m T} & f_m < 1/MT \\ \dfrac{1}{\sqrt{M}} & f_m > 1/MT \end{cases} \qquad (2\text{-}16)$$

In Fig. 12, we plot the averaging factors of (2-15) and (2-16) for M = 10.

We see that PALM should achieve a substantial multipath error reduction when $f_m > 1$ Hz. Using (2-13), one can determine the geometric region over which this should be advantageous. Two examples of this are shown in Fig. 13. In these cases, it is assumed that the aircraft velocity heading will vary ±1° about centerline. We see that motion averaging is primarily effective as the aircraft nears threshold (e.g., at the category II decision height). In this region, it provides a very high rejection (≈10 dB) against reflections from aircraft on taxiways.

Fortunately, when the landing aircraft is not near threshold, the reflections from aircraft on taxiways will be sharply reduced due to the very small glancing angle of incidence needed to yield specular reflections. To illustrate, we find in Fig. 13 that the angle of incidence would generally be less than 10°. For tailfins in this situation, the level is $\approx K\sqrt{\sin \theta_i}$, where

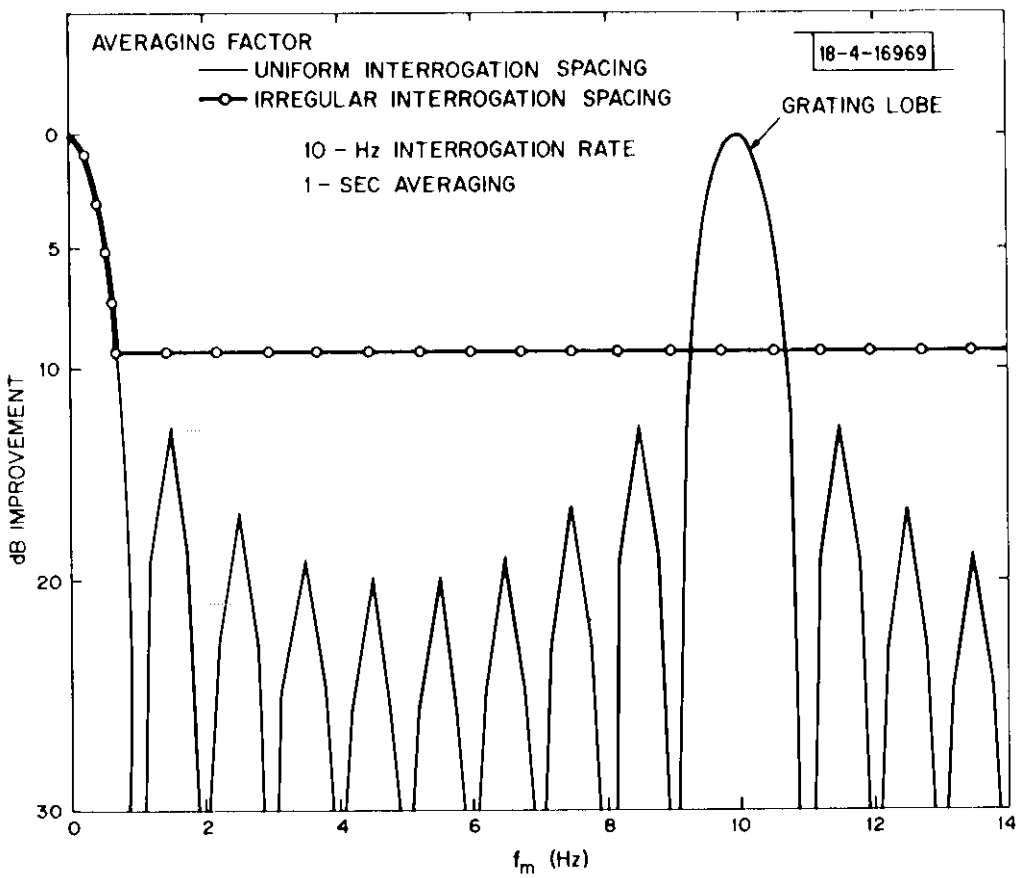

Fig. 12. PALM motion averaging factor.

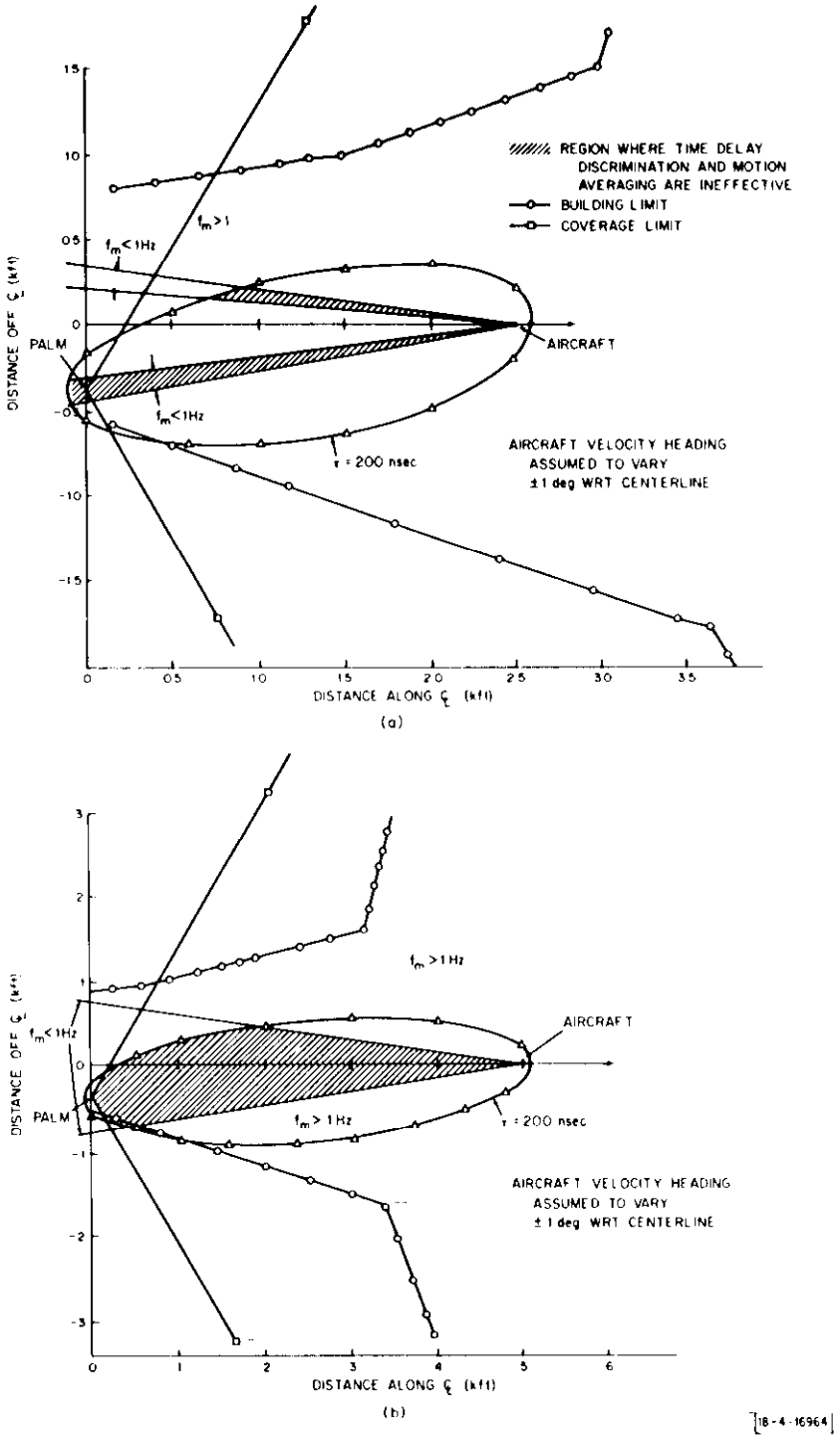

Fig. 13. Time delay discrimination combined with motion averaging for PALM elevation sensor.

$K \approx 0.26$, and θ_i is the angle of incidence, so that the oblique angle of incidence provides a multipath reduction of approximately 8 dB. Since the tailfin level was already 12 dB down, this 8-dB factor should reduce the tailfin multipath to the 20-dB level, and hence, virtually eliminate it as a threat.

2.3 Ambiguity Resolution

So far the design of the PALM sensor has been concerned only with the proper choice of the end-pair spacing of the basic interferometer. However, the angle estimate is being derived from the relation

$$\sin e = \frac{\phi}{2\pi\ D/\lambda} \tag{2-17}$$

where the phase angle is measured by a phase detector modulo 2π. Therefore unambiguous angle estimates are possible only if the range of elevation angle is always less than $\sin^{-1} \lambda/D$. We have already found that reasonable performance can be obtained only if the end pair is spaced by at least 25.5 wavelengths. This would restrict coverage to a 2.25° region, which, for the PALM application, is inadequate. Coverage over a wider region can be obtained, of course, by reducing the end-pair spacing, but this would result in an estimate having a larger rms error than was desired. It is possible, however, to use the poorer estimate to restrict the size of the unambiguous region and hence bootstrap to a larger end-pair spacing for which the estimate will be more accurate. The basic idea is illustrated in Fig. 14 which shows the equivalent antenna pattern for two interferometers of different spacing. It is clear that the closer pair, having a wider beamwidth, would give a poorer angle estimate but one that was good enough to identify the correct lobe of the narrow beam larger aperture system.

It was found that for the PALM application, 5 antenna elements were needed having spacings 2D, 4D, 6D and 9D, where 9D = 25.5 λ resulting in the spacings 17/3 λ, 34/3 λ, 17 λ, and 25.5 λ. In the remainder of this section an intuitive justification for these choices will be given.

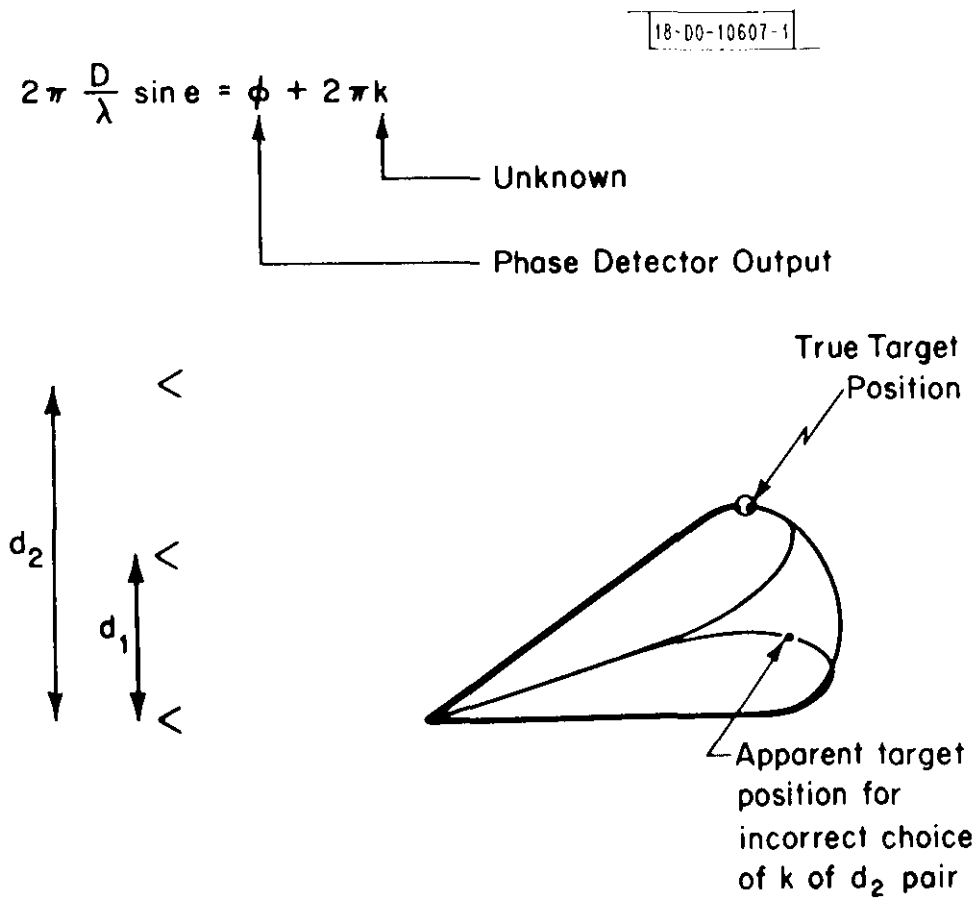

Fig. 14. Ambiguity resolution.

The experimental system was designed to provide ambiguity resolution over a 10° coverage sector.* This is achieved using the 2D-spacing since, from (2-17)

$$\sin^{-1}(1/2D) = \sin^{-1}(3/17) = 10.2° \tag{2-18}$$

If we let σ_o and σ_1 denote the rms error for the 9D-and 2D-end-pair spacings, then from (2-12) it follows that

$$\sigma_1 = \frac{9}{2}\sigma_o \tag{2-19}$$

From Fig. 7 at 1° in elevation, σ_o = 2.7 milliradians or 0.16 degree which means that an estimate made on the smaller end pair will have an rms error of 0.7°. If we let $\hat{e}_1$ denote the angle estimate made using this pair and assume that the error is Gaussianly distributed† about the true elevation angle e, then

$$I_1 = \{e: \ \hat{e}_1 - 3.5\,\sigma_1 \leq e \leq \hat{e}_1 + 3.5\,\sigma_1\} \tag{2-20}$$

represents a 99.95% confidence interval for the true angle value. This has the effect of reducing the unambiguous region of the angle estimate from 10 degrees down to 7 σ_1 degrees, which, since σ_1 = 0.7° at 1° in elevation is 5 degrees wide. From (2-17) it follows that an unambiguous angle estimate

---

*Unambiguous coverage can actually be obtained over a 20° sector by synthetically forming an antenna pair of spacing D by subtracting the phases measured at the 6D-and 2D-antenna pairs from that measured at the 9D-antenna pair (i.e., $\phi_{9D} - \phi_{6D} - \phi_{2D} = \phi_D$).

†This assumption is being made more for pedagogical reasons than technical. It is actually a conservative assumption since multipath errors peak at about the 2-sigma point. The small signal suppression effect of the hard limiters enters in here via the relationship between phase rms error (σ_i) and multipath/direct signal ratio at the input to the mixer.

can be made on this smaller angle interval, provided another antenna is added spaced 4D = 34λ/3 wavelengths from the bottom reference antenna. Using this antenna pair, another angle estimate, denoted $\hat{e}_2$, can be made having an rms error, denoted σ_2, given by

$$\sigma_2 = \frac{9}{4}\ \sigma_o \tag{2-21}$$

which, at 1° in elevation will be 0.36°. Then

$$I_2 = \{e: \hat{e}_2 - 3.5\ \sigma_2 \leq e \leq \hat{e}_2 + 3.5\ \sigma_2\} \tag{2-22}$$

represents another 99.95% confidence interval for the true angle value. Therefore the region of uncertainty in the estimate of e is reduced to an interval of width $7\ \sigma_2 = 2.5°$.

From (2-17), we see that this smaller interval can be unambiguously covered by another antenna pair spaced 6D = 17 wavelengths from the reference antenna. Another angle estimate, $\hat{e}_3$, can be made using this pair whose rms error σ_3 is given by

$$\sigma_3 = \frac{9}{6}\ \sigma_o \tag{2-23}$$

which, at 1° in elevation, is 0.24°. With essentially 100% confidence the true elevation angle will lie somewhere in the interval

$$I_3 = \{e: \hat{e}_3 - 4.7\ \sigma_3 \leq e \leq \hat{e}_3 + 4.7\ \sigma_3\} \tag{2-24}$$

which is an unambiguous region 2.2° wide. This is precisely the unambiguous region that can be covered by the antenna pair having the 9D = 25.5 wavelength separation specified in an earlier section of the report. Hence by using the

bootstrapping technique to locate the smallest unambiguous region and the 25.5 wavelength end-pair spacing, an angle estimate that is unambiguous over the 10° sector can be made with the theoretical rms error shown in Fig. 7 for elevation angles above 1°. The probability that the final estimate will be ambiguous is much less than .1% and becomes even smaller at higher elevation angles. This performance can be achieved using 5 antennas having pair spacings 5.7, 11.3, 22.7 and 25.5 wavelengths relative to the bottom antenna.

2.4 Use of All Sensor Data Simultaneously To Reduce Multipath

From the preceding sections, we conclude that ambiguity resolution should proceed satisfactorily, but that the elevation angle estimates based only on the (ambiguity resolved) end-pair phase measurement will not meet the objective of 1-mrad accuracy for elevation angles above 1 degree due to specular ground reflections. In this section, we discuss an algorithm based on using all the phase measurements simultaneously to "optimally" estimate the aircraft elevation angle.

Our objective here is to take advantage of the cyclic spatial variation in error caused by the specular ground reflections. It is trivial to show (see, e.g., [9] and [10]) that the observed phase difference between antennas at heights h_{ref} and $h_i (h_i > h_{ref})$ above a flat specularly reflecting ground plane is:

$$\Delta\phi\ (h_{ref},h_i) = \frac{2\pi(h_i-h_{ref})}{\lambda}\ \sin e + \tan^{-1}\frac{\rho_i \sin(\theta+\Delta\theta_i)}{1+\rho_i\cos(\theta+\Delta\theta_i)} - \tan^{-1}\frac{\rho_{ref}\sin\theta}{1+\rho_{ref}\cos\theta} \qquad (2\text{-}25)$$

where

ρ_i = ratio of multipath amplitude to direct signal amplitude at the i^{th} antenna

θ = phase of multipath relative to the direct signal at the reference antenna

$\theta + \Delta\theta_i$ = phase of multipath relative to direct signal at the i^{th} antenna

$\Delta\theta_i = 4\pi(h_i-h_{ref})[\cos\tau \sin(e+\tau)]/\lambda$

τ = ground plane tilt in the along range position as shown in Fig. 15.

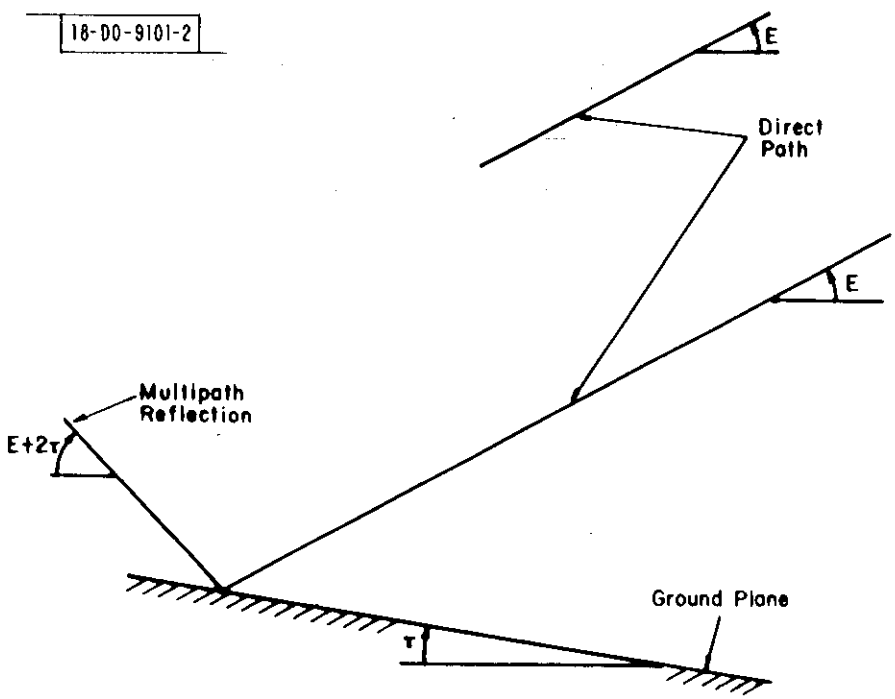

Fig. 15. Geometry of specular ground errors for interferometer pair.

If all phase differences are measured relative to a bottom "reference" antenna, one can then consider $\Delta\phi$ to be a function of the single variable h_2 with the additive error term $e_{ref} \triangleq \tan^{-1}\{\rho_{ref} \sin\theta/[1 + \rho_{ref} \cos\theta]\}$. In Fig. 16, we see that $\Delta\phi$ is a periodic function of h_i with a spatial frequency of $2 \cos\tau \sin(e + \tau)$.

The processing algorithm attempts to take advantage of the cyclic nature of the multipath error shown in Fig. 16, while keeping in mind from the start several factors which would obscure the cyclic pattern:

(i) The front end receiver noise.

(ii) The possibility that the ground reflection multipath could be substantially smaller than that predicted in earlier sections due to ground roughness and divergence effects.

(iii) The multipath reflection angle may not equal $e + 2\tau$ if the ground is tilted differently at different azimuths. This would affect both the amplitude of the multipath and its "period."

(iv) The multipath magnitude could vary from antenna to antenna due to directivity differences and/or the fact that the ground surface contributing to the multipath (e.g., the first Fresnel zone) is not the same for all antennas.

We have attempted to account for the above possible variations in ground reflection multipath errors by considering these errors to be sample functions of

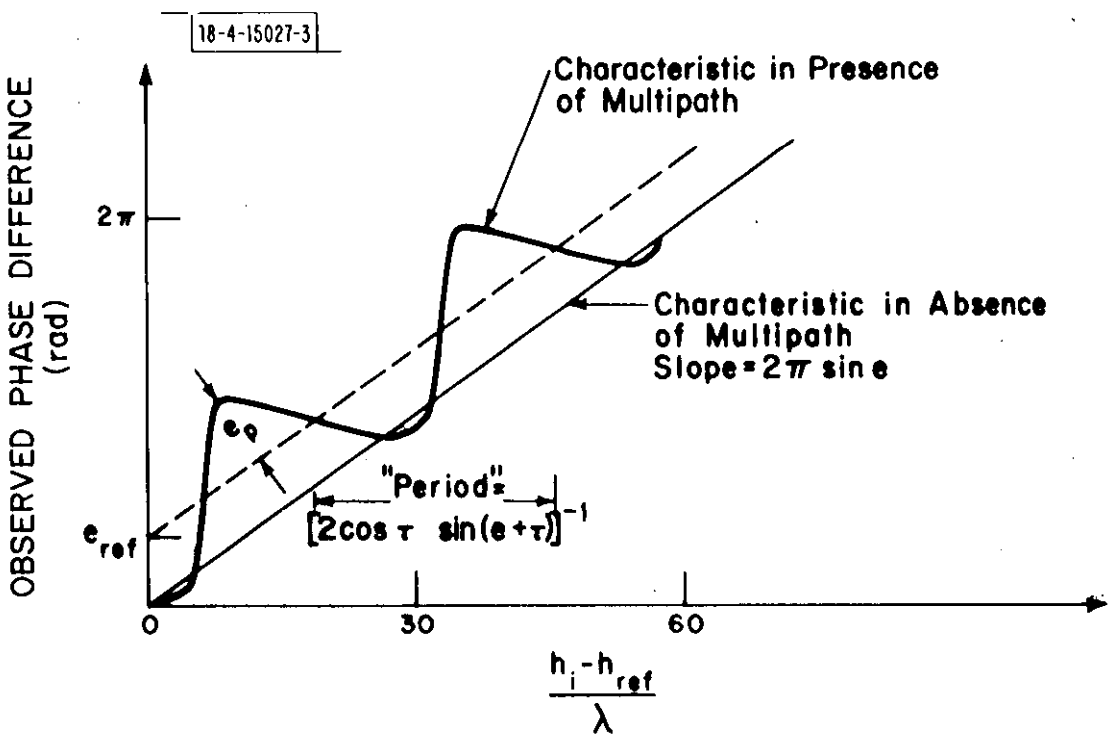

Fig. 16. Pair phase error due to ground reflection as a function of antenna separation.

a spatial Gaussian random process which should have a variation with antenna height similar to that shown in Fig. 16. This "noisy" multipath model is then incorporated with a receiver front end noise model to develop a method of improving the angle estimation performance.

It is appropriate to ask whether any algorithm can achieve the desired improvements. In particular, we call attention to the work of Schweppe, Sklar and Pollon [20,21] in computing Cramer-Rao bounds* for angle estimation with multiple targets. Although they have not specifically considered the bounds for interferometers (they assume amplitude information is also available as well as phase information), their results for the apertures ($\approx 30\lambda$), minimum target separations ($>2°$), and signal-to-noise ratios characteristic of our application do not preclude the possibility of obtaining the desired improvement.

By expanding the inverse tangent terms in (2-25) and maintaining first-order terms in ρ_i, we see that the multipath phase error, m_i, at the i^{th} antenna is a sinusoid of magnitude ρ with a frequency $2 \cos\tau \sin(e + \tau)$ in normalized vertical separation space, $\tilde{h}$, where

$$\tilde{h} = 2\pi \, (h_i - h_{ref})/\lambda \tag{2-26}$$

Averaging over possible variations in reflection angle and reflection magnitude, we propose to model the wavenumber spectrum of the multipath phase error as

$$S(\omega) = [\langle\rho^2\rangle/2]\left[e^{-(\omega-\omega_o)^2/2B^2} + e^{-(\omega+\omega_o)^2/2B^2}\right] 1/(2\pi B^2)^{-1/2} \tag{2-27}$$

*The use and utility of Cramer-Rao bounds for estimating angular performance are described in References [8] and [22].

where

ω_o = 2 cos τ sin(e + τ)

B = rms uncertainty in ω_o

$\langle\rho^2\rangle$ = mean square specular reflection coefficient

Inverse transforming (2-29), we find that the cross correlation function of the multipath phase error between two identical antennas with a normalized separation of $\tilde{h}$ is

$$\psi(\tilde{h}) = E[m_i m_j | \tilde{h}_i - \tilde{h}_j = \tilde{h}] = \langle\rho^2\rangle e^{-B\tilde{h}^2/2} \cos(\omega_o \tilde{h}) \qquad (2\text{-}28)$$

Assuming that the phase error due to front-end noise is independent from antenna to antenna with an rms value of σ_n, we find that the autocorrelation function between phase estimates for the antenna pairs, h_i-h_{ref} and h_j-h_{ref}, is:

$$R_{ij} = \psi(\tilde{h}_i - \tilde{h}_j) - [\psi(\tilde{h}_i) + \psi(\tilde{h}_j)] + \langle\rho^2\rangle + \sigma_n^2(1 + \delta_{ij}) \qquad (2\text{-}29)$$

where δ_{ij} = 1 if i=j and 0 otherwise.

Next, we assume the phase error process is Gaussian, whereupon the likelihood ratio of the observed (ambiguity resolved) phase differences

$$\underline{\Phi} = [\phi_1, \phi_2 \cdots \phi_N]$$

between antennas 1, 2, ...,N and the reference given η = sin e is:

$$p(\underline{\Phi} | \eta = \sin e) = \left[2\pi^{N/2} |\Lambda|\right]^{-1/2} \exp\left[-\frac{1}{2} (\underline{\Phi} - \eta\underline{\tilde{h}})^t \underline{\Lambda} (\Phi - \eta\underline{\tilde{h}})\right] \qquad (2\text{-}30)$$

where

$\underline{\Lambda}$ = $[R]^{-1}$ is the inverse of the correlation matrix

$\underline{\tilde{h}}$ = is the row vector of antenna-reference separations as normalized in (2-26)

The maximum likelihood estimate of η, denoted $\hat{\eta}$, is obtained from the equation

$$\frac{\partial \ln p(\underline{\phi}|\eta)}{\partial \eta} = 0 \qquad (2\text{-}31)$$

Applied to (2-30) this yields (after some algebra)

$$\hat{\eta} = \frac{\underline{\phi}^t \underline{\Lambda}\, \underline{\tilde{h}} + \underline{\tilde{h}}^t \underline{\Lambda}\, \underline{\phi}}{2\, \underline{\tilde{h}}^t \underline{\Lambda}\, \underline{\tilde{h}}} = \left\{ \underline{\phi}^t \frac{\underline{\Lambda}\, \underline{\tilde{h}}}{\underline{\tilde{h}}^t \underline{\Lambda}\, \underline{\tilde{h}}} \right\} = \underline{\phi}^t\, \underline{g} \qquad (2\text{-}32)$$

Equation (2-32) defines the "optimal"* estimator of target location. We see that the measured phase differences are multiplied by the weighting coefficients $\{g_i\}$ and summed to give the optimal estimate. When $\langle \rho^2 \rangle = 0$ in (2-28)(i.e., no multipath), $g_i = \tilde{h}_i / (\sum_i \tilde{h}_i^2)$ which can be shown to yield an unbiased estimator whose variance achieves the Cramer-Rao bound.

In utilizing this in practice, one needs to know ρ and sin e in order to compute R_{ij}. We propose using the estimate of sin e obtained from the end pair alone and the known τ_i to give ω_o in (2-28). The value of ρ is then

*It must be emphasized that this estimator is truly optimal only when the actual observed phase differences coincide with the mathematical model proposed here. The maximum likelihood estimator is asymptotically unbiased and gives (asymptotically) the lowest variance achievable by any unbiased estimator [22].

obtained from an appropriate table of reflection coefficient times directivity factor. The bandwidth B is chosen to accommodate the expected terrain variations as well as the fact that our value of ω_o is slightly in error. Given these parameters, we note that the signal processor defined by (2-32) is linear, so that we do not expect its performance to degrade spectacularly, provided one is above the ambiguity resolution "threshold."

The performance of the algorithm has been investigated theoretically in two ways. First, since the maximum likelihood estimator asymptotically achieves the Cramer-Rao bound on the error, one can plot the Cramer-Rao bound

$$\sigma_e \geq \sqrt{\frac{1}{\underline{\tilde{h}}^t \underline{\Lambda} \underline{\tilde{h}}}} \qquad (2\text{-}33)$$

as a function of elevation angle as is done in Fig. 17 (keep in mind that Λ is a function of elevation angle). We see that this bound suggests that angular errors less than 1 mrad can be achieved at all angles above 1.5 degrees.

One difficulty with this bound is that it represents an average over all possible values of θ at each elevation angle, whereas in practice $\theta \approx 4\pi(h_{ref}/\lambda)(\cos\tau)[\sin(e+\tau)]$.* Thus, this bound may overestimate the errors at some elevation angles and underestimate the errors at other angles.

To better assess the probable performance in the real world environment, a large number of simulations of the algorithm were run for the case of perfectly flat terrain in front of the PALM array. The simulations were accomplished as follows:

---

*This equation is exactly true if h_{ref} is the vertical height above the ground plane on which the reflection occurs.

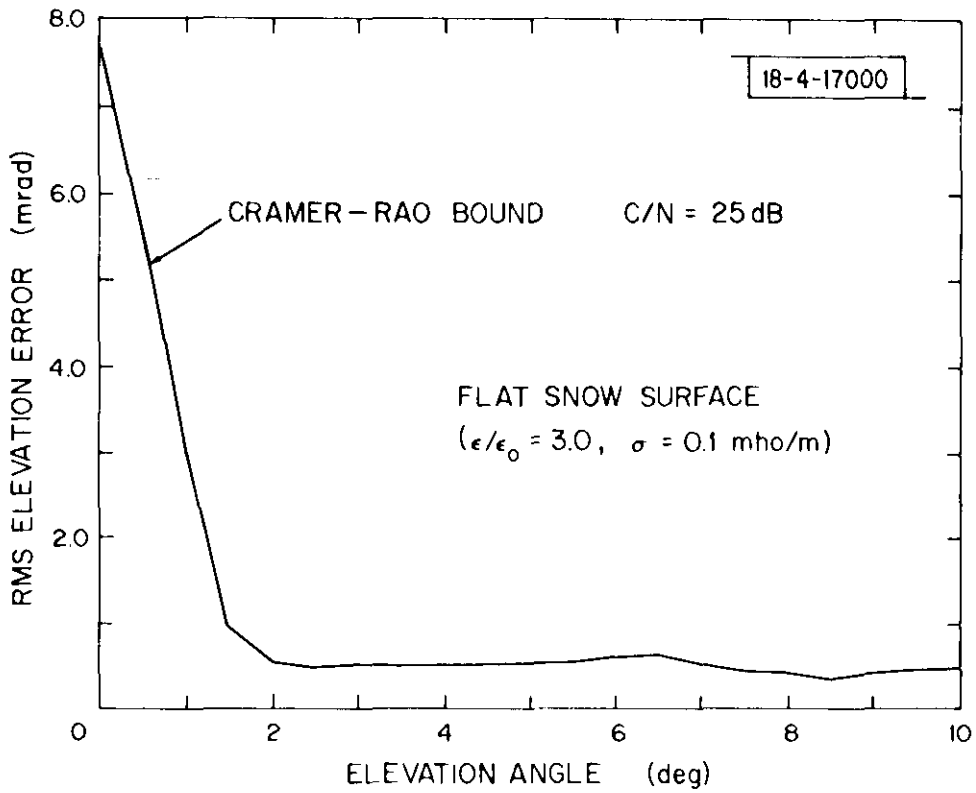

Fig. 17. Cramer-Rao bound on accuracy of "optimal" phase measurement processor.

1. The multipath magnitude at a given elevation angle was determined using the measured PALM antenna patterns and the theoretical Fresnel reflection coefficients for a perfectly flat surface of the specified dielectric properties.
2. The measured phase values at each antenna were computed from (2-25) with $\theta = 4\pi(h_{ref}/\lambda) \sin e$.
3. Ambiguity resolution was checked and a first-order estimate of elevation angle generated from the phase difference between the top and the reference antennas.
4. This initial estimate of elevation angle was then used to choose the appropriate set of weighting coefficients $\underline{g}$.
5. The optimal estimate was then determined from (2-32).
6. Receiver noise and instrumental errors were assumed to be present in generating the coefficients $\{g_i\}$, but not present in the generated phase data, since we were primarily concerned with the ground reflection multipath induced error.*

In Fig. 18 we show the results of one such simulation over smooth fresh snow. We see that the "optimal" processor should achieve the desired

*Section 2.2 showed that the "worst case" error in first-order estimate from nonmultipath sources was $\approx$0.3 mrad. The choice of the $\{g_i\}$ is quite unaffected by errors of this magnitude. Since (2-32) is a linear weighting, it is straightforward to determine the error contribution for various amounts of front-end noise and instrumental errors.

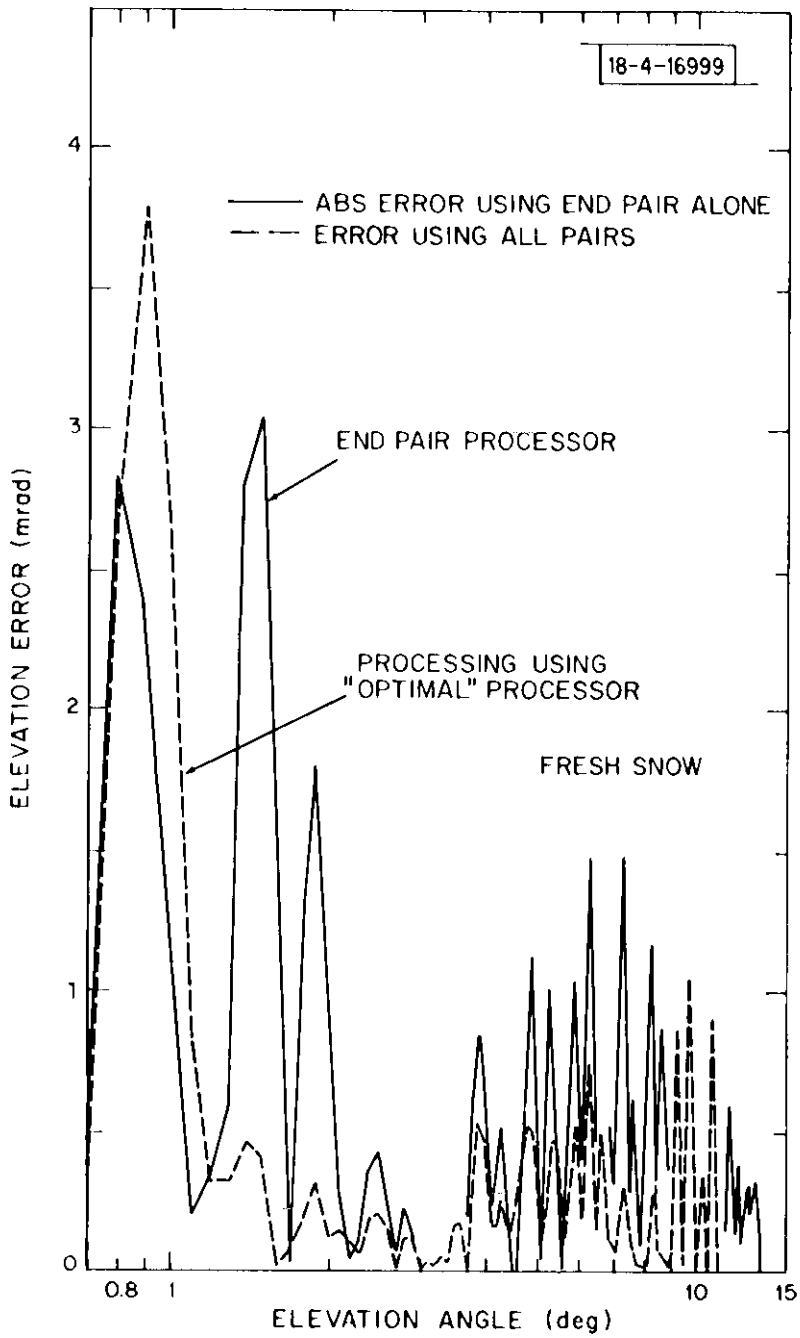

Fig. 18. Simulation of PALM error over flat, fresh snow surface.

1-mrad accuracy at all elevation angles above 1°, whereas the end-pair processor performance would not meet the goal between 1° and 2° and between 6° and 9°. Both schemes would have a very small error due to ground reflection multipath for elevation angles in the important range of 2° to 4°; this occurring because the PALM antennas have a sharp null at approximately -3° elevation angle.

The errors between 6° and 9° represent ground reflections coming in through the first sidelobe of the PALM array. The sidelobe leakage can easily be eliminated in future designs by using antenna patterns with - 20-dB sidelobes. Consequently, the principal utility of the optimal processing should be in improving performance at elevation angles below 2°.

It was not possible to execute flight profiles at elevation angles less than 2° at the Lincoln antenna range due to signal blockage by trees and airspace restrictions. Thus, we could not experimentally demonstrate the improved performance at less than 2° in the tests conducted to date. However, at Hanscom Field in Bedford, Mass., it will be possible to operate at elevation angles as low as 0.5°.

Similarly, it was not possible to fly and track profiles at elevation angles greater than 6° for this initial set of flights. Thus, the indicated improvement between 6° and 9° using "optimal" processing could not be assessed experimentally.

3.0 EXPERIMENTAL HARDWARE

3.1 Introduction

This section is devoted to describing the experimental system. The hardware has been designed and fabricated specifically to experimentally validate the performance of the PALM approach and is not intended to be representative of operational hardware.

The equipment (Figs. 1 and 19) consists of a receiving antenna subsystem (containing five antenna elements mounted on a 28-ft vertical support), a far field calibration source (to largely eliminate phase drifts, e.g., due to antenna motion or receiver variations), a theodolite (to measure the true aircraft position) and a self-powered electronics van. The van contains an ATCRBS interrogator with a roof mounted broad beam antenna, an operator's console, a five-channel receiver, timing and control circuitry and equipment to digitize the data and store it on magnetic tape for off-line processing on a general purpose computer. The data stored includes amplitude for each of the five antennas, differential phase (in-phase and quadrature) for four antennas referenced to the fifth, theodolite bearing, round trip delay, meteorological data and time of day.

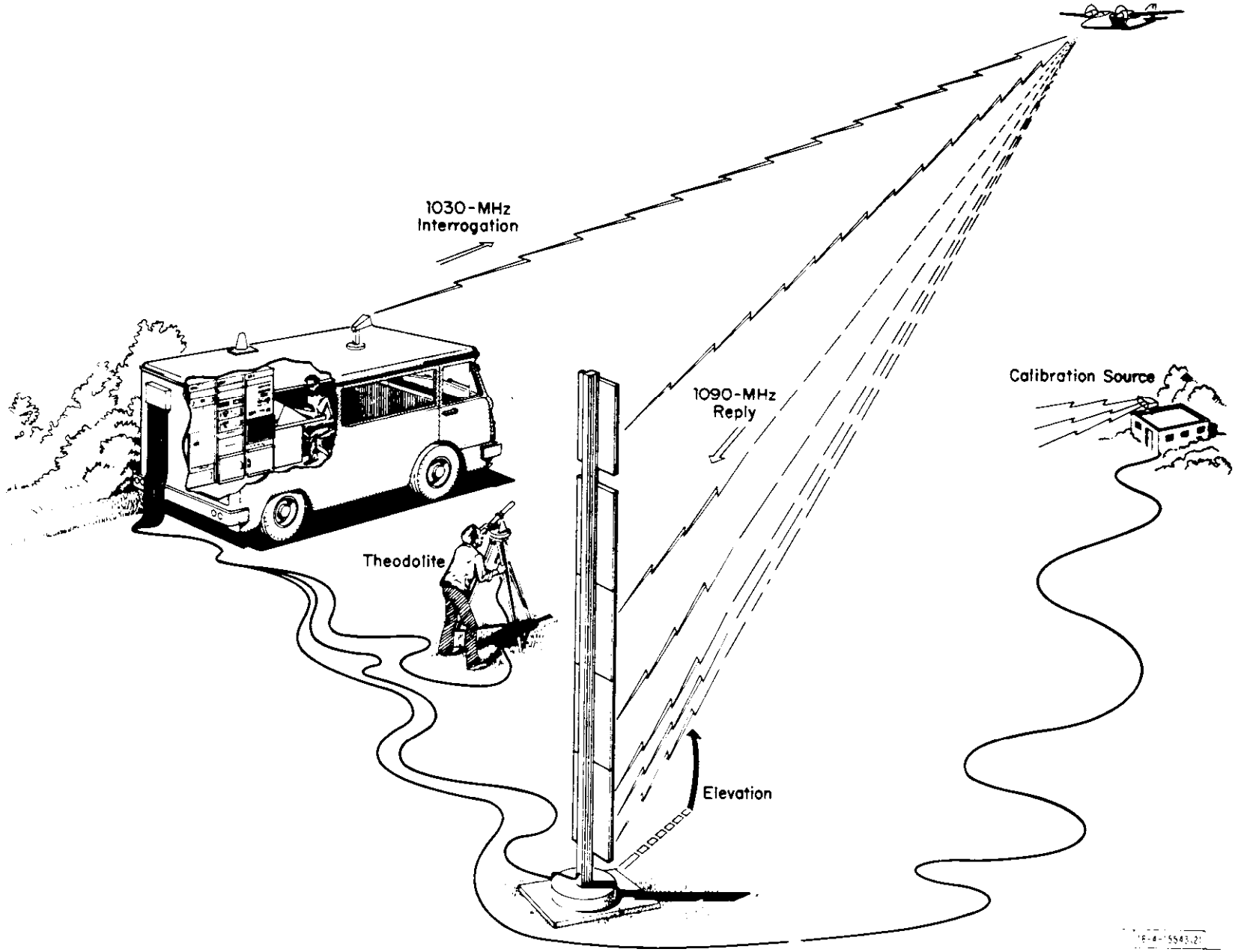

Fig. 19. PALM Phase I experimental configuration.

3.2 Experimental Antenna

The experimental antenna system consists of five identical antennas mounted on a vertical mast. Referenced to the bottom antenna, the pair spacings are $17\lambda/3$, $34\lambda/3$, 17λ and 25.5λ, the spacings being chosen to provide for ambiguity resolution, as described in Section 2.3. Each of the five antennas was fabricated using printed circuit techniques with strip line feeds on a polyolefin board (Fig. 20). The antenna consists of nine radiating dipoles (with half-wavelength spacing) over a 15-inch ground plane. The measured azimuthal pattern for a typical dipole over a ground plane is indicated in Fig. 21. The design for an operational installation would have an azimuthal coverage approximately twice as large (120°), and a 3-dB lower gain.

As detailed in [12], the design of the feed network to achieve the elevation pattern has been based on an adaptation of results obtained for the design of low pass digital filters for minimum transition bandwidth subject to passband and stopband constraints. The dipole coefficients were synthesized to realize an equiripple approximation to the "sector beam" pattern which has a constant magnitude over the mainlobe region and zero-magnitude elsewhere. This equiripple approximation is believed to provide the maximum rolloff at the horizon, subject to constraints on the maximum allowable errors from the desired pattern in the mainlobe and sidelobe region and the number of array elements. This design procedure yielded the relative driving current amplitude and phase of the excitation delivered to a dipole column to give the elevation pattern shown in Fig. 22. Antennas were fabricated to meet this specified

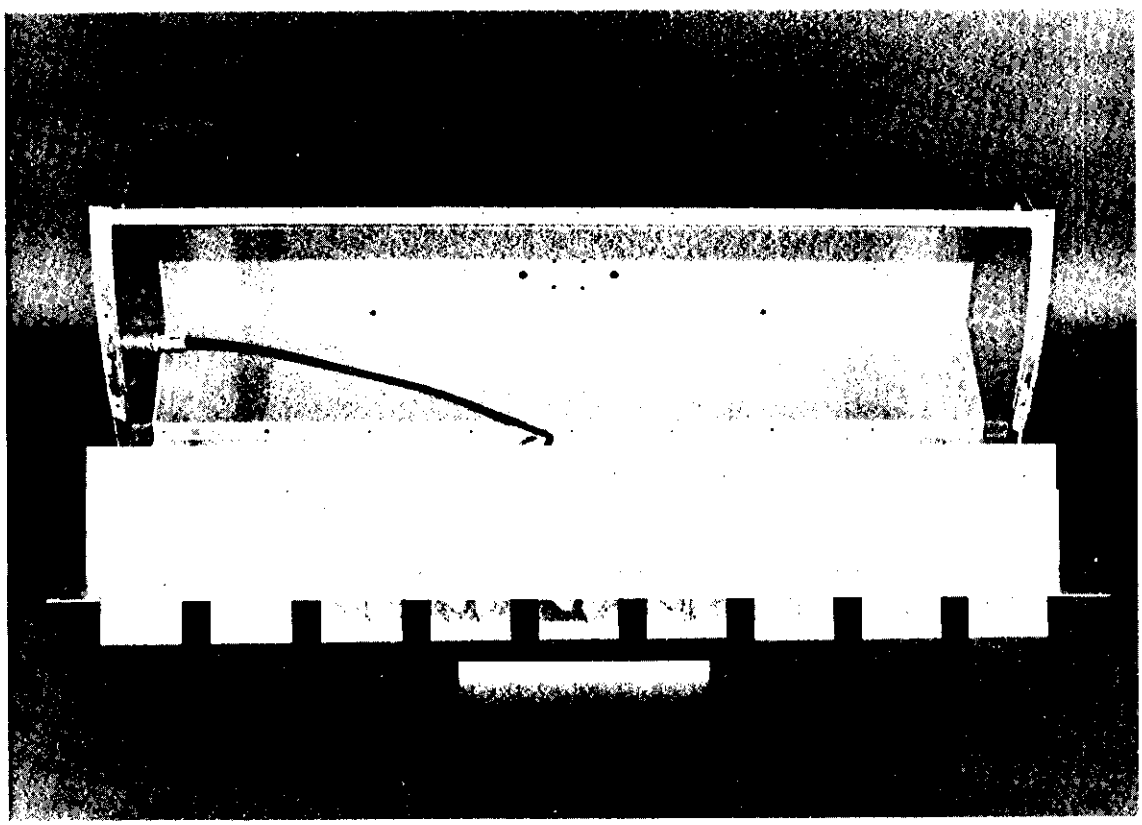

Fig. 20. Antenna feed network.

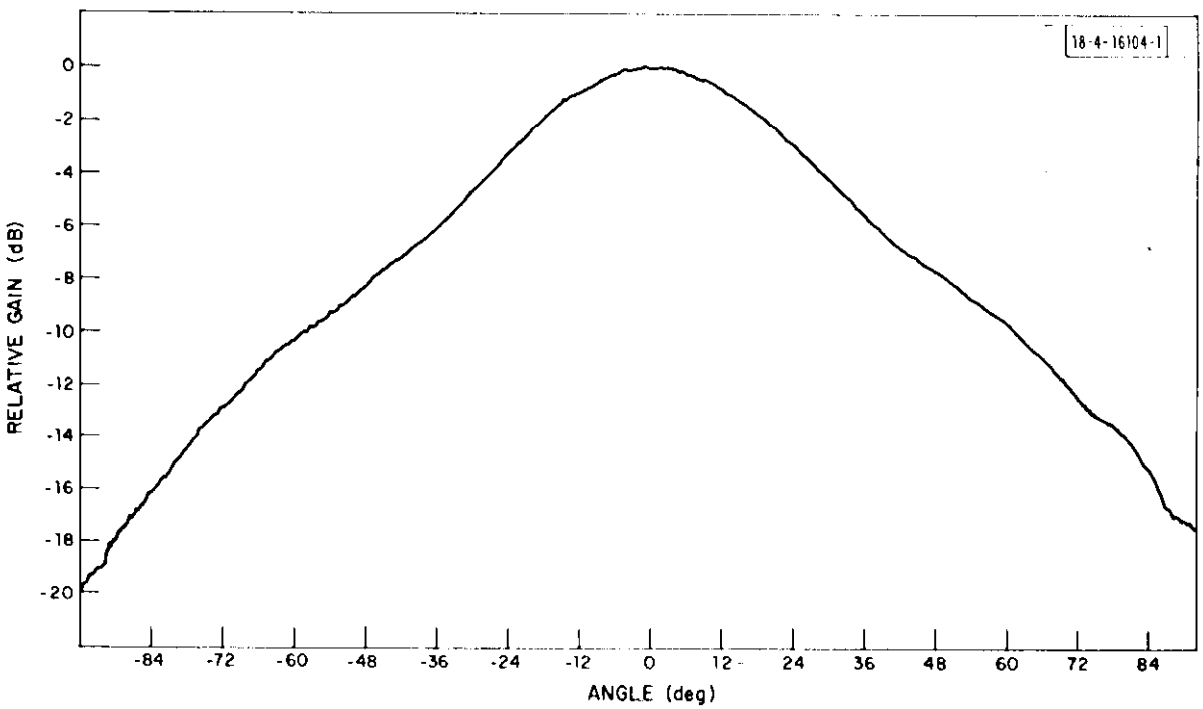

Fig. 21. Measured azimuth pattern for PALM antenna.

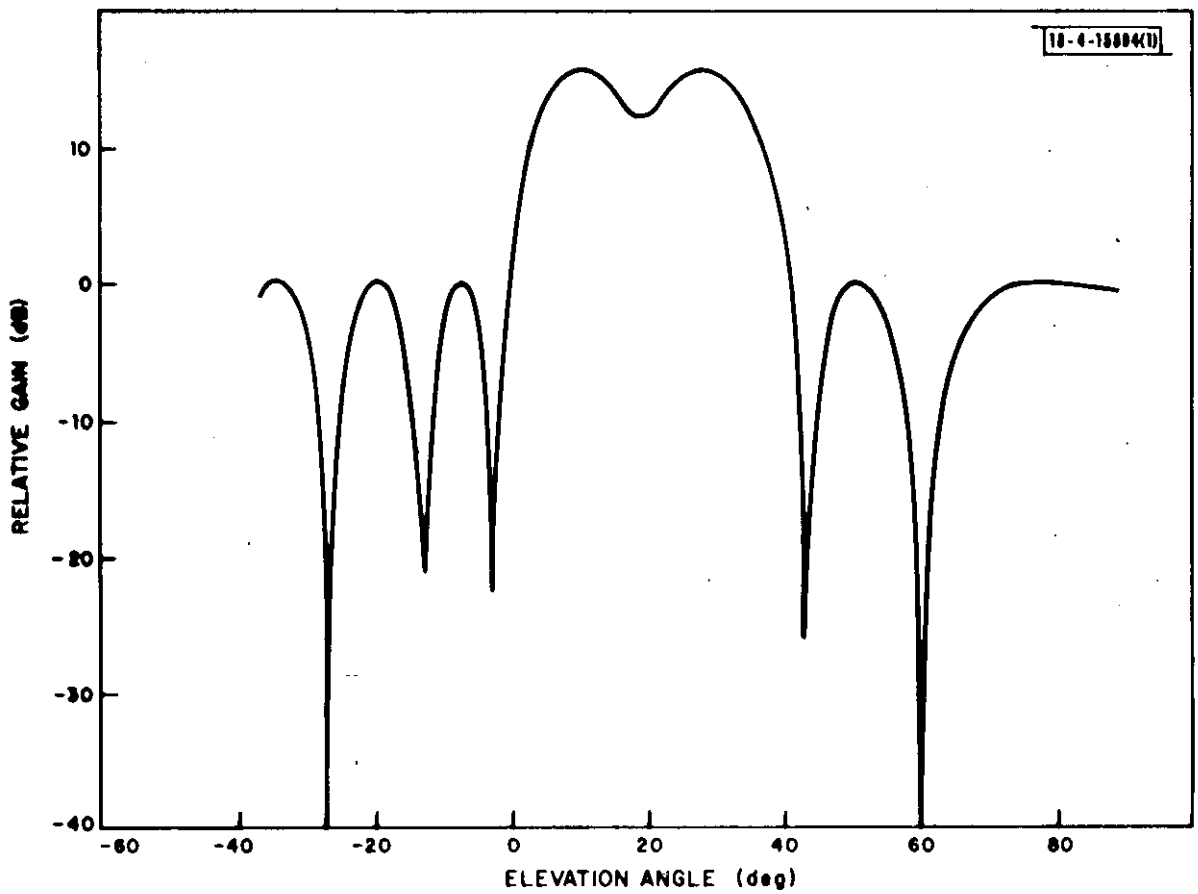

Fig. 22. Elevation pattern through azimuth boresight.

design. Measured patterns for the five antennas used in the experiments (as indicated in Fig. 23) indicate a close match over the coverage region. These antennas have been aligned on a vertical support to make the gain at the horizon (12 ± 0.2 dB) down from the peak gain. Measurements inband (1090 ± 3 MHz) indicate that the antennas exhibit the following properties:

Gain = 15.3 ± 0.5 dB

VSWR < 1.2 : 1

cross polarization isolation $\geq$ 20 dB in the 1° to 40° elevation coverage region

18-4-16902

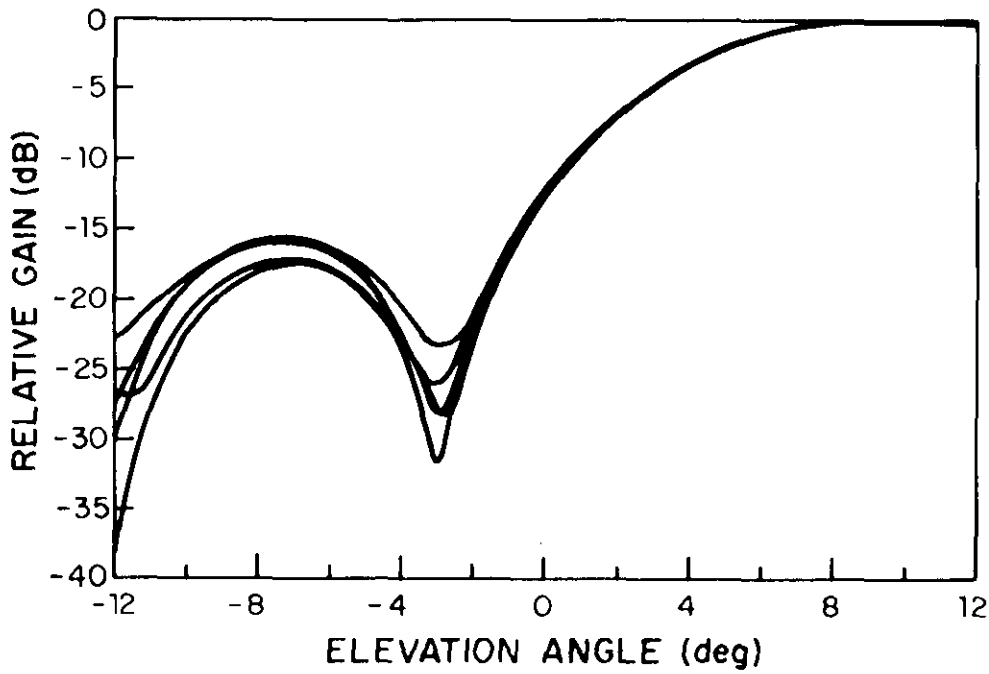

Fig. 23. Elevation patterns for the five PALM antennas.

3.3 Experimental Receiver Subsystem

The receiver subsystem, which was located inside the van (Fig. 24), is connected to the antenna using 50 ft of RG-214/U coaxial cable. The total attenuation between the antenna output ports and the mixer preamplifiers is 5.5 dB. A block diagram of the receiver subsystem is shown in Fig. 25.

The mixer preamplifiers have measured noise figures in the range, 7.8 to 8.0 dB. The IF filters are linear phase five-pole Bessel filters with a noise bandwidth of 5.5 MHz, matched in gain and phase with respect to the reference receiver IF filter to within ±0.2 dB and ±1.5°, as shown in Fig. 26. The resultant receiver transient amplitude and phase response for a 450-nsec pulse at 1090 MHz is shown in Fig. 27. Measurements indicate a differential phase stability of better than ±1° over a 24-hour period. Quadrature phase detectors are used, each having an unambiguous $\pm\pi/2$ phase range. The quadrature phase measurements are processed in software to derive an unambiguous 0-to-2π phase measurement. A digitally controlled phase shifter in the reference receiver and a test signal network permit the injection of CW or ATCRBS pulsed reply signals into the receiver front end for testing and premission calibration. The digital phase shifter and test signal attenuator permit tests over the full amplitude range and 2π-radian phase range. The five receiver channels are equalized for group delay to within 1.5 nsec in order to minimize differential phase error due to ATCRBS downlink signals (which can vary by ±3 MHz around 1090 MHz).

The downlink power budget for the experimental system is shown in Table 2. The principal differences between this and an operational system are

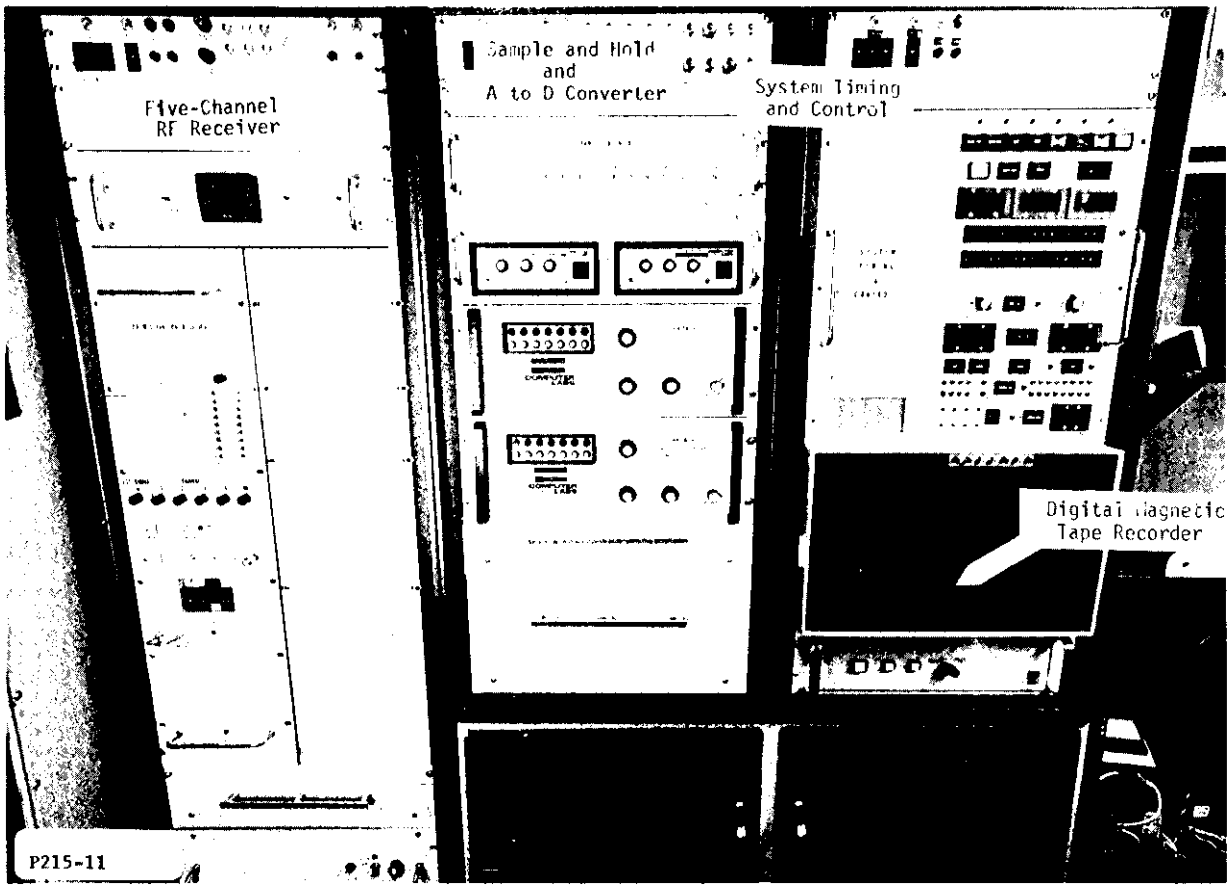

Fig. 24. Van interior photo.

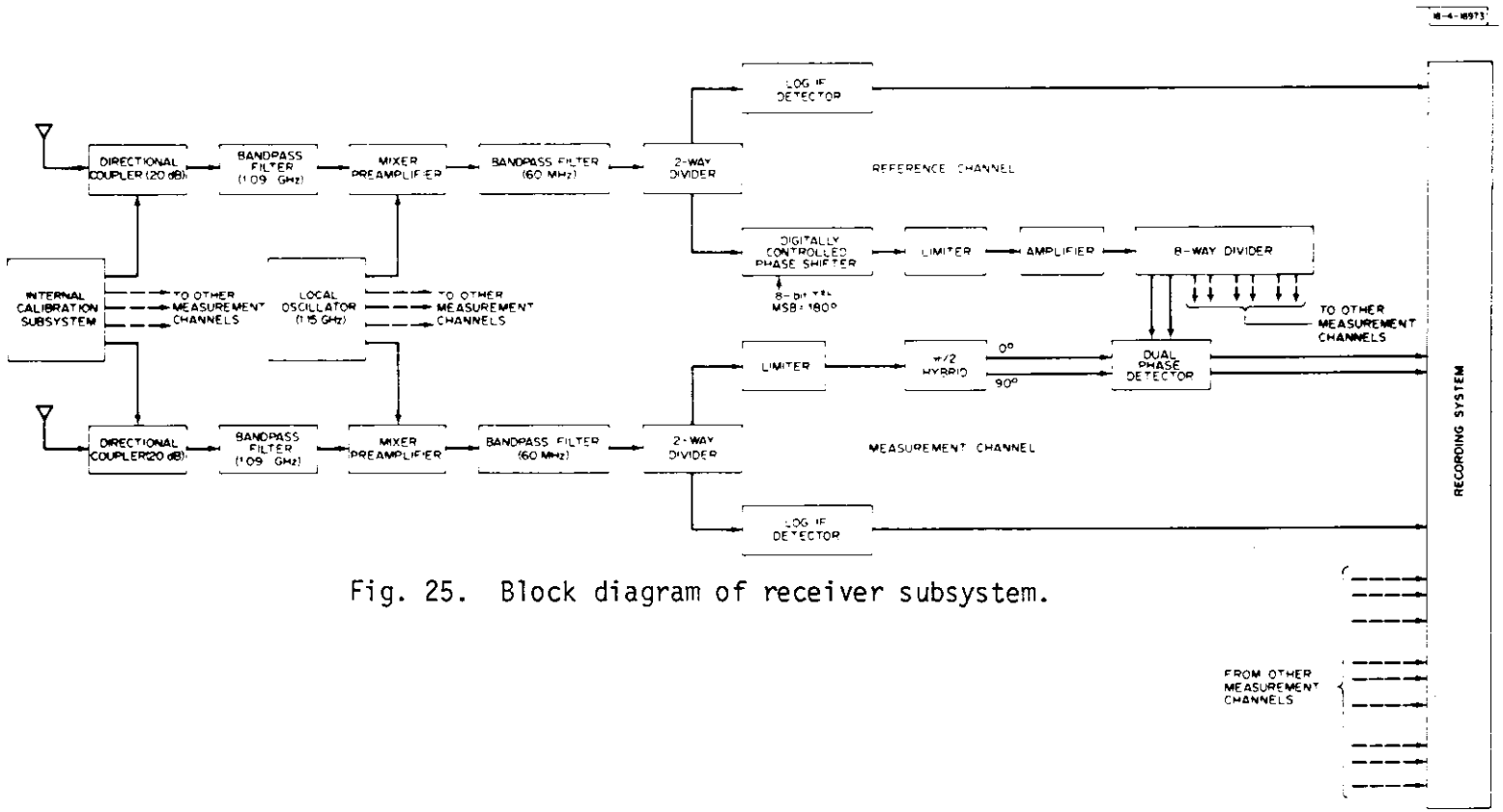

Fig. 25. Block diagram of receiver subsystem.

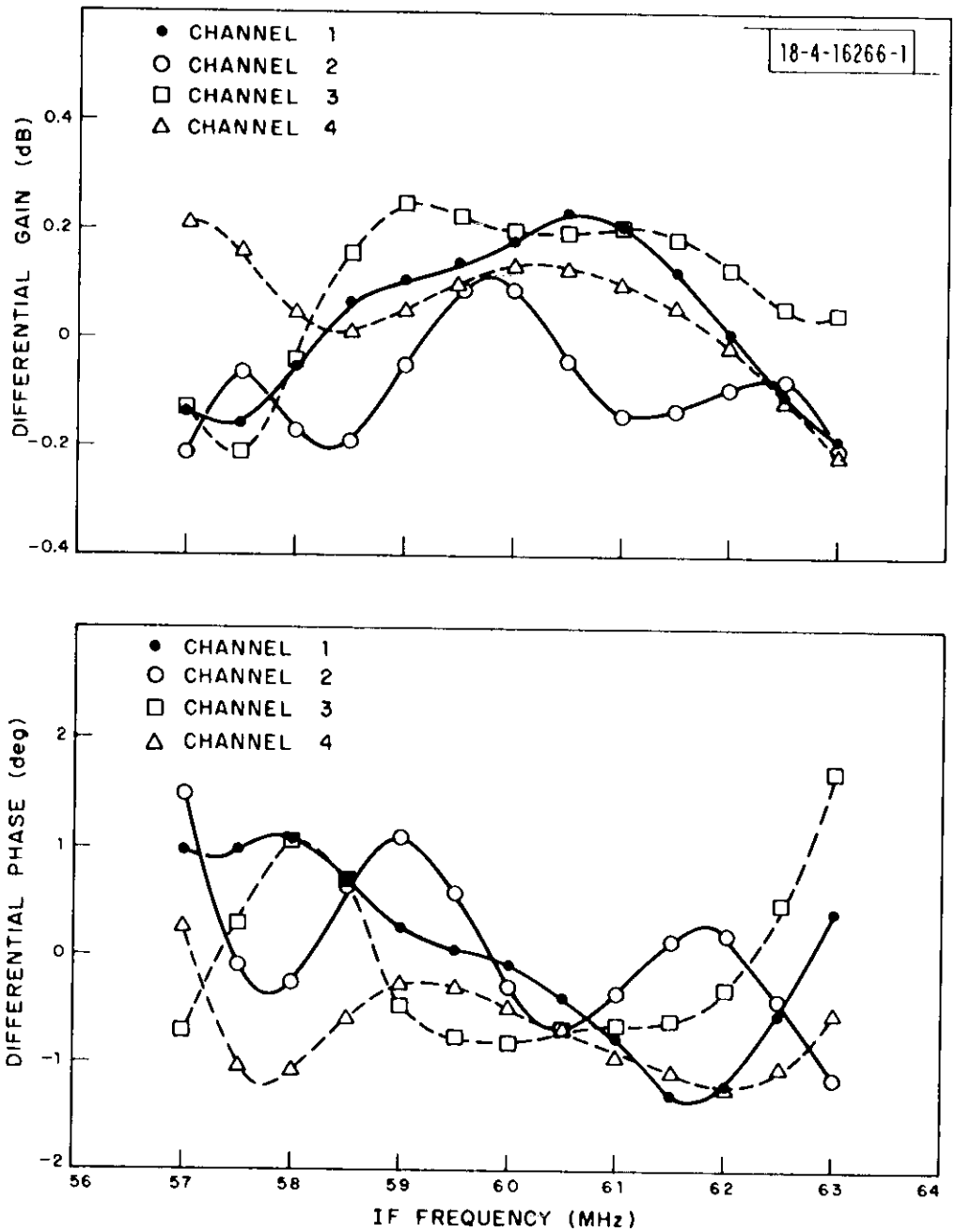

Fig. 26. Channel differential amplitude and phase response.

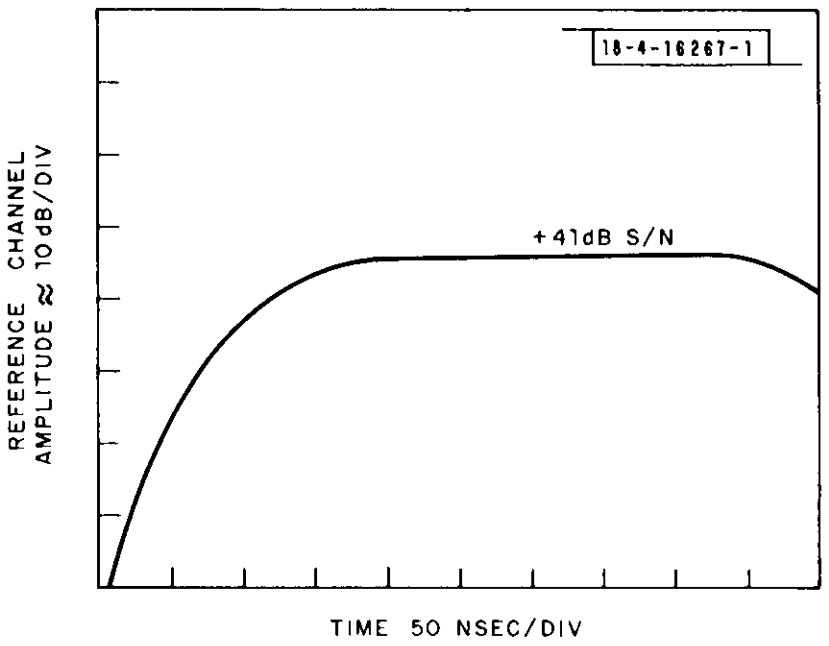

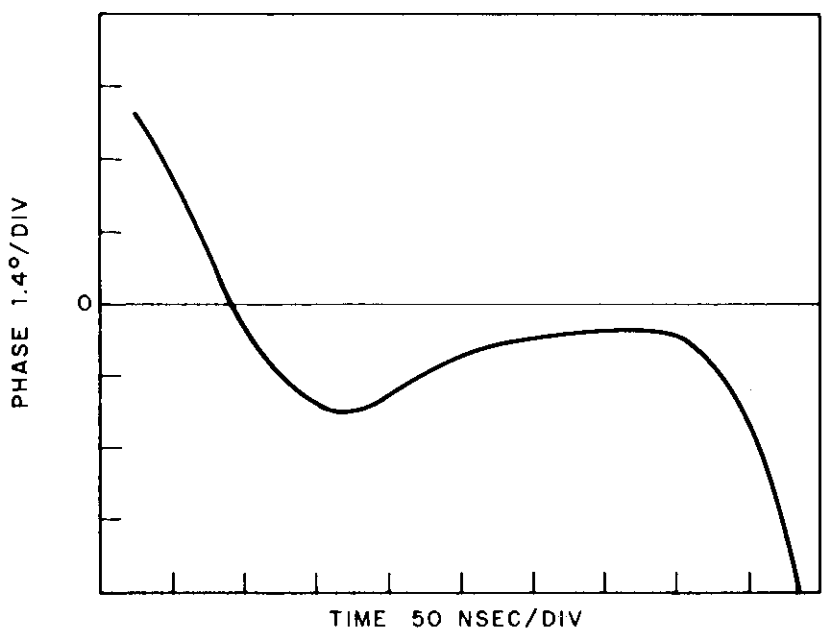

Fig. 27. Transient amplitude and phase response.

Table 2. Downlink Power Budget for Experimental System

Aircraft ERP	21 dBW	125 watts
Path Loss	-118 dB	10 miles
Receiver Antenna Gain	7 dB	1° elevation
Loss at Beam Edge	-3 dB	25° off boresight
Multipath Fading Loss	-5 dB	1° elevation
Effective Noise Power Density	-190 dBW/Hz	At antenna
Line loss		6 dB
Noise figure		8 dB
Antenna temperature		300°K
Receiver Bandwidth	67 dB Hz	5.5 MHz
E/N_o	25 dB	
Required E/N_o for 1-mrad Accuracy	16 dB	With 25.5-wavelength spacing
Margin	9 dB	

the azimuthal coverage (50° versus 120°) and the effective noise power density (-190 dBW/Hz versus -199 dBW/Hz). In an operational implementation, microwave front ends could be mounted on the antennas and low noise (2-dB noise figure) solid state L-band preamplifiers could be used ahead of the mixers.

3.4 Data Processing Subsystem

The processing of received pulse amplitude and phase data, as well as auxiliary data, is accomplished using special purpose system control and timing hardware shown pictorially in Figs. 24 and 28. The system is designed to record the instantaneous amplitude and phase of the pulsed signals incident on the PALM array transmitted from cooperative aircraft equipped with ATCRBS transponders.

In normal operation, ATCRBS interrogations are transmitted using a van-mounted L-band horn antenna (beamwidth approximately 30°) at a pulse repetition frequency (PRF) of 10 Hz. A range gate is manually positioned to bracket the reply signal, and velocity is manually adjusted to place the signal in track. Range and range-rate circuits use 50-nsec logic providing range precision to 7.5 meters, and velocity to ± 3.75 meters/sec. The reply signal is held within a 1500-nsec window, referred to the leading edge of the F1 pulse, for data collection. In the record mode, an amplitude insensitive pulse leading edge detector, shown schematically in Fig. 29, is enabled during the first 1500 nsec of the range window. A pulse which exceeds threshold in this interval (S/N =16 dB) triggers the measurement cycle for this reply. Samples of the 8-phase and 5-amplitude channels are taken 250 nsec after the pulse leading edge, and stored in sample-and-hold (S/H) circuits for subsequent processing. The S/H circuits acquire the analog samples of phase and amplitude to within ±0.6 degree, and ±0.3 dB, respectively. After an 800-nsec delay to allow for S/H output amplifiers to settle, the samples are sequentially gated through a 14-channel analog multiplexer, shown

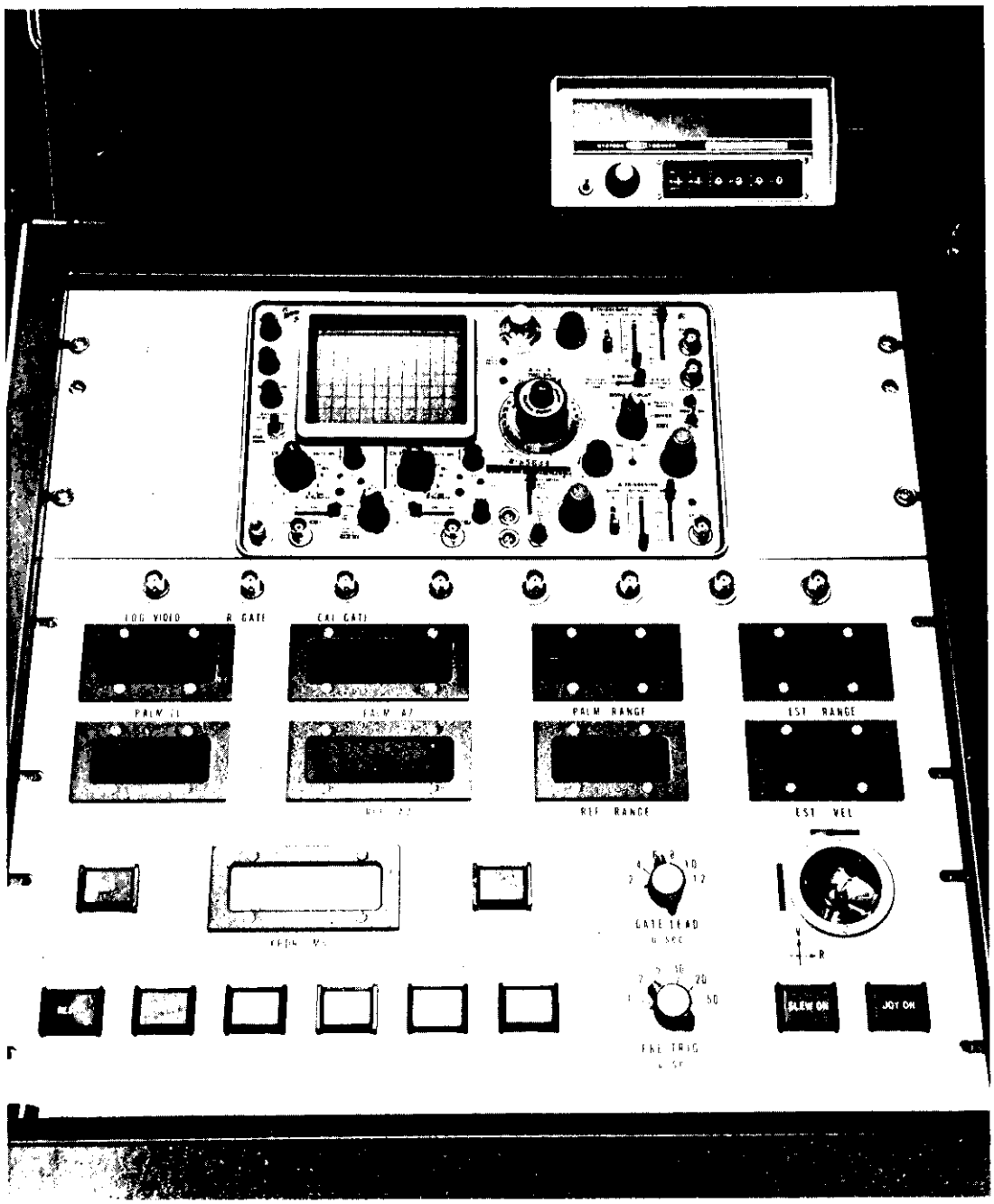

Fig. 28. Operator's console.

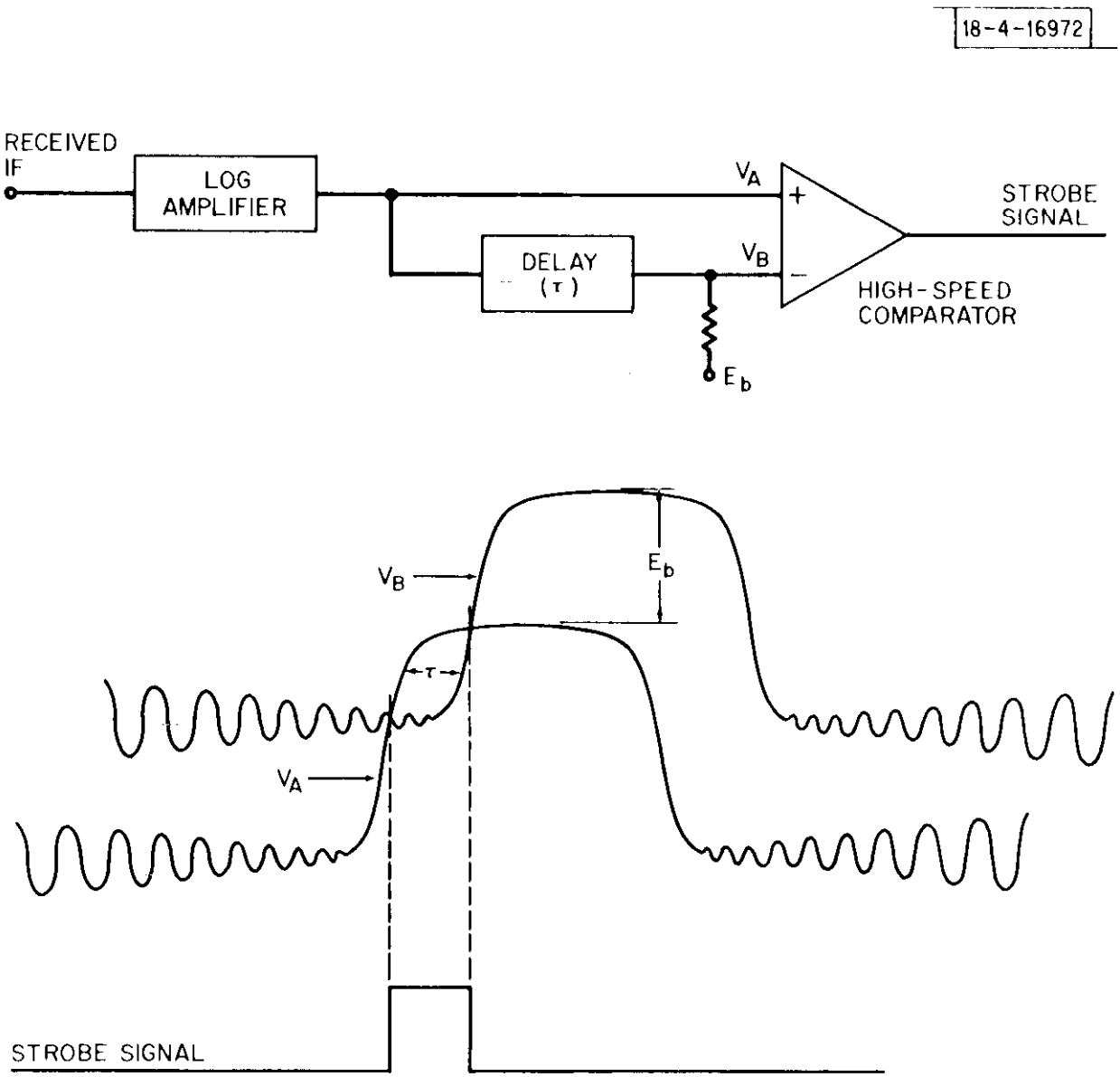

Fig. 29. Log video strobe generator.

schematically in Fig. 30, to a 7-bit A/D converter. The A/D operates at a 5-MHz rate (200 nsec/sample), and the digitized samples are stored in an 8-bit by 256-word bipolar random access memory (RAM). The complete measurement cycle of a single received pulse is completed in 3750 nsec. There is, therefore, adequate time to sample, digitize, and store measurements of every fourth reply pulse (1.45 μsec pulse-pulse spacing) at 4350-nsec intervals. Strobes are developed to sample each pulse interval for aircraft verification, and to sample, hold, and measure pulses C_2, A_4, D_1, and B_4 of a typical ATCRBS reply.

After each reply is processed, the RAM data is transferred to a slower speed dual 8-bit by 2K-word tape system buffer memory, along with auxiliary data such as received code, time of day, theodolite elevation/bearing, etc. When ten interrogation/reply cycles have been completed, the contents of the dual tape buffer are transferred to a 9-track 800-BPI tape in IBM compatible format. Time and space have been allowed for the inclusion of measurements, using a five-channel azimuth interferometer, without requiring modification to the timing and control subsystem. A simplified flow chart of one "scan" of measurement is shown in Fig. 31. Each scan consists of ten interrogation/reply measurements performed in one second, followed by a manually selectable dwell interval of 2 to 16 seconds.

The observed errors of the measurement system (not including the antenna system) are 0.5 dB rms for amplitude, and 2 degrees rms for phase. This is approximately equivalent to a 0.2-mrad rms elevation estimate error referred to the maximally spaced pair.

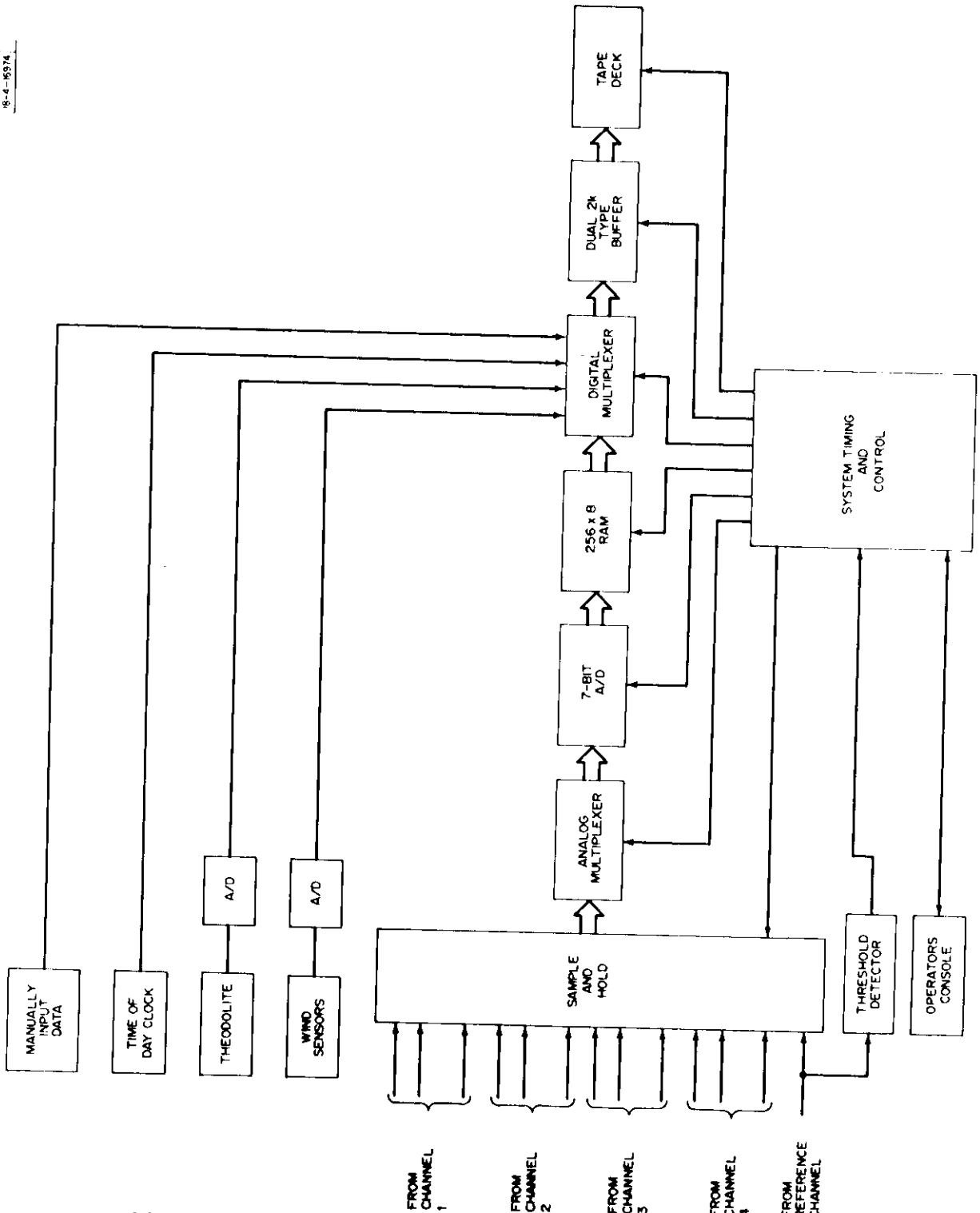

Fig. 30. Block diagram of data processing subsystem.

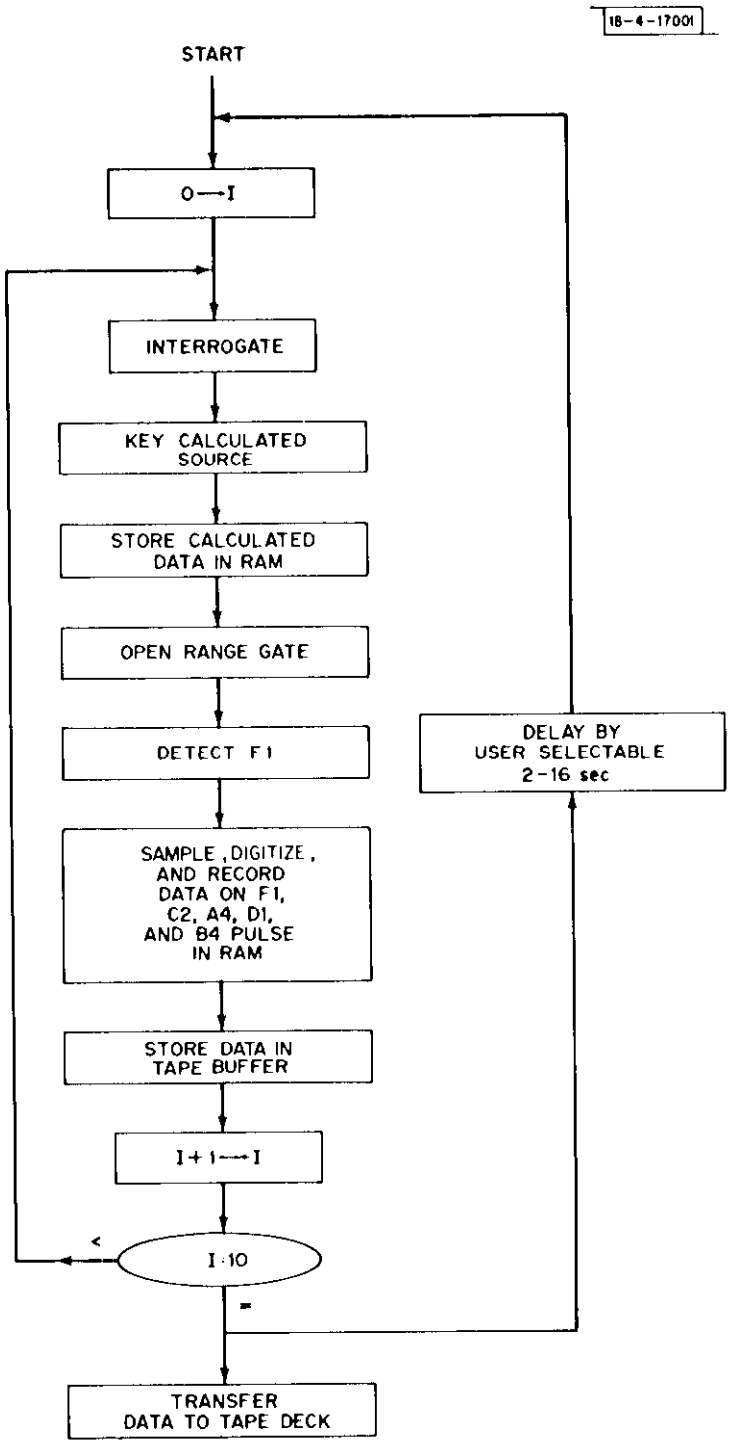

Fig. 31. Simplified measurement flow diagram.

The timing and control subsystem is designed as a hard wired special purpose processor using synchronous digital logic to realize the required flow diagrams. It consists of 750 dual-in-line packages, including small and medium scale T^2L, and Schottky T^2L logic. All clocks are synchronously related to a 20-MHz system clock. The functions include the derivation of a range filter, range measurement, control of all analog measurement equipment, tape buffer, tape deck and diagnostic self-test functions. All control signals are conducted along twisted pairs within back-planes and 100-ohm coaxial transmission line between rack drawers.

3.5 System Calibration

Calibration of the PALM instrumentation system is accomplished in several phases. Pre-operation and post-operation internal calibration records are produced to develop look-up tables for channel amplitude and phase samples. The full system is dynamically calibrated in real time against antenna movement and equipment drift. Finally, the true elevation angle to the test aircraft is measured independently using a surveyed optical instrument and recording of its elevation angle along with the live data for off-line comparison.

3.5.1 Internal Calibration

The Internal Calibration Subsystem is shown schematically in Fig. 32. A CW calibration signal (at 1090 MHz) having identical amplitudes and phases is generated using a 60-MHz crystal oscillator and a sample of the system local oscillator at 1150 MHz. The amplitude of the calibration signal is controlled using a digitally controlled attenuator to insert known signals ahead of the receiver system front ends. System Timing and Control (STC) is used to control the 8-bit IF attenuator which sets a prescribed CW carrier-to-noise ratio, and to write corresponding amplitude records onto the magnetic tape along with measured samples out of each log amplifier channel. Using this technique, the system can be calibrated over the range of received signals from -30 dBm to -80 dBm. Channel differential phase is calibrated using the digitally controlled phase shifter in the reference channel IF processor shown in Fig. 25. STC is used to control the 8-bit digital phase shifter and to write phase records onto the magnetic tape along with channel in-phase and quadrature-phase samples. The system is calibrated over the full 0-to-2π range. In addition,

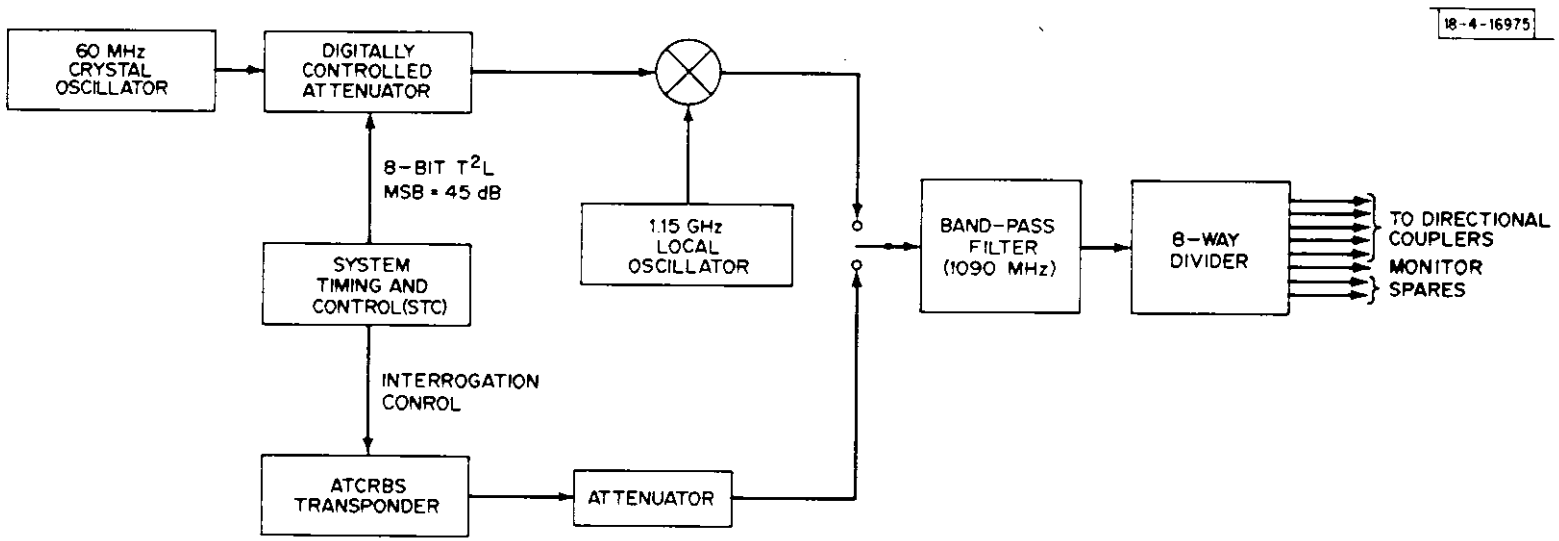

Fig. 32. Internal calibration subsystem.

a standard ATCRBS transponder can be triggered via the STC and its 1090-MHz downlink signal inserted into the receiver system front ends instead of the CW calibration signal. This signal is used to check the operation of the full instrumentation system with standard ATCRBS pulses and also for the purposes of calibration.

3.5.2 External Calibration

A fixed reference source in either the near or far field of the 5-antenna array is used to calibrate the system in real time. Following each interrogation, an ATCRBS transponder connected to an L-band horn antenna is triggered and transmits a single pulse which is timed to arrive at the array before the earliest possible aircraft reply. Channel differential phase is measured and recorded and is subsequently used to correct for antenna motion and/or phase drift. Aircraft replies are processed within approximately 200 μsec of the reference strobe, and the system is assumed to be stationary over this time interval. This measurement is repeated for each interrogation/reply sequence (10 Hz). Since the measurement system phase drift has been found to be negligible ($\leq 1°$ in 24 hours), all of the measured phase error is assumed to be wind induced motion of the array antennas.

3.5.3 Absolute Calibration

The actual elevation angle to the test aircraft is continuously measured by manually tracking the aircraft with a D. White Balloon Theodolite, Model 6061. The rms error of this measurement is estimated to be 0.25 mrad, based on the component errors shown in Table 3, and zero cross-track velocity. The FAA has observed rms errors related to tracking of 0.84 degree/degree/sec cross-track rate [15]. The theodolite elevation angle error voltage is digitized

Table 3. Theodolite System Errors

1.	Opto-Mechanical-Electronic Alignment	σ_1 = 0.008 deg
2.	Elevation Potentiometer (0.2% LIN)	σ_2 = 0.005 deg
3.	A/D Quantization Error (8-bit)	σ_3 = 0.005 deg
4.	Human Static Target Track Error	σ_4 = 0.010 deg
	Total Error	σ_T = 0.014 deg (0.25 mrad)

(8-bit A/D) and recorded once per second on the system magnetic tape, along with other auxiliary data. The theodolite operator utilizes a foot switch to flag the data when the aircraft is on boresight.

4.0 EXPERIMENTAL RESULTS

An extensive flight testing program was undertaken to gather data to validate the ability of the PALM sensor to produce accurate unambiguous estimates of aircraft elevation angle in the presence of large ground reflection multipath. The latter condition was guaranteed by mounting the PALM antenna at the Lincoln Laboratory Antenna Test Range where the terrain had been constructed to be level to within ±1 inch over a region 200 ft in width by 2000 ft in extent. The basic experiment was to fly an aircraft at constant elevation angle on outbound and inbound radials from the PALM antenna. Local regulations prohibited operation at altitudes below 875 feet with respect to the PALM antenna; hence, the experimental flight profile, called plan Bravo, took the form shown in Fig. 33. Data was obtained during the duration of the entire flight, but the most reliable theodolite data is, of course, obtained beyond the 3-nmi range where the elevation angle is essentially constant and the manual tracking errors are small. A particularly good portion of the flight path was found extending from approximately 4.5 nmi to 5.5 nmi in range for which the aircraft was able to maintain a fairly constant elevation angle. The theodolite data and the PALM elevation angle estimates are plotted in Fig. 34 as a function of pulse number or time since data for 10 pulses are collected every 2 sec. Since the theodolite tracker appears to be relatively stable, it is likely that the theodolite estimates are quite a good representation of the true aircraft elevation angle. Hence, the difference between the theodolite and PALM estimates is a good measure of the system errors. These are plotted in Fig. 35. Statistical analysis

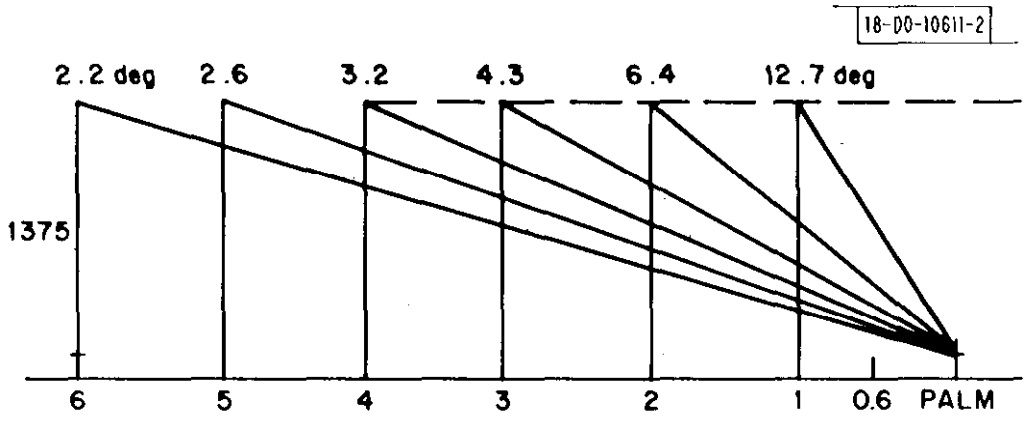

(a) PLAN "ALFA"

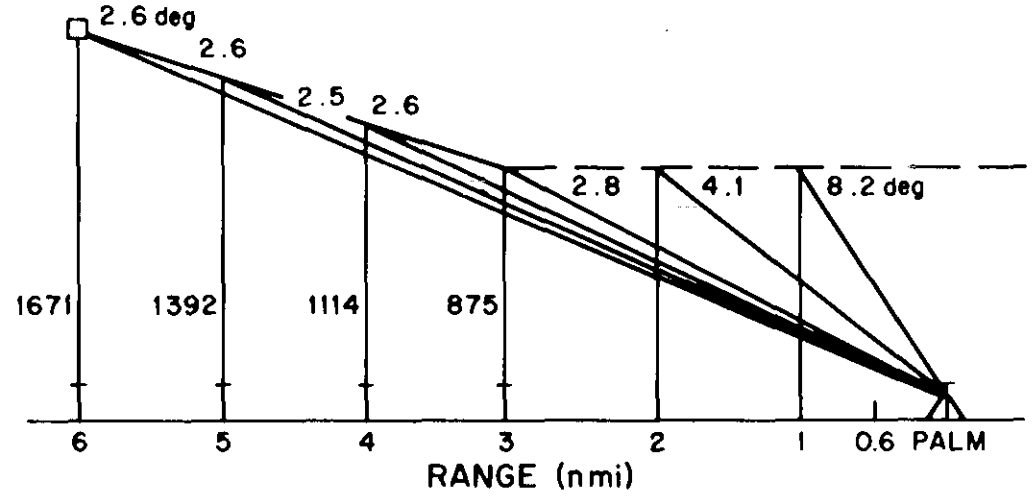

(b) PLAN "BRAVO"

Fig. 33. Test flight profiles.

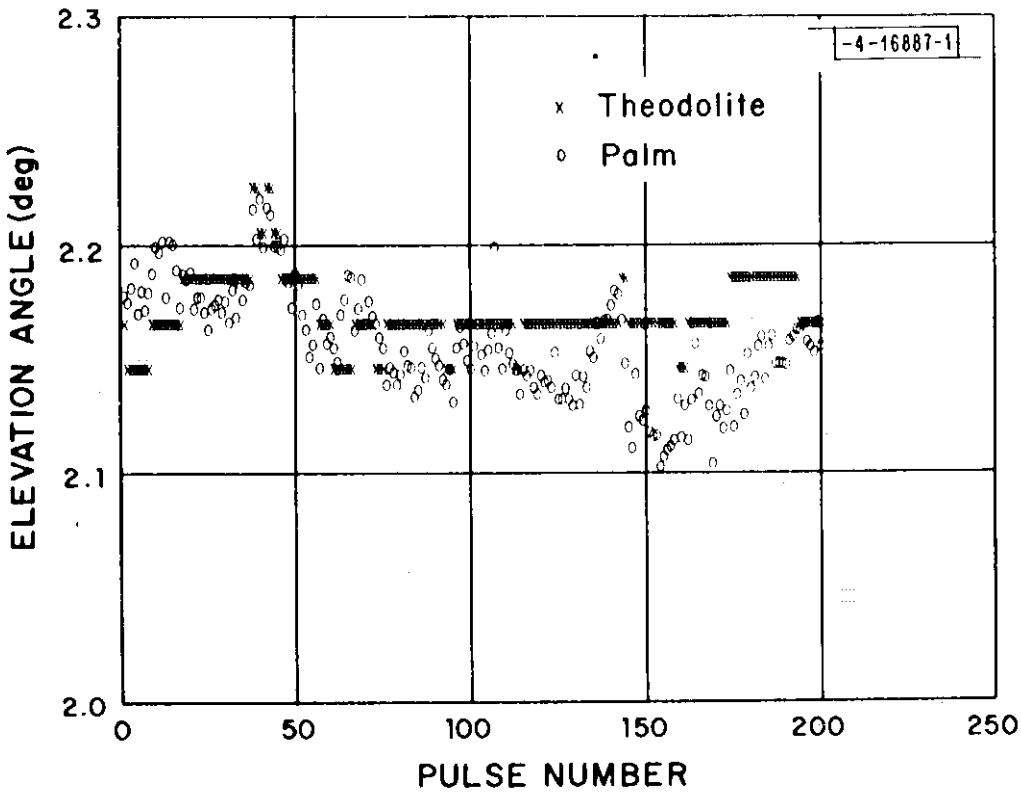

Fig. 34. Elevation angle estimates versus pulse number (time).

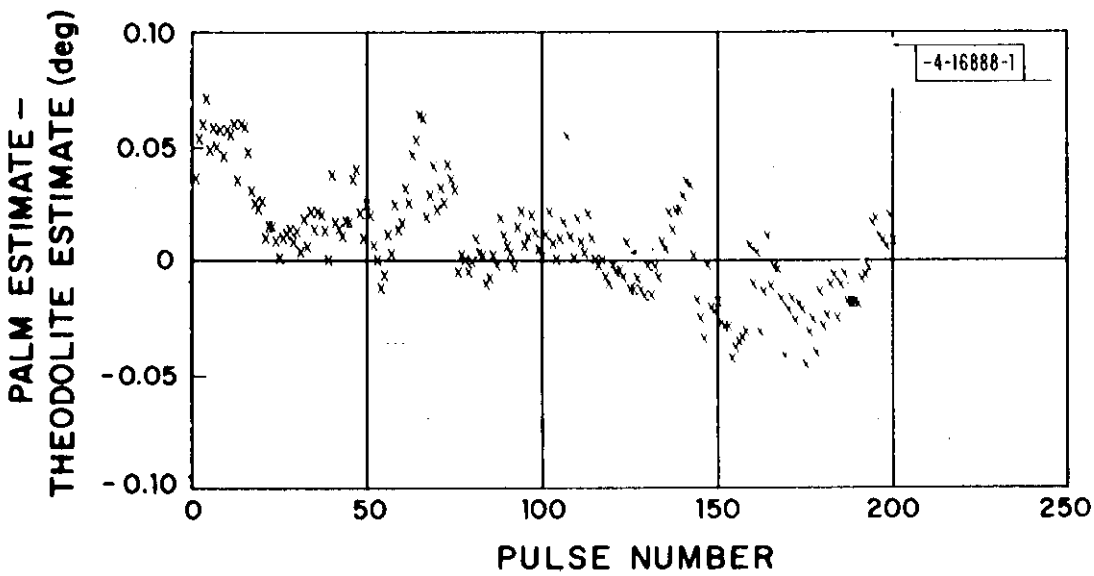

Fig. 35. PALM estimate error versus pulse number (time).

of this data reveals a bias error of 0.008 degree (0.14 milliradian) and a standard deviation of 0.024 degree (0.42 milliradian). This gives an rms error of less than 1/2 milliradian which is even better than the 1-milliradian performance predicted in Fig. 7. It should be noted that certain phase calibration constants were adjusted to reduce the bias error in this data to produce the essentially zero value. Although it appears that significant drift in these constants is unlikely, their temporal characteristic is still not completely understood but will be a high priority issue to be resolved in future tests. These phase calibration constants were then held fixed, and the remainder of the outbound and inbound data for that flight was processed. The PALM and theodolite estimates for the flight are plotted in Fig. 36, and the corresponding errors (assuming the theodolite is a good measure of truth) are shown in Fig. 37. In the angular sector from 1.75 to 2.25 degrees, the rms error was less than 1/2 milliradian, while in the region from 2.25 to 2.50 degrees, it was less than 3/4 milliradian.

As another test on system performance, the aircraft was flown at constant altitude which, of course, results in changing elevation angle with range. This flight profile is called plan Alpha and is shown in Fig. 33. Theodolite tracking is a little more difficult in this case, and the error analysis may not be as indicative of system performance as in the case of the Bravo flights. In Fig. 38 the theodolite and PALM elevation angle estimates are plotted as a function of aircraft range. The lack of data at the 22,000-ft range is due to the extremely conservative data editing routine in the software processor that simply eliminates data

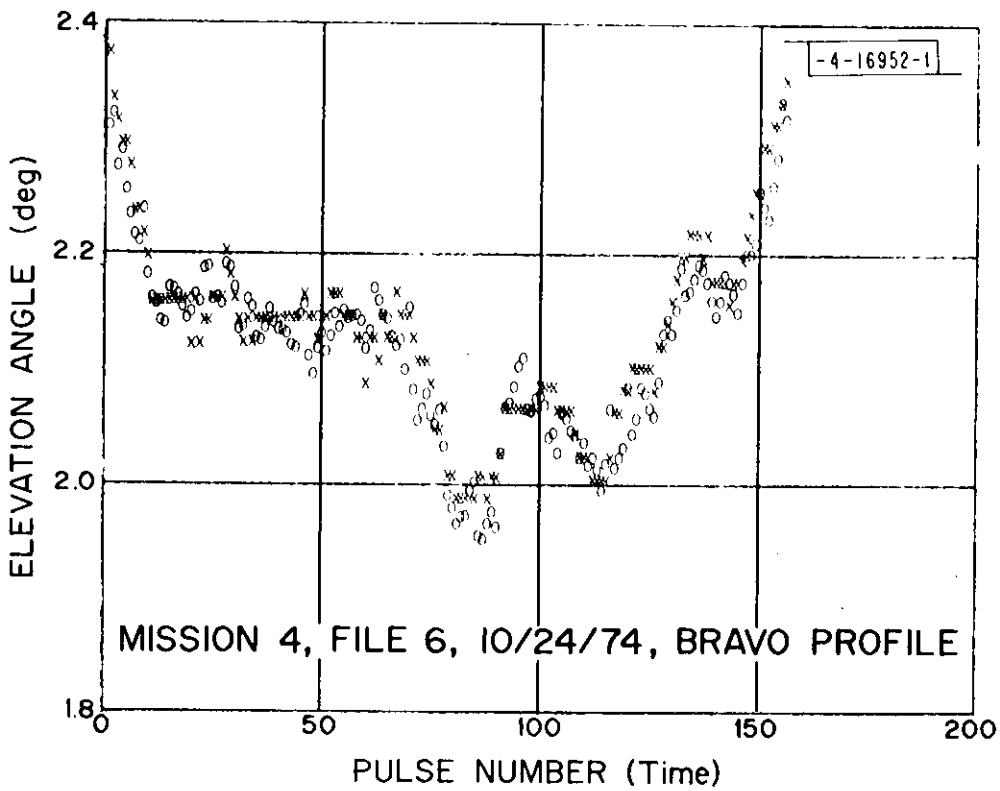

Fig. 36. End-pair elevation angle estimates versus pulse number (time).

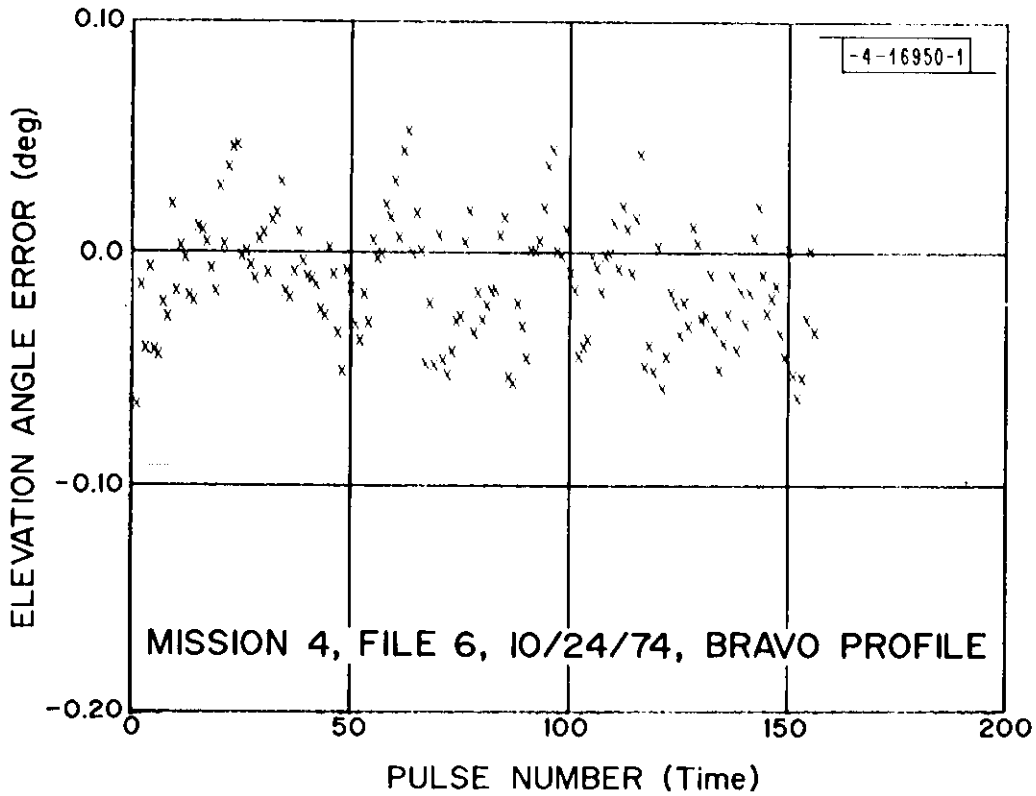

Fig. 37. End-pair PALM estimate error versus pulse number (time).

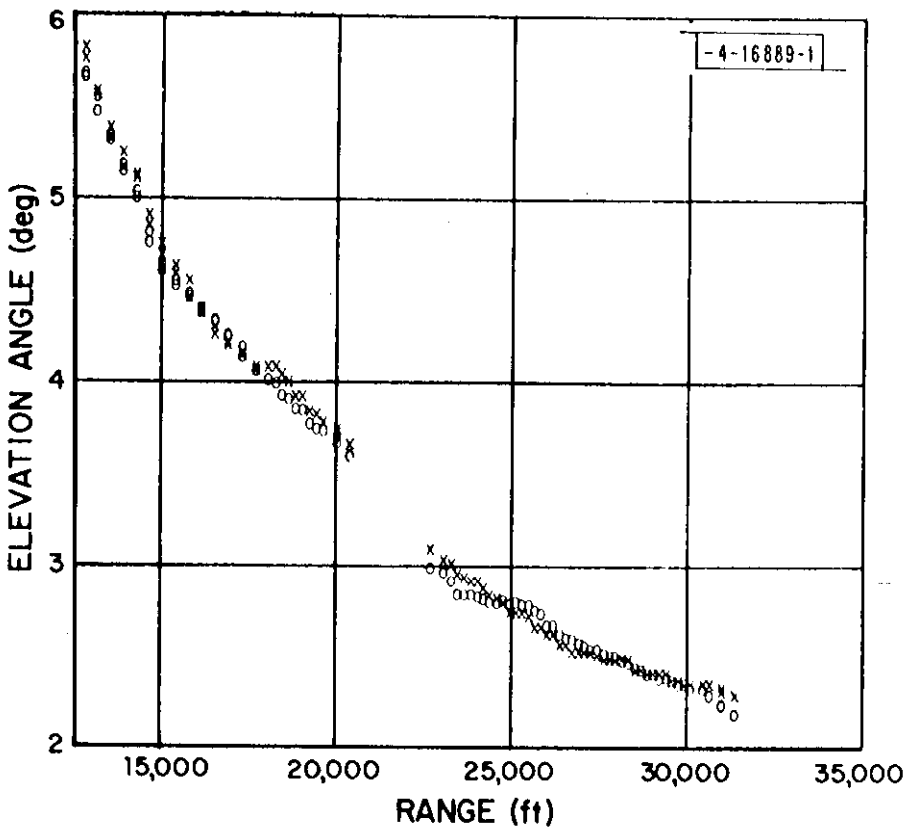

Fig. 38. Elevation angle estimates versus range (time).

for an entire reply whenever there is some indication that fruit is present in the reply. In this case, it may be that the desired reply was synchronously garbled during a short period of the flight path. The reply processor planned for operational use (Appendix A) would eliminate long term data dropouts. If we again assume that the theodolite represents the true aircraft elevation angle, a measure of the PALM error can be obtained as shown in Fig. 39. Data for the entire flight profile was reduced at a slower rate (1 hit/sec) and plotted in Fig. 40 to show both the outbound and inbound portions of the flight. The errors in the PALM estimates are shown in Fig. 41.

In an attempt to discover multipath related errors that should be dependent on elevation angle, the flight path from 2.25° to 6.0° was subdivided into 1/4° angular sectors. The PALM errors for the data corresponding to the theodolite estimates falling into each of these sectors were averaged to generate an rms error. In Fig. 42 these rms errors are plotted as a function of elevation angle. Also plotted on Fig. 42 is the theoretically predicted rms error obtained from Fig. 7. The experimental results confirm the fact that for angles greater than 2 degrees, the PALM design makes the elevation angle estimate essentially independent of elevation angle and furthermore, the errors are of the same order of magnitude which indicates that extremely good agreement between theory and practice is being realized.

Therefore, we conclude that the PALM concept is capable of producing unambiguous, accurate elevation angle estimates in the presence of ground reflection multipath. The hardware and software have performed as anticipated, and the experimental results agree quite well with the theoretical

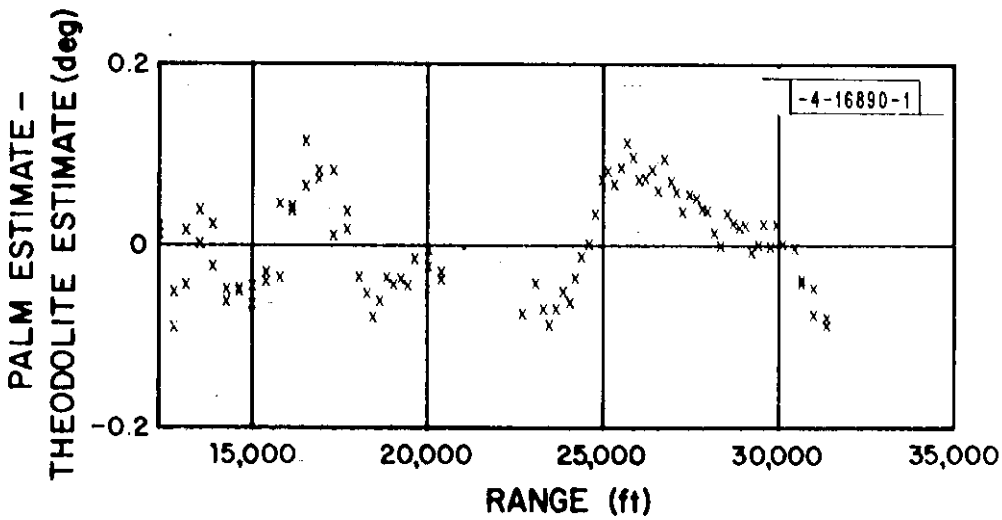

Fig. 39. PALM estimate error versus range.

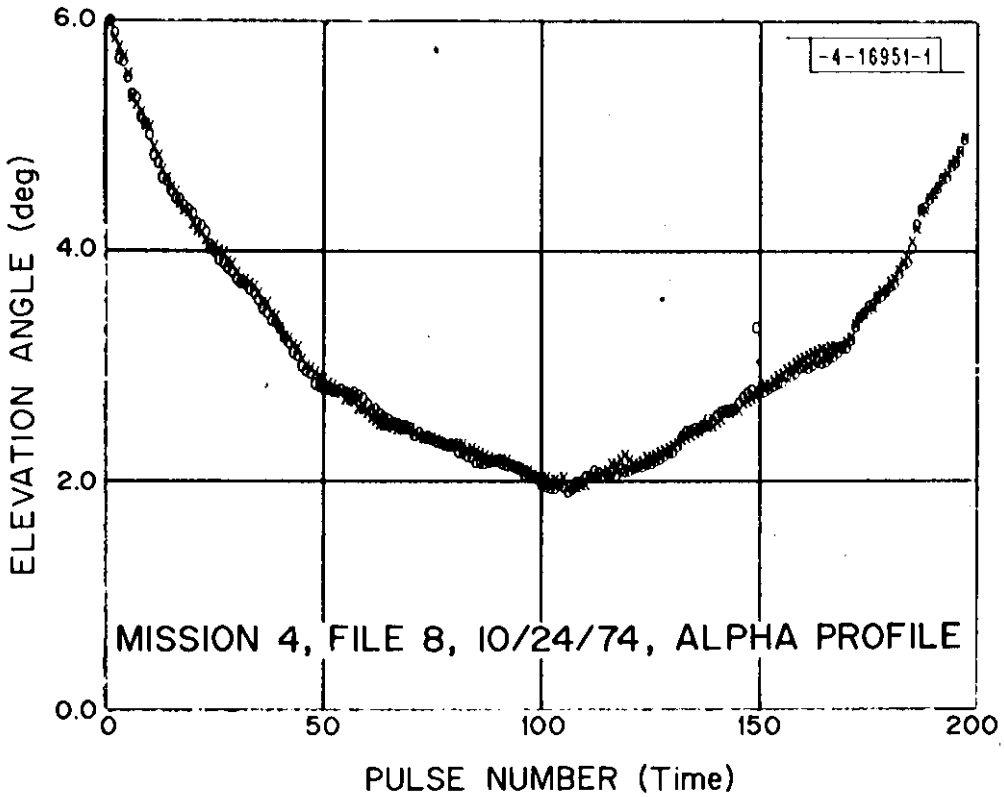

Fig. 40. End-pair elevation angle estimates versus pulse number (time).

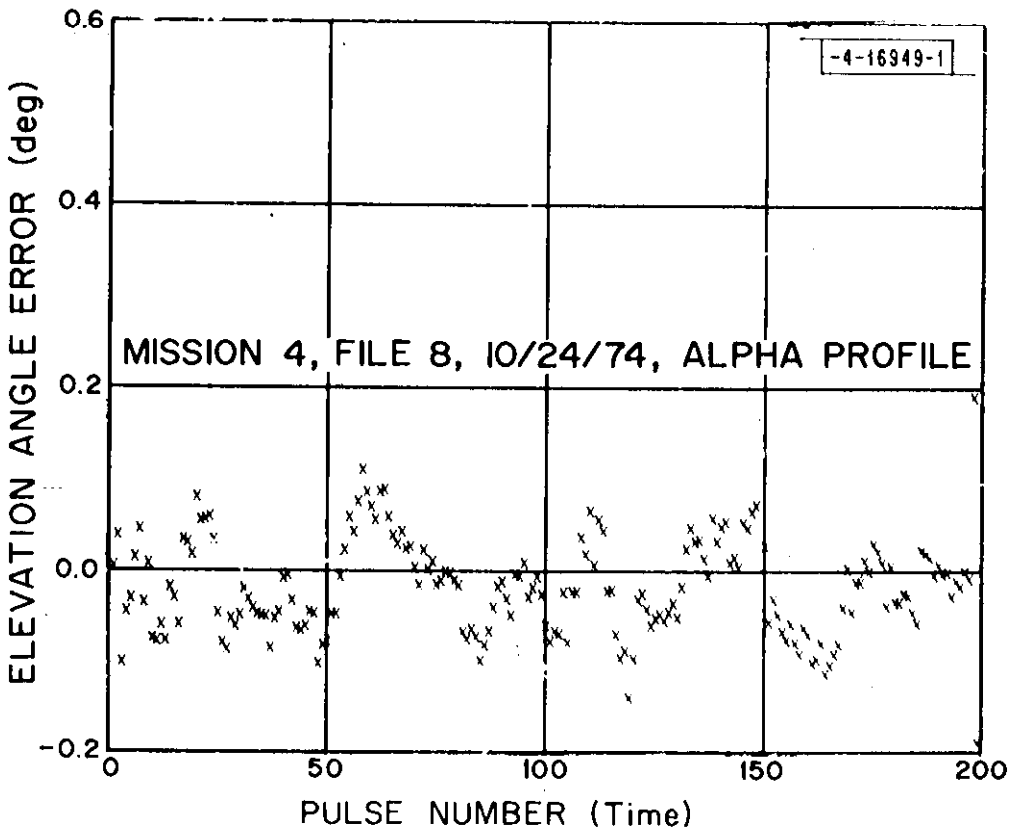

Fig. 41. End-pair PALM estimate error versus pulse number (time).

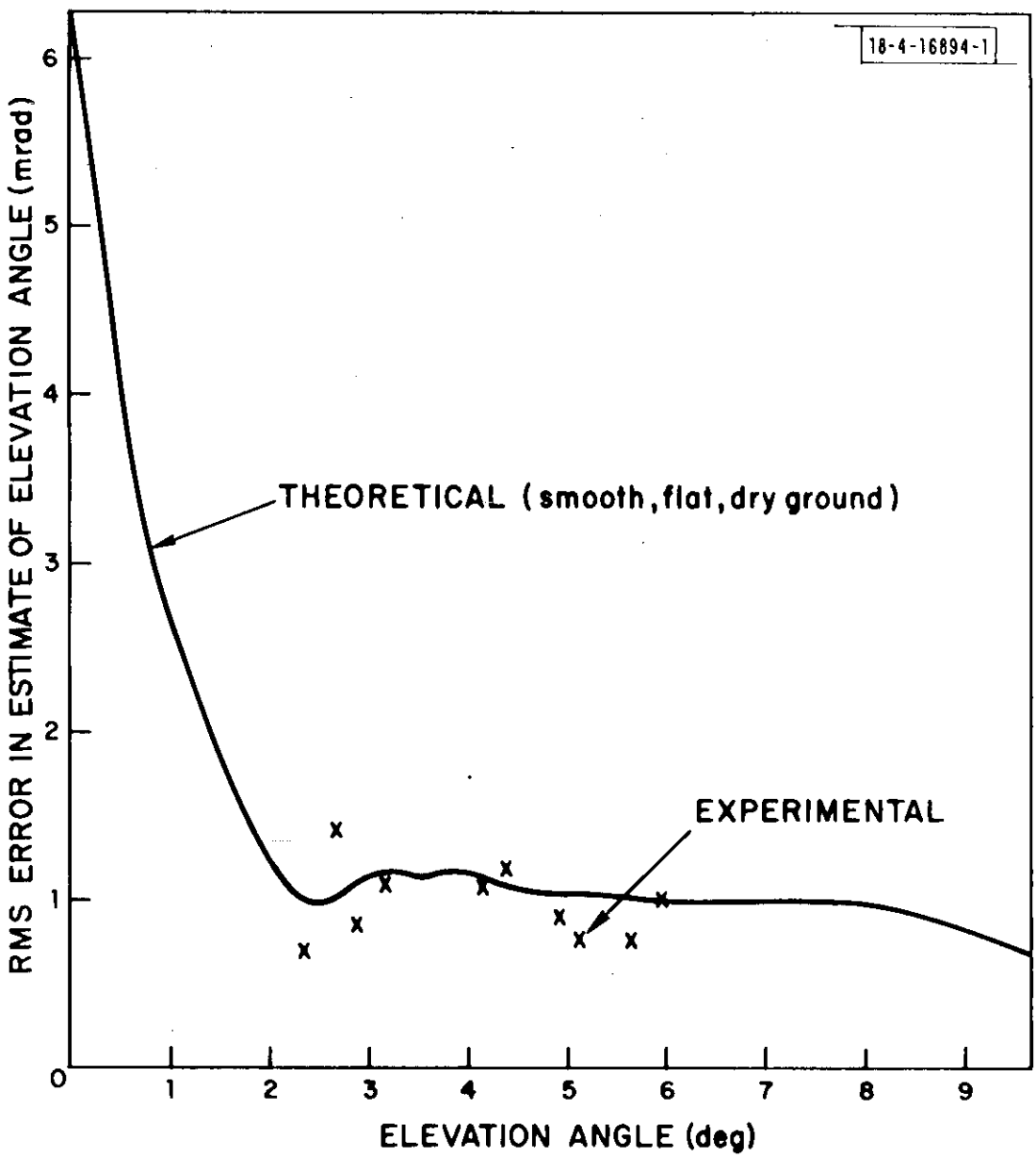

Fig. 42. Rms error versus elevation angle.

predictions. In the next series of flight tests proposed for Hanscom Field , it should be possible to explore the elevation angle dependence further, since it will be possible to have unobstructed line of sight down to 0.5° in elevation. Furthermore, the site is typical of an airport multipath environment so that the multipath sensitivity issue can be explored once again. Finally, with a new installation at Hanscom, a very careful phase calibration can be performed which is compatible with the more recently developed software programs so that day-to-day phase calibration drifts can be recorded and studied as possible sources of error in an operational system. The function of the external phase calibration system can then be evaluated as a candidate for removing this error.

Appendix A

THE EFFECTS OF ASYNCHRONOUS FRUIT ON PALM REPLY PROCESSING

A.0 Introduction

Because PALM provides simultaneous coverage over an airspace sector 40° (in elevation) by 120° (in azimuth), the equipment would have to function in a high fruit environment. This Appendix summarizes the results of a simulation and analysis of the susceptibility of the reply processor to asynchronous fruit.

Because of the high accuracy and data rate implicit in the PALM design, the reply processor is able to employ track file data to provide a range and angular reference for confidence checking to confirm the correctness of the current position estimate. This tracker-aided reply processor avoids the need for F1 pulse correlation checking and therefore permits the track file to be updated as long as a single clear pulse can be found in the reply. The track file data is also to be used in the data editing process to select the clear pulse. It follows, therefore, that the failure rate of the tracker-aided reply processor is given by the probability that at least one clear pulse does not exist in the target reply.

In order to estimate this probability, it was first necessary to determine the maximum number of replies that would overlap the desired target reply. To do this, an estimate of the peak omnidirectional fruit rate was made assuming 800 aircraft in line of sight of the sensor, each responding to interrogations at the rate of 275 fruit/sec. This corresponds to a measured

fruit rate of 30,000 fruit/sec which is three times larger than most predictions for the 1980 era. Due to the 120° beamwidth, the extremely high fruit rate could lead to as many as three fruit replies overlapping some portion of a desired ATCRBS target reply that could cause some, none, or all the target pulses to experience interference.

By making minor modifications to an existing computer simulation of the DABS sensor and the DABS/ATCRBS reply processor, it has been possible to estimate the probability that any ATCRBS target reply will have at least one clear pulse on which a good range and angle estimate can be made. If track file data were not to be used by the reply processor and no revision made to the existing DABS/ATCRBS reply processing algorithm, then it was found that only 61% of 300 replies had an interference-free angle estimate. This is inadequate even for a high data rate system and establishes the need for a different reply processing algorithm. If, on the other hand, the processor were allowed to use the range and angle data stored in the aircraft's track file, then it was found that interference may have affected the range and angle estimates of the 300 replies in, at most, 6% of the cases. Therefore, if a specially designed though inexpensive tracker-aided reply processor is used, no serious long-term data dropouts due to fruit are expected to occur. Furthermore, the ranging accuracy should be the same as in the ATCRBS system, or 275 ft.

In the next sections we briefly document the analysis to support the preceding conclusions and provide a brief discussion regarding the data dropout problem and the method by which target acquisition might be performed.

A.1 The Tracker-Aided Reply Processor

With the tracker-aided reply processor, the range and angle information that is stored in the track file is used to process a new reply as it arrives. This is done by using the range information to locate a range gate around the location of the anticipated reply. This means that the ability to detect replies depends neither on the bracket detector logic, since it is known a priori that there is a reply in the range gate, nor on the need to eliminate phantom F1-F2 pairs, since the range gate eliminated the possibility that a phantom exists. The only question that the reply processor must address is to determine which pulse in the reply is free of interference. This is done by making an angle estimate on those samples for which a leading edge has been detected and comparing this estimate to the angle stored in the track file. A range estimate is also made on this clear pulse by measuring the time of arrival of the leading edge and the number of 1.45-μsec intervals that have elapsed with respect to an F1-F2 bracket detection which establishes the arrival time of the F1 pulse. Since the fruit is distributed over a 120°-azimuth sector, the resolution capabilities are considerable and it will be relatively easy to determine the samples which correspond to a clean target pulse. Further discrimination is possible by storing amplitude data, but since the azimuth estimate is much more sensitive to interference than is amplitude, it is unlikely that this additional discriminant will be necessary.

It is reasonable to conclude, therefore, that the detection probability of the tracker-aided reply processor will be near unity and that it will be possible to update the range and angle track by isolating interference-free

pulses. The question that remains to be answered is whether or not there will be any pulses within the target reply that are interference free in the first place. This is, of course, a function of the background fruit rate.

A.2 Fruit Statistics

In order to determine the probability that any one target reply has at least one clear pulse, we first try to estimate the number of mainbeam fruit replies that are likely to overlap some portion of the desired reply. Although estimates can be calculated using projections of measured fruit rates and assuming Poisson statistics, we shall take a more conservative distribution-free approach. It has been estimated from aircraft density predictions for the region around New York City in 1980 that there will be a maximum of 800 aircraft within line of sight of a DABS sensor at Philadelphia* [16]. It has also been estimated from recent airborne measurements of that environment that if all ATCRBS interrogators are SLS equipped, there will be, on the average, approximately 275 ATCRBS fruit replies generated each second by each aircraft [17]. It should be noted that directional peaking is unlikely to be the problem for the dual parallel approach monitor as it might be for DABS, since the beamwidth is 30 times larger (120° vs 3°); hence, considerable averaging is implicit. Therefore, the peak omnidirectional fruit rate can be estimated at 220,000 fruit/sec (800 a/c × 275 fruit/sec/ac). For the 120° antenna, one

*It should be noted that the dual parallel approach monitor design is less sensitive than a typical DABS sensor; hence, less than 800 aircraft would be within its line of sight.

would reasonably expect the mainbeam fruit rate to be 73,000 fruit/sec (120°/360° × 220,000 fruit/sec). If the F1 leading edge of a target reply arrives at time t_0, then a fruit reply will be a potential source of interference only if its F1 leading edge arrives somewhere in the interval (t_0-21, t_0+21) μsec. Assuming independent fruit arrival times, the number of fruit replies that may overlap the target reply is 3 (73,000 fruit sec × 42 μsec). It may be worth noting that the estimated omni fruit rate of 220,000 fruit/sec corresponds to a measured fruit rate, using a 4° beamwidth, -26-dB sidelobe antenna of 33,000 fruit/sec which is 3 times larger than most estimates of what the interference level is likely to be [18].

Therefore, we conclude that in an extremely malign environment, there will be at most 3 ATCRBS fruit replies that may overlap some portion of the target reply. Focusing on these 3 replies, it remains to determine the probability that there will remain at least one clear target pulse in the desired target reply.

A.3 Computer Simulation Results

Since there is an almost unlimited number of ways that the 3 fruit replies can produce interference on the target pulses, it is very difficult to analytically compute the probability of at least one clear pulse. Therefore, we have employed the existing computer simulation program of a DABS sensor that has been used to study the effects of interference on the DABS/ATCRBS reply processor [18]. The results generated using this simulation will tend to be conservative, since the computer logic requires that F1-F2 pulse pairs must be detected in order to declare a valid reply, which, as discussed

previously, is not a necessary condition for the detection aspect of the tracker aided reply processor, although it is necessary for updating the range estimate. Furthermore, of necessity, we have been required to maintain the 4° main beamwidth which reduces the resolution capability of the azimuth correlation checks. In the dual parallel approach monitor case, the 3 fruit replies would be spread over the entire 120° azimuth sector and, hence, provide for much greater azimuth discrimination capabilities. Finally, it is noted that the azimuth estimates are being made using a monopulse processor, so that the interference-free pulses will perform almost as well as the dual parallel approach monitor processor. The simulation program is defined in detail in reference [18], but, in summary, we note that on each Monte Carlo trial, the 3 ATCRBS fruit replies are specified by choosing arrival times, azimuths and amplitudes at random according to reasonable statistical models for these parameters. The arrival times are chosen uniformly on the interval (0, 42) μsec, the azimuths uniformly over the 20-dB beamwidth, and the amplitudes are chosen by selecting the associated range uniformly over the line of sight of the sensor. The target reply is specified to arrive at 20.1 μsec, at 1/2° off boresight with an amplitude corresponding to a 30-dB signal-to-noise ratio. For all replies, the presence of code pulses was completely random, being on or off with equal probability. Data were accumulated for 300 trials and processed by the DABS/ATCRBS reply processor.

In the first case, it was assumed that track file data could not be used by the reply processor and that no revision could be made to the existing

DABS/ATCRBS reply processing algorithms. The idea here was to make the processor a carbon copy of the DABS/ATCRBS processor. Of the 300 replies, 15 were lost due to the inability to detect an F1-F2 bracket pair, and another 79 were eliminated as phantoms. This gives a reply detection probability of only 69%. Of the replies that were correctly detected, 20 of them had no monopulse azimuth estimate because the F1 pulse experienced interference and resulted in an erroneous azimuth estimate that would not correlate with any of the other estimates made in the reply even though there were obviously one or more interference-free pulses. An additional 3 replies satisfied the F1 correlation criterion, but the estimates were significantly in error, probably as a result of strong interference overlapping the F1 pulse and some other pulse in the reply. Therefore, only 61% of the replies produced an interference-free azimuth estimate. This is too low even for a high data rate system and establishes the need for an alternate reply processing algorithm that capitalizes on the special characteristics of the approach monitoring problem.

Since there are relatively few aircraft in track for approaches for landings, it is reasonable to utilize the range and azimuth data in the track file to assist the reply processor in a heavy fruit environment. The simplest addition to the present algorithm is to use the track file range to locate a range gate around the anticipated target reply. In this case only 17 replies were lost by the bracket detection logic, which resulted in a reply detection probability of 94%. Of the 283 replies that were detected, 41 failed to produce azimuth correlations with the F1 pulses, and another 29 which did correlate

produced a poor azimuth estimate. Therefore, the probability of a clean azimuth estimate is still only 61%.

The problem with the preceding algorithms is that they depend on an azimuth correlation check which is always related to the F1 pulse. Fortunately, there is no need to depend on only the F1 pulse for providing the azimuth reference, since one already exists in the track file which is an integral feature of the PALM system design. The range and angle update can, therefore, be taken on any clear pulse in the reply being processed and the clear pulse can be found by using conservative consistency checks with the track file azimuth estimate. The probability of successfully updating the track file therefore depends on the probability that there is at least one clear pulse in the detected reply. For the 283 replies for which an F1-F2 bracket was detected, all of them had at least one clear pulse. Therefore, the probability of a successful tracker update is at least 94%.

A.4 Ranging Accuracy

Using the preceding reply processing algorithm, it is possible to determine a clear pulse on which to make the azimuth and range estimate. Of course, the range estimate is ambiguous within some multiple of 1.45 μsec. However, this ambiguity can be resolved as long as the bracket detector can provide a time reference that is accurate to within 0.725 μsec. The simulation results showed that even for the cases for which the F1 pulse experienced interference, the largest ranging error was found to be less than 0.2 μsec. Furthermore, as required by FAA transponder specification [19], the separation of code pulses relative to the F1 pulse can be in error by at most 0.1 μsec. In addition,

hardware has been built which can determine the location of a leading edge to within 0.05 μsec. Therefore, the largest pulse-to-pulse jitter is less than 0.35 μsec (.2+ .1+ .05), hence, there should be no cases in which the range ambiguity cannot be resolved. Therefore, the ranging accuracy should be as good as it would have been if clean F1 pulses were available all of the time. Since the error in the transponder turn-around delay must be less than 0.5 μsec [19], and since the leading edge of a clean pulse can be located to within 0.05 μsec, the PALM ranging error is the same as that for a standard ATCRBS system, namely 0.55 μsec or 275 ft. Finally, it may be worth noting that the performance of the range tracker depends only on the reply-to-reply jitter, which is required to be less than 25 nsec 1-sigma for all pulses in the reply [19].

A.5 The "No-Reply" Probability

From the preceding study, it is seen that a conservative estimate of the probability that fruit causes no reply to be received is 6%. In addition, there is also the possibility that the SLS circuitry in each of the transponders causes the target transponder to be shut off and, hence, not receive the PALM based uplink interrogation. This has been estimated at 5% at 20 miles with the likelihood of being considerably smaller as the aircraft drops below 1/2 mile, since in this case there will be fewer nearby interrogators for which the aircraft will be in line of sight and, hence, susceptible to SLS. Therefore, we must expect that 11% of the time there will be a data dropout (only 6% of this is due to the PALM configuration). Unfortunately, none of the tracker studies concerned with the approach monitoring problem considered the possibility of data dropouts, hence, it is difficult to say

for sure whether or not the question is of any relevance since the tracker may very well be able to coast through one or two missed returns with no loss in performance.

Until such a study is undertaken we can only assume the worst: that it is essential to be able to maintain a fixed data rate with no dropouts. For the PALM system, which doesn't have any antenna scheduling problems, this is most easily achieved by simply repeating an interrogation whenever an anticipated bracket pair is missed. Since the probability of a missed reply is 0.11 and the misses are indeed independent from interrogator to interrogation (since it is due to fruit and transponder SLS), the probability of a miss on two replies is 0.012 and on three replies is 0.001. These interrogations could be scheduled at a higher PRF (400 pps, for example) in order to keep the 1- to 10-Hz tracker update going smoothly.

A.6 Target Acquisition

Since airports in which PALM is likely to be employed will be ARTS III equipped, that system can be used to perform the target acquisition function and to establish the basic target track files (containing range, azimuth and a/c code data) which can be passed directly to the PALM computer. If for some reason it is desired to perform the acquisition operation under the control of the PALM interrogator, this could be done by transmitting a burst of 20 pulses at 400 pulses per sec every 4 sec which would provide exactly the same data base as the beacon system. The detection and acquisition logic would then be the same as that of the ARTS III system. Unless PALM was required to provide independent stand-alone operation, economics would dictate that the acquisition function be performed by the ARTS equipment and simply have the track file data passed to the PALM computer.

Appendix B

THE EFFECTS OF PALM ON ATCRB UPLINK RELIABILITY AND DOWNLINK FRUIT RATES

B.0 Introduction

Since the 120° PALM beamwidth is so much larger than that for the other sensors in the ATCRBS system, there is some concern that the 10-Hz data rate might lead to significant increase in the background fruit rate and possibly a decrease in the uplink reliability. In this section we look at these issues analytically and find that within the anticipated lifetime of the ATCRBS system the addition of a limited number of PALM sensors should cause no significant degradation in its performance.

B.1 Uplink Interference

For the case of uplink interference, we note that every 4 sec the ASR interrogates any one aircraft approximately 18 times over a sweep duration of 0.04 sec (4° beamwidth, 4-sec data rate, 400 pulse/sec). Since any one aircraft being scanned by the ASR is interrogated by PALM once every 0.1 sec, it is clear that at most only one ASR interrogation out of the 18 could possibly be interfered with by PALM. Since a mode A PALM interrogation effectively occupies the transponder for 30 μsec (8 μsec for the interrogation, 20 μsec for the reply), and since the ASR interrogations are 1/400 sec apart, the probability that the one interrogation from the ASR is blocked out by a PALM interrogation is simply $30\times10^{-6}/(1/400) = 0.012$. Therefore, PALM will cause

the ASR to lose one interrogation per scan only 1% of the time, which will have an insignificant effect on the uplink reliability.

B.2 Downlink Interference

On the downlink, PALM will cause every aircraft within its coverage region to generate 10 replies/sec which then adds directly to the background fruit rate. Estimating the overall effect is difficult since it requires knowledge of the total number of aircraft within the coverage region. Working from recently acquired ARTS tapes, studies at Lincoln Laboratory have shown that within a 30-mile range of JFK airport in New York there are likely to be as many as 55 transponder equipped aircraft. For the 120° PALM beamwidth, this number can be reduced to 18 (55 a/c × 120°/360°) which in turn leads to an additional 180 fruit/sec. Fruit rate measurements have produced estimates of the order of 2000 to 3000 fruit/sec. Hence, the additional fruit caused by a single PALM sensor contributes to an increase in the total background fruit level of 10% at most.

REFERENCES

1. J. B. Allen and E. J. Denlinger, "Parallel Approach Surveillance," Project Report ATC-13, Lincoln Laboratory, M.I.T. (14 August 1972), DDC AD-747744.

2. A. L. Haines, "Reduction of Parallel Runway Requirements," MITRE Technical Report MTR-6283, The MITRE Corporation (2 February 1973).

3. D. L. Parks, M. M. Hayashi and J. R. Fries, "Development of an Independent Altitude Monitor Concept," Report No. FAA-RD-73-168, Boeing Commercial Airplane Company (September 1973).

4. H. D. Hoekstra, E. B. Perry and S. Huang, "Altimeter Display Study, Part 2 - Analysis of Altitude Accidents," Report No. FAA-RD-72-46, 11, Flight Safety Foundation (May 1972).

5. "Engineering and Development Plan - Performance Assurance," Report No. FAA-ED-21-2, Systems Research and Development Service, Federal Aviation Administration (May 1973).

6. "Tentative MLS Functional Requirements Specification of November 1974," adopted by FAA MLS Central Assessment Group (November 1974).

7. J. T. Mengel, "Tracking the Earth Satellite, and Data Transmission, by Radio," Proc. IRE 44, 755-760 (1956).

8. M.I. Skolnik, Introduction to Radar Systems (McGraw-Hill, New York, 1962).

9. J. W. Duncan, "The Effect of Ground Reflections and Scattering on an Interferometer Direction Finder," IEEE Trans. - Aerospace Electron. Systems AES-3, 922-932 (1967).

10. D. K. Barton, "Multipath Error in a Vertical Interferometer," Proc. IEEE, 53, 543-544 (1965).

11. R. Horonjeff, Planning and Design of Airports (McGraw-Hill, New York, 1962).

12. J. Evans, "Synthesis of Equiripple Sectorial Antenna Patterns," submitted for publication in IEEE Trans. Antennas-Propag.

13. "Final Report of the MLS Scanning Beam Working Group," for Department of Transportation Federal Aviation Administration (December 1974).

14. "Final Report of the MLS Doppler Working Group," for Department of Transportation, Federal Aviation Administration (December 1974).

15. E. A. Zyzys, "Evaluation of Radio Telemetric Theodolite Using Kinn Model KEC-4029 UHF Transmitter," Memorandum Report Project No. 320-101-01V, National Aviation Facilities Center (January 1966).

16. "Development of a Discrete Address Beacon System," Quarterly Technical Summary, Lincoln Laboratory, M.I.T., (1 July 1972), 4-6, and (1 October 1972), 5-6, DDC AD-747789.

17. "Development of a Discrete Address Beacon System," Quarterly Technical Summary, Lincoln Laboratory, M.I.T. (1 April 1973), Fig. II-3, DDC AD-762071.

18. R. J. McAulay and V. Vitto, "A Simulation of the DABS Sensor for Evaluating Reply Processor Performance," Project Report ATC-28, Lincoln Laboratory, M.I.T. (16 September 1974), DDC AD-787633/7.

19. "Selection Order: U. S. National Aviation Standard for the Mark X (SIF) Air Traffic Control Radar Beacon System (ATCRBS) Characteristics," Order 1010.51A, 8 March 1971.

20. J. Sklar and F. Schweppe, "The Angular Resolution of Multiple Targets," Technical Note 1964-2, Lincoln Laboratory, M.I.T. (14 January 1964).

21. G. E. Pollon and G. Lank, "Angular Tracking of Two Closely Spaced Radar Targets," IEEE Trans- Aerospace Electron. Systems AES-4, 541-550 (1968).

22. H. L. Van Trees, Detection, Estimation and Modulation Theory, Parts I - III (John Wiley & Sons, New York, 1968).

23. W. B. Kendall, "Unambiguous Accuracy of an Interferometer Angle-Measuring System," IEEE Trans. Space Electron. Telemetry, 62-79 (1965).